LOS ALAMOS SCIENTIFIC LABORATORY
OF THE UNIVERSITY OF CALIFORNIA o LOS ALAMOS NEW MEXICO

RADIATION EFFECTS ON LITHIUM HYDRIDE

LEGAL NOTICE

UNIVERSITY OF CALIFORNIA
LOS ALAMOS SCIENTIFIC LABORATORY
(CONTRACT W-7405-ENG-36)
P.O. BOX 1663
LOS ALAMOS, NEW MEXICO

IN REPLY
REFER TO:

June 13, 1962

To: Copyholders of LA-2463

From: Report Library

Please staple this notice to the inside front cover of LA-2463, Radiation Effects on Lithium Hydride.

Page	
55	Fig. 15. On Curve C, 0.17% should read 0.1%.
56	Lines 16-17. Substitute $1/2\ E_c$ for E_c, so that end of the paragraph reads "... by $(1/2\ E_c + U) = 0.75 \pm 0.05$ ev, from which $1/2\ E_c = 0.2_2 \pm 0.1$ ev."
60	Fig. 16. F^1 center shown on + ion site, but ee should be at - ion site.
112-113	Values of E(displ) approximated by the expression at the bottom of p. 112 are in error. The calculation does not converge rapidly enough for any significance to be placed on the numerical values given for E(displ) in Table A.2; but the difference of 8 ev in the calculated E_B values obtained for LiH and LiF is noteworthy.

LA-2463
CHEMISTRY
TID-4500, 16th ed.

LOS ALAMOS SCIENTIFIC LABORATORY
OF THE UNIVERSITY OF CALIFORNIA LOS ALAMOS NEW MEXICO

REPORT WRITTEN: September 15, 1960

REPORT DISTRIBUTED: August 24, 1961

RADIATION EFFECTS ON LITHIUM HYDRIDE

by

Frank E. Pretzel
Dwayne T. Vier
Eugene G. Szklarz
W. Burton Lewis

Contract W-7405-ENG. 36 with the U. S. Atomic Energy Commission

ABSTRACT

Extensive measurements of the effects of radiation have been made on various compositions of Li hydrides containing combined T. The isothermal expansions of samples exposed to a flux of tritium β radiation equivalent to 16.8 Mr/hr have been observed at 12 temperatures between -196° and 400°C for maximum exposures up to 7 years. The results of these measurements are correlated with other data and are used to formulate a model for radiation damage in the Li hydrides.

That the Li hydrides are essentially ionic in character is shown by various properties. Single crystals of Li hydrides of various compositions were prepared from the melt. These were used to measure various physical properties, such as electrical conductivity, and to study radiation effects on the optical absorption of plates cleaved from the single crystals. The Li hydrides conduct electricity primarily by cation diffusion through a lattice-vacancy mechanism with an activation energy of 0.53 ev in a manner completely consistent with results obtained for the Li halides. The color-center model, which has been proposed to explain the effects of radiation damage to the alkali halides, is shown also to be suitable to explain the radiation-induced optical and electron-spin paramagnetic-resonance absorption observed in the Li hydrides.

Mechanical properties, phase separation, gas evolution, and other properties of the samples exposed to intense β radiation from combined T were also observed and correlated with the isothermal expansion data to formulate a model for the radiation effects. Equations are presented for the mechanisms involved, and comparisons between simplified calculations based on the model and observed expansion rates are given. One interesting conclusion obtained from these studies is the result that little dissociation and cavitation occurs in samples stored at temperatures below -7°C, whereas these effects are extensive and tend to lead to the disintegration of samples stored at 23°C or higher.

ACKNOWLEDGMENTS

The authors gratefully acknowledge the very substantial assistance they received from other members of the Laboratory. Much of the work required specialized techniques and could not have been performed without such assistance.

Significant contributions included the preparation of all of the LiH, except the single crystals, by A. Briesmeister of Group CMF-4, pressing of the LiH bars by C. Gutierrez and P. Stone of CMB-3, assistance with mass spectrometric analysis of the gas samples by T. Roberts of CMF-9, design of dies for pressing by J. Livingston of CMB-7, and calorimetry of LiT for T content by L. Treiman of CMB-3.

The first measurements of linear growth and outgassing were begun by T. W. Newton and E. J. Huber, Jr., of CMF-2, and they were continued by J. D. Farr of CMB-3. M. J. Jorgenson continued the observations in cooperation with the present authors. E. J. Huber, Jr., initiated the strength measurements. J. Jackson, CMF-2, made nuclear magnetic-resonance measurements of He, H_2, and Li contained in old, heavily damaged samples containing LiT.

Single crystals of Li hydrides in all the various isotopic compositions were prepared to study some of the basic physical and photochemical properties of the material. George Rupert, CMB-3, designed and constructed many of the components of the apparatus. C. L. Mader, G. V. Gritton, C. C. Rushing, R. J. Friauf, and E. K. Storms helped to prepare many of the single crystals and made some of the measurements on them. E. M. Cramer, CMF-5, measured the microhardness of the cleavage faces of LiH and other crystals. R. L. Petty, CMB-3, made low temperature measurements of crystal lattice expansion using an X-ray diffractometer technique. P. Waldstein, CMF-2, made some of the ESR measurements on single crystals and assisted in the interpretation of ESR data.

CONTENTS

CONTENTS (Continued)

TABLES

ILLUSTRATIONS

ILLUSTRATIONS (Continued)

ILLUSTRATIONS (Continued)

CHAPTER 1

INTRODUCTION

Because of the comprehensive nature of this report, which covers over 7 years of measurements, the inclusion of all the data would have made the report excessively long. Accordingly we have chosen to present representative results in a graphical form for brevity and clarity. Details of measurements on individual samples, along with discussions of techniques and probable errors, are left for separate reports of more limited scope.

Lithium hydride containing lithium tritide offers an excellent means for the study of radiation damage to this material under various conditions, such as temperature, at a well-known dose rate over long periods of time. However, it is necessary to know something about the bonding and the general character of the material before one can expect to interpret the mechanism for radiation damage to it.

The beta decay of tritium (with a 12.26 year half-life[1] to form helium-3) occurs at constant rate which is independent of the nature of bonding the T or of external variables such as temperature. Still, the distribution of the product He^3 throughout the LiH is not independent of these factors, and neither is the nature of the immediate products nor the state of the stoichiometric quantity of Li formed (whether atoms, metal, or color centers). The net reaction for the decay of the T after the dissipation of the energy

(18 kev maximum energy, 5.6 kev mean energy[1]) of the β particle is:

$$LiT \longrightarrow \left(\begin{array}{l}\text{Intermediate}\\ \text{Metastable}\\ \text{Products}\end{array}\right) \longrightarrow He^3 + Li$$

The β particles must lose their energy during passage through the material; the mechanism by which this energy is dissipated and the net resultant radiation damage to the material are primarily dependent on the chemical and thermodynamic properties of the material. It seems most reasonable to assume that the net effect of radiation damage on LiH will result in the chemical dissociation of the material with the possibility of recombination by a back reaction as indicated in the equation:

$$LiH \underset{\longleftarrow}{\overset{\beta}{\longrightarrow}} \left(\begin{array}{l}\text{Intermediate}\\ \text{Metastable}\\ \text{Products}\end{array}\right) \underset{\longleftarrow}{\longrightarrow} Li + \tfrac{1}{2}H_2$$

The extent to which the back reaction occurs in the first stage of the latter equation is most important to the resistance of the material to permanent radiation damage. If recombination is rapid and the steady-state concentration of metastable products is comparatively small, the net effect of the radiation on the material may be nearly negligible because all of the energy is dissipated as heat. On the other extreme, all of the energy could go to form dissociation products which do not recombine at all under the conditions of the irradiation; this could lead to the dissociation of about 300 molecules of LiH per β particle, assuming that 20 ev is required per dissociated molecule.

In recent reviews[2-4] of radiation damage, solid materials have usually been divided into four types, which differ in their response to exposure to the three types of radiation: electromagnetic, charged particles, and neutral particles. Seitz and Koehler[2] list the four basic solid types according to

the nature of their chemical bonding as metallic, valence, molecular, and ionic. Of course, many materials exhibit chemical properties which are intermediate between those of two or more of the basic types, and the explanation of radiation effects on these materials will usually involve comparison with more than one of the basic types. Metals are, in general, resistant to electromagnetic radiation, since most electronic excitation is readily dissipated as heat, and they suffer most damage through atomic displacements produced by heavy particle irradiations. Valence crystals, such as silica, diamond, silicon, and germanium, behave similarly to metals in their resistance to radiation by being primarily damaged by atomic displacements in their pure state. Molecular crystals, consisting of discrete molecules held together by van der Waals or other weak forces, are electronically excited by all types of radiations and, as a class, they probably suffer the greatest damage. Some molecules lose energy much more rapidly than others and suffer less permanent damage; thus aromatic organic compounds, such as naphthalene, dissipate energy readily, partly by fluorescence. Other molecular crystals, such as ice, aliphatic organic compounds, and even complicated molecular structures, such as polyethylene, suffer through the rupturing of bonds or ionization to form free radicals or ions which serve as intermediates for the production of new molecular species. Simple ionic salts, such as the alkali halides, suffer damage primarily as a consequence of electronic excitation by any type of radiation. Ionization causes displacements which act as electron or hole traps to produce metastable products called color centers. Color centers have pronounced effects on the properties of the salts, but in simple ionic materials they can be induced to recombine by moderate annealing or by bleaching with light of suitable wavelength. The irradiation of salts involving complex ions, such as the alkali azides or nitrides, forms color centers like the alkali halides; but the covalently bonded

anions behave like molecules in that they dissociate after excitation to form new molecular species. Damage to such materials is relatively permanent and is not easily removed by annealing. Comparison of radiation effects in the Li hydrides to those observed in the four basic solid types is useful for the interpretation of the results, and it also gives additional evidence as to how the Li hydrides should be classified among the four basic chemical bond types.

Insofar as it can be considered ionic, LiH is unique as the lightest and simplest of all possibly stable ionic solids. It has a simple NaCl type of lattice and is the only salt that consists solely of ions with the He configuration of electrons. These properties have made LiH attractive for theoretical treatment, and calculations of lattice parameters and crystalline cohesive energy of LiH have been made using various quantum-mechanical approximations.[5-9] The classical calculation of the lattice energy based on the Born-Mayer model has been performed by Baughan[10] although a reliable experimental value for the compressibility of LiH is not available. Kasarnowsky[11] reversed the calculation to obtain the compressibility from the experimental lattice energy computed by means of the Born-Haber cycle, and his values are in fair agreement with the average of estimates obtained from experiments.

Calculations by Herzberg[12] and others have shown that the bond in the diatomic LiH gas molecule is predominantly covalent. By using electronegativities to calculate the covalent contribution to bonding between neighboring ions in a NaCl-type lattice following Pauling,[13] 12.5% covalent character is found for LiH compared to 10% obtained by Pauling for LiI. Homopolar bonding[9] has been used to account for the 6 to 9% discrepancy between the observed cohesive energy and the results of Lundqvist[7] in a more recent calculation. X-ray-scattering results have been used to ascribe a large

degree of covalency to the bonding in solid LiH,[14] but others have shown that this interpretation is in error in the case of LiH and, indeed, that no conclusion can be made regarding the character of the bonding in crystalline LiH from the X-ray data.[15,16] Some pertinent physical and chemical properties of crystalline LiH are given in Table 1. It is seen that many properties are similar to those of the alkali halides.*

*The properties of LiH are discussed in greater detail in Reference 17.

Table 1. Properties of Li Hydrides Compared to Alkali Halides

Property/Material	LiH	LiD	LiF	NaCl	References
Molecular Weight	7.948	8.954	25.94	58.45	18
Lattice Constant (Å)	4.083_5	4.068_4	4.0270	5.6402	19, 20
Crystal Density (25°C, g/cc)	0.7750	0.8826	2.601	2.162	*, 21, 20
Hardness (DPN or kg/mm^2)	36.6	36.6	97.0	17.5	*
Compressibility (10^{-12} cm^2/dyne)	2.8	2.8	1.53	4.18	*, 10, 22, 23
Coefficient of Thermal Expansion (10^{-5}/deg)	3.6	(3.6)	3.4	4.04	24, 25, 26, 23
Thermal Conductivity (cal/deg cm sec at 100°C)	0.025	(0.025)	0.022	0.014	22, *, 27, 28
Debye Temperature (°K)	815, (920)	(611, 744)	610, 780	281, 330	29, 30, *, 31
Melting Point (°C)	688	(688)	842	801	32, 22, 33
Lattice Energy (kcal/mole)	-217.8	-218.8	-244	-185	34, 22, 35, 36
Heat of Formation (kcal/mole)	-21.67	-21.78	-143.6	-98.2	34, 22, 35, 36
Gas Pressure at Melting Point (mm of Hg)	~600	~600	~0.06	~0.10	*, 21
Electrical Conductivity (ohm^{-1}/cm at 600°C)	3×10^{-3}	10^{-3}	10^{-5}	10^{-5}	*, 37, 38
Dielectric Constant	12	(12)	9.3	5.6	*, 39
Refractive Index at 5892 Å	1.984_7	1.985_6	1.391_6	1.5442	19, 40

*This work

CHAPTER 2

MEASUREMENTS

This chapter on measurements is by no means complete, but it is included to give the reader some idea of the experimental methods employed in this investigation. The purpose of the measurements can be divided into three categories: (1) to determine the physical and chemical properties of LiH, (2) to study radiation-damage effects and color-center formation in crystalline LiH, and (3) to study such gross effects as expansion and outgassing in samples containing LiT as functions of the logical variables, in such a way as to permit the interpretation of the results in terms of a reasonable model. Table 1 contains the measured values for some of the properties determined under the first category for LiH and LiD along with others from the literature; also, literature values for the properties of LiF and NaCl are included for comparison. With the exception of such properties as density and Debye characteristic temperature, which depend more directly on the mass of the hydrogen isotope, the other tabulated properties of LiH and LiD may be assumed to be identical without introducing errors greater than 1% or so. Similarities in crystal structure, lattice energy, and such physical properties as hardness, compressibility, thermal expansion, and thermal conductivity between LiH and the two alkali halides are quite evident from the table. The values for LiH are frequently in the logically intermediate

position between those of LiF and NaCl. The value given in the table for the melting point of LiH may seem relatively too low, and that given for the electrical conductivity of LiH may seem too high; but these properties are discussed later in more detail and found to fit logically into the sequence of Li halide properties. On the other hand, the comparatively low heat of formation of LiH from the elements reflects the relatively high bonding energy of H_2 in its standard state, compared to the halogens, and results in the instability of LiH toward chemical reaction in oxidizing atmospheres or toward dissociation of vapor molecules at temperatures near the melting point. (The high chemical reactivity of LiH requires that all handling of this material must be carried out either in vacuum or in an inert atmosphere. A dry box flushed with dry He or Ar was commonly used for achieving the latter.) Since the vapor is predominantly dissociated at the melting point and metallic Li has a limited solubility in the molten salt, a H_2 pressure in excess of the high value given in the table is required to obtain pure, colorless LiH of stoichiometric composition from the melt. The comparatively low electron affinity of H is also in agreement with the above observations and with the expectation that H^- ion should be more easily polarized than F^- or Cl^- ions. The comparatively high polarizability of H^- ion is verified by the high refractive index of LiH.

2.1 Measurements on Single Crystals

Single crystals of LiH and LiD were grown from the melt for use in a study by optical and magnetic-resonance (ESR) techinques of color-center formation. Many types of irradiation were used, including X rays, Co^{60} γ rays, β rays from 10^{-5} to 10 mole % LiT included in several crystals, neutrons from a homogeneous reactor, and ultraviolet light. Except for the ultraviolet light, which was very ineffective for the production of color

centers at low temperatures, all methods of irradiation produced the same optical absorption bands. Neutron irradiation proved to be the most efficient means for obtaining densely colored crystals because of the highly energetic $Li^6(n, \alpha)T$ reaction. A 1 min exposure to a flux of 5×10^{11} n/cm^2 sec is roughly equivalent to exposing the sample of LiH to X rays from a copper target operated at 40 kv and 20 ma for 2 days. To prevent the destruction of the color centers first formed and also prevent their aggregation to form more complex color centers, many of the irradiations were done at low temperatures. Temperatures in the range from -196° to -73°C proved to be adequate for this purpose, and they were attained by the use of boiling nitrogen or mixtures containing solid CO_2. Samples of single crystals containing LiT were most useful for studying the kinetics of radiation damage at chosen temperatures by comparing optical and ESR measurements of color-center growth to flotation and X-ray measurements of crystal expansion.

Samples were also cleaved from the single crystals to measure the electrical conductivity, hardness, and density of LiH and LiD. The results of these determinations are included in Table 1. Electrical conductivity is discussed in more detail in a later section. All of the tabulated hardness values are for "strain-free" samples of single crystals and were obtained from measurements made with a Kentron microhardness tester applying a load normal to the (100) cleavage faces of the crystals. Flotation densities obtained for "pure" samples of LiH and LiD agree with the calculated crystal densities obtained from X-ray lattice parameters within the small limits of error of the measurements. This is taken as a measure of the high degree of purity of some of the single crystals prepared. A similar flotation method was used to follow the expansion of crystals containing LiT stored at low temperatures, which is described in the following section. Measurements of the lattice expansion of samples prepared from a LiH crystal containing

5.56% LiT were made using a low temperature vacuum stage on an X-ray diffractometer. The free surfaces of the powdered samples were protected by a 0.00025 in. Mylar film, which was adequate protection during transferences and storage under liquid N_2.

The single crystals of LiH and LiD were prepared by slow crystallization of the molten salt in the apparatus shown in Figure 1. The apparatus was pressurized with H_2 or D_2 to a total pressure of 2.7 atm to prevent dissociation of the salt. Because of the chemical reactivity of LiH and of the still higher reactivity of the Li metal from which it is made, nonmetallic impurities such as oxides and nitrides were more troublesome than metallic impurities. When attempts were made to grow clear crystals with theoretical density from the purest salts obtainable, the products were made cloudy by the presence of dense impurities. The first step in the procedure adopted to produce suitably pure crystals of LiH was the removal of the less volatile impurities by vacuum distillation of Li metal into a clean thin-walled crucible made of pure iron. The lid of the crucible containing the freshly distilled Li was tamped into place and welded to the crucible by induction heating under vacuum. The crucible was then heated to about 750°C in H_2. Further stages in the preparation of a pure single crystal of LiH are illustrated by the temperature-time curves in Figure 2. At this temperature and 2.7 atm of pressure, H_2 diffused through the thin Fe walls of the crucible, with complete synthesis of pure molten LiH after about a week's exposure to the gas. Next, with the heat conduction down the crucible support giving a vertical thermal gradient through the melt of about 30°C/cm, the stabilized power supplied to the furnace was automatically and slowly reduced to grow a single crystal. The crystal was then cooled more rapidly under reduced thermal gradient to room temperature. The approximately 2 in. long and 5/8 in. diameter single crystal was finally freed by cutting through the thin-walled

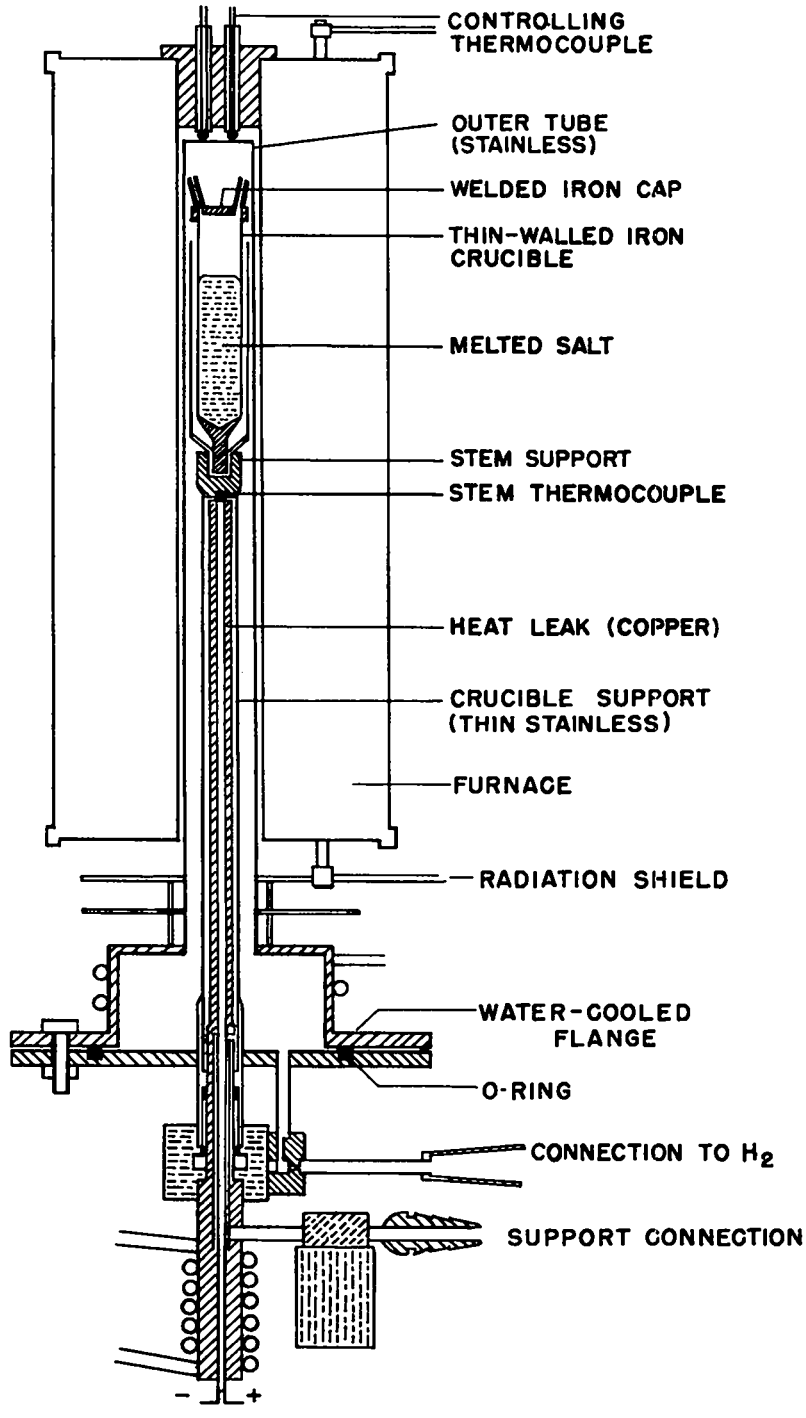

Fig. 1 Apparatus for the preparation of single crystals of LiH from the melt. Note water-cooled Cu heat leak sealed inside the crucible support to establish a thermal gradient through the melt.

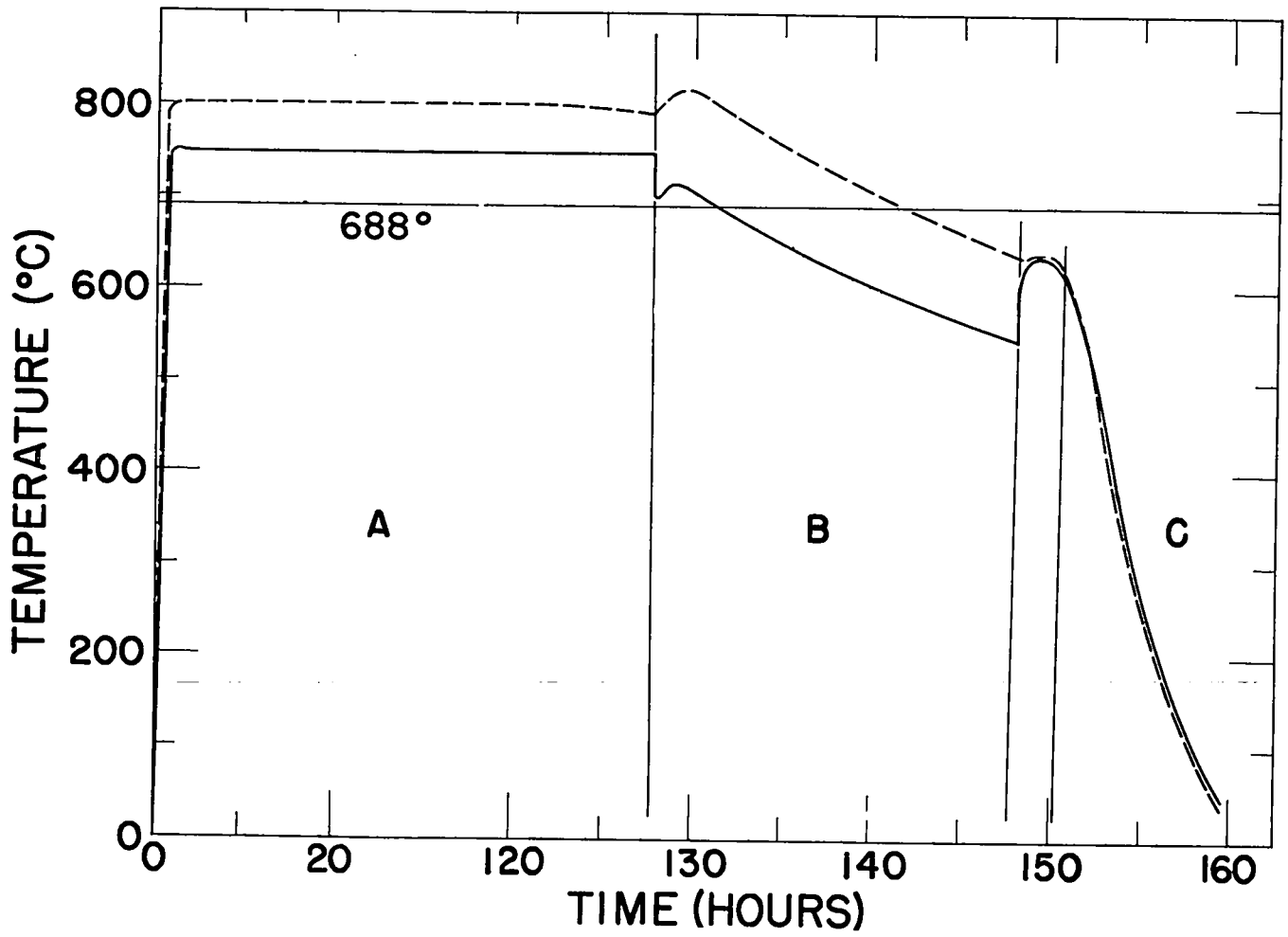

Fig. 2 Preparation of LiH single crystal illustrated by temperature traces compared to the melting point of LiH. The dashed and solid lines indicate the temperature at the top of the apparatus and at the crucible support, respectively, as determined by the thermocouples illustrated in Fig. 1. (a) The synthesis of molten LiH (normally requiring from 4 to 7 days), (b) crystallization by slow cooling at maximum thermal gradient, (c) cooling the crystal.

crucible and then tearing and peeling it away from the crystal.

The purity requirements for some of the measurements are very severe because very low concentrations of crystal defects are entirely responsible for the property under observation. In the color-center studies it was found that centers associated with divalent impurity ions had greater stability than those formed in a "pure" crystal lattice. These impurity centers are responsible for the predominant absorption bands formed by the irradiation of crystals containing 0.05 to 0.5 mole % Mg^{++} ion at room temperature, but the effects of such divalent ion impurities are minimized in "pure" crystals which are more heavily irradiated at low temperatures. Experiments show that the addition of Mg metal to LiH before crystallization improves the optical properties and cleavage characteristics of the single crystals prepared from LiH starting material. As with the alkali halides and other ionic crystals, it was found that aliovalent metallic impurities introduce defects which are responsible for the low temperature electrical conductivity of LiH in even the purest crystals. Analyses of the "pure" crystals indicated that the most important divalent impurity was Mg at 2 to 5 molar ppm and Cu and Fe at 0.5 to 2 molar ppm in both LiH and LiD. From the flotation density measurements it is estimated that the concentrations of nonmetallic impurities, calculated as oxide, in the purest crystals varied from a few molar ppm up to 0.1 mole %.

2.2 Measurements on Samples Containing Large Concentrations of LiT

No large single crystals containing more than 5.56 mole % LiT were prepared, but several small 0.1 to 20 mg crystals containing 40 or 50 mole % of the tritide were obtained from melts and were adequate for several studies. Samples near to the minimum size were used to study Li formation in the salt by observing the intensity and shape of the electronic-spin paramagnetic-resonance absorption of the metal over a period of 500 days in samples

stored at 23° and -196°C. Also, density measurements were made to study the expansion of crystallites stored at -196°C. Densities were computed from flotation temperature measurements on small crystals immersed in an inert calibrated liquid which was contained in a sealed quartz tube and stored under boiling N between determinations. A similar method was used for single crystal samples containing 1 to 6% LiT mentioned in the preceding section, but in that case flotation liquids were chosen so that the measurements could also be made at -80° to -20°C instead of at room temperature or above. The high sensitivity of the flotation method makes it valuable for samples which expand at a low rate, but the limited density range obtainable with a given liquid restricts the period of observation for rapidly expanding samples and also the utility of the method.

Extensive observations of the expansion of Li hydrides as a function of LiT content, storage temperature, and age of the material were made on larger samples of the salt prepared from pressed powder. The material was prepared as a melt, reacting H_2 containing T_2 with the metal, which was then cooled and ground. Most of the samples were hot-pressed bars of the ground salt which were compacted to 95 to 100% of the crystal density at 400°C and contained 2 to 4 g of material with 20 to 70 mole % LiT in a shape that was $3 \times 1/2 \times 1/4$ in. Small circular markings near the ends of the bars or bar fragments were used as indices for periodic measurements of length with a traveling microscope. Volume expansions were computed from observations of linear growth after first ascertaining the isotropic nature of the expansion by measuring increases in all three dimensions on many samples. All measurements were made at 23°C although the bars were stored at many temperatures from -22° to 400°C.

The outgassing of the bar samples was observed by periodically pumping the sealed sample containers and measuring the total gas evolved in a

calibrated volume. Samples of the gas were analyzed on a Consolidated-Nier mass spectrometer, and the analyses were frequently checked for He content by burning a portion of the gas in a CuO train with a trap to remove the H_2. A record of the quantities of He^3 and the H_2 isotopes evolved as a function of storage time under different conditions of temperature or composition was obtained. The observations also yielded information on possible leakage of the sample containers.

After long storage, the presence of radiation-damage products in the samples was verified by nuclear magnetic-resonance spectroscopy.

Mechanical properties such as bending stress and hardness were studied as functions of age on some of the bar samples. The bending stress data were scattered -- largely because of incipient cracks formed during sample preparation. They indicate a general decrease of strength with storage time. Hardness data were more easily obtained from the samples, and they show a consistent increase in hardness with increasing storage time at room temperature. A Rockwell hardness tester using 1/8 and 1/16 in. diameter ball indenters under reduced load was used to make the measurements. The machine was calibrated on a number of samples, and the results were cross-checked against a Kentron microhardness tester so that all data could be presented in DPH (or DPN) units, which have a more direct physical meaning, in terms of kg of force supported by 1 mm^2 of the material, than the Rockwell number values. Other physical changes were observed visually, often with the aid of a microscope. These included observations of microcleavages and Li extrusion from surfaces, as well as observations of microscopic fracturing and disintegration of samples.

CHAPTER 3

DISCUSSION OF RESULTS

3.1 Expansion

The expression $E = E(x_T, t, T)$ relates the expected dependence of the volume expansion on three logical variables: concentration of LiT, age, and storage temperature. The dependence of the expansion on the latter two variables is the main subject of the illustrations and discussions contained in the remainder of this paper. It is evident that the dose rate is dependent on the LiT concentration in the salt. The room temperature expansion of salts of varied LiT concentrations can be described more simply by combining the concentration and age parameters into one "equivalent damage" parameter represented by $t' = x_T t$.* Since most of the data are taken from observations

*This relation breaks down after t' exceeds about 120 effective days with salts of lower LiT concentrations showing larger total expansions on the E vs t' plot. If mean temperatures of the more concentrated tritide salts were raised by radioactive heating -- which must always be considered in these experiments -- the reverse effect would be expected. The "effective damage" formulation describes the production of decay and damage products by a zero-order mechanism dependent on the dose rate. Higher-order mechanisms are obviously involved in the recombination of the damage products at the differing concentrations in which they are produced in the various tritides. Thus, the lowered total expansions of the more concentrated LiT salts, after considerable damage, is not unexpected. After 1 year effective storage, these variations became small compared to total expansion.

made on material containing 40 mole % LiT, for simplicity the uncorrected age has been used in preparing most of the figures.

The general effects of age and temperature on the expansion of Li hydrides containing 40 mole % LiT are shown by the isotherms plotted in Figure 3. The isotherms are given for temperatures of -22°, 23°, 50°, 75°, 150°, 300° (dashed line), and 400°C and extend to the first 680 days of expansion. Note that the temperature dependence is very large, affecting both the magnitude of the expansion and the shape of the curve. The 300°C curve is particularly notable since it starts at very low values and then rises with age to cross many of the other expansion isotherms.

Other samples stored at 125°, 200°, and 250°C had short lifetimes due to the breaking of the samples (discussed in Section 3.3). For clarity these expansion curves are plotted along with other curves in the 23° to 400°C storage temperature range in an expanded scale shown in Figure 4. Changes in the slopes and shapes of the expansion curves as a function of increasing storage temperature are again quite striking. The data for the incomplete curve at 150°C were obtained with a different set of samples having a less well-defined thermal storage history from those used for the 125° to 400°C curves. The short jagged lines on the 125°, 200°, and 250°C curves indicate fracture or disintegration of the bar samples. Visual observations and particle-size determinations made on the residue of some of these disintegrated samples indicate that the breakup of the material occurred primarily at the grain boundaries. The mean lifetimes of the bars were probably reduced by a combination of factors including the extreme brittleness induced in the material and the high strain rate to which samples were exposed.

The expansion data obtained from samples stored at lower temperatures are best illustrated in the scale chosen for Figure 5. These isotherms illustrate the relatively minor influence that temperature has on the expansion

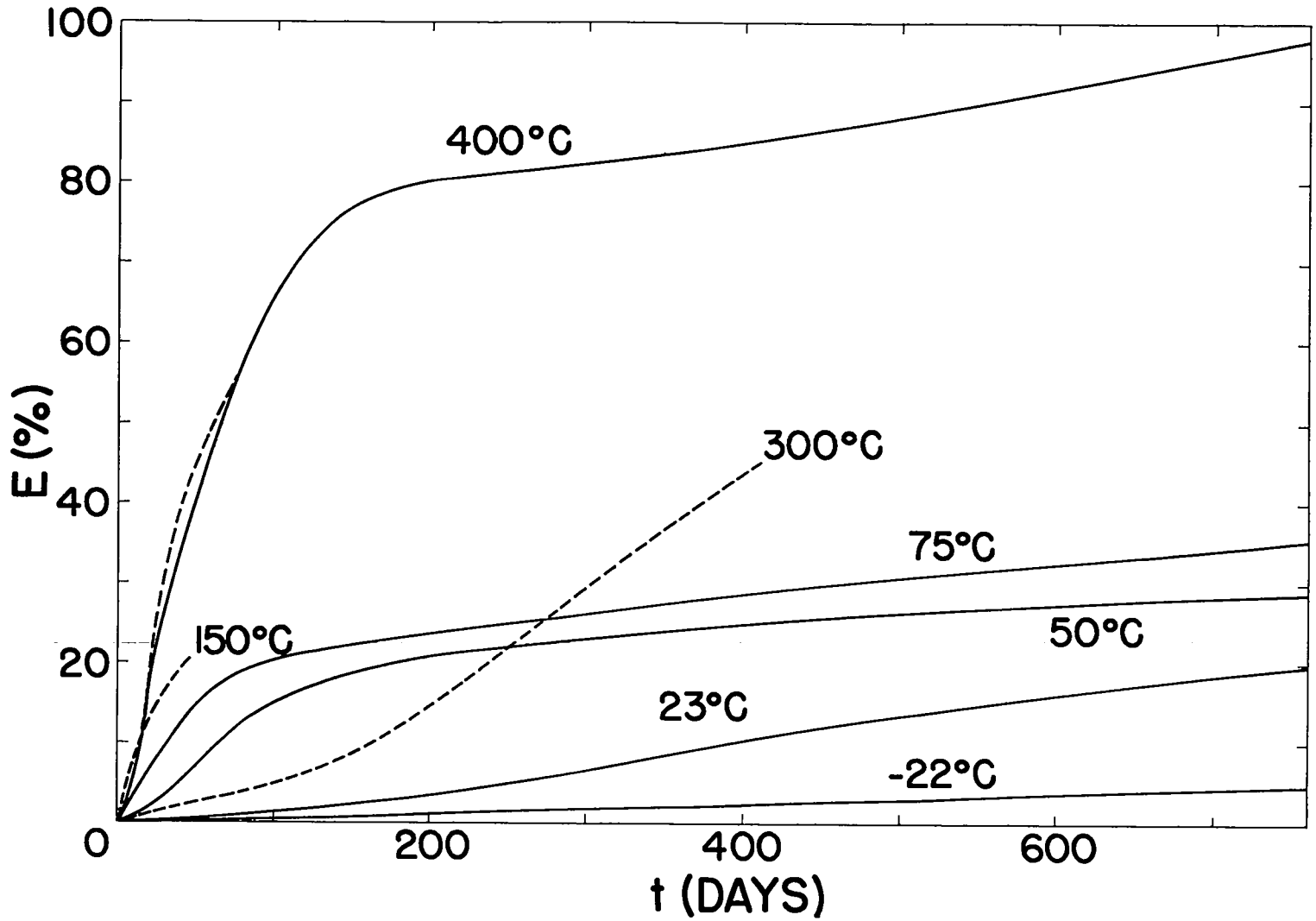

Fig. 3 Expansion isotherms for LiH samples containing 40 mole % LiT stored at the indicated temperatures. The variation of the 400°C data and the isotherms obtained at 150° and 300°C are shown as dashed lines.

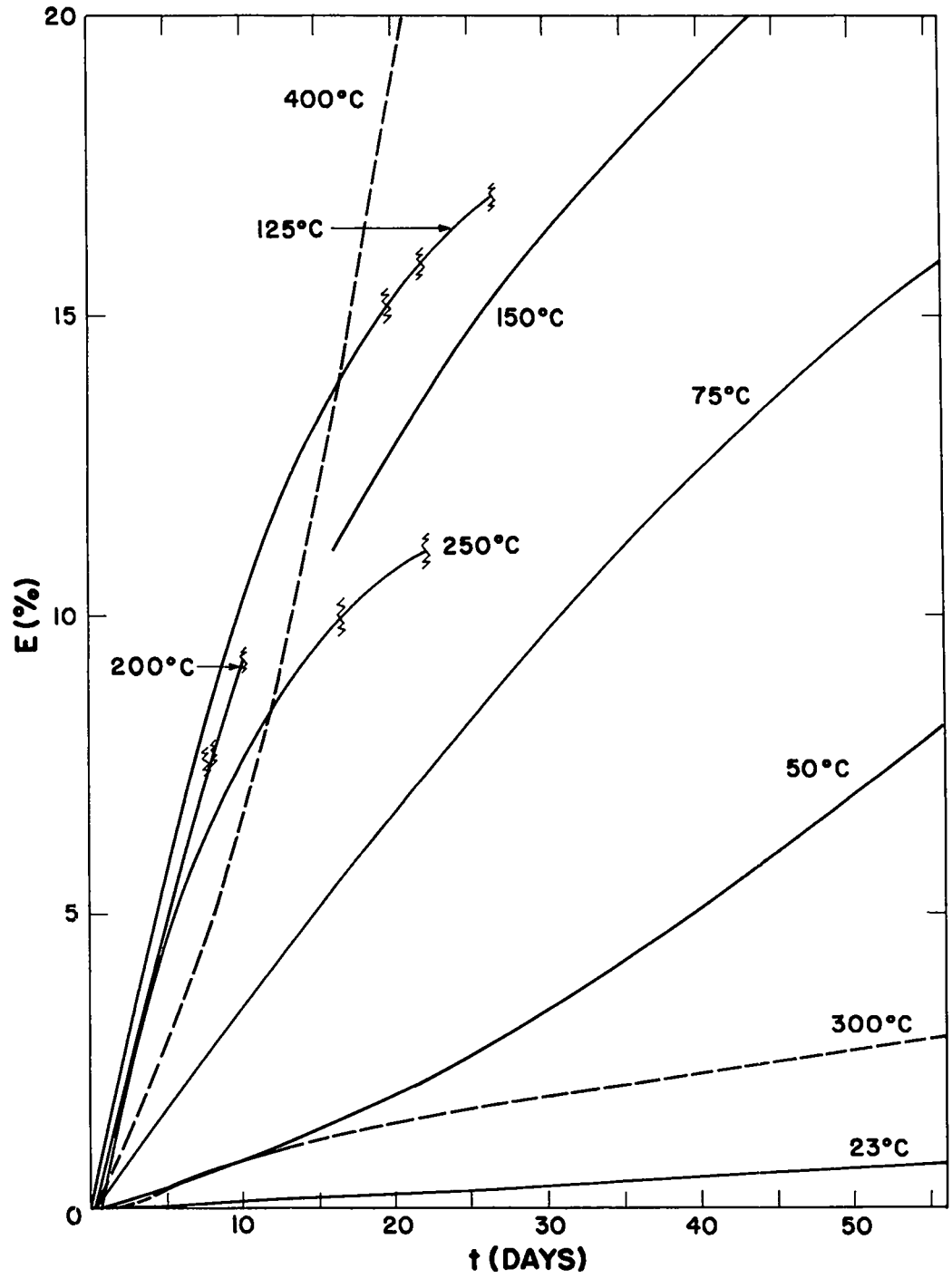

Fig. 4 Expansion isotherms of short-lived samples of LiH containing 40 mole % LiT stored at temperatures above room temperature. The jagged marks on some of the curves indicate the rupture of a sample.

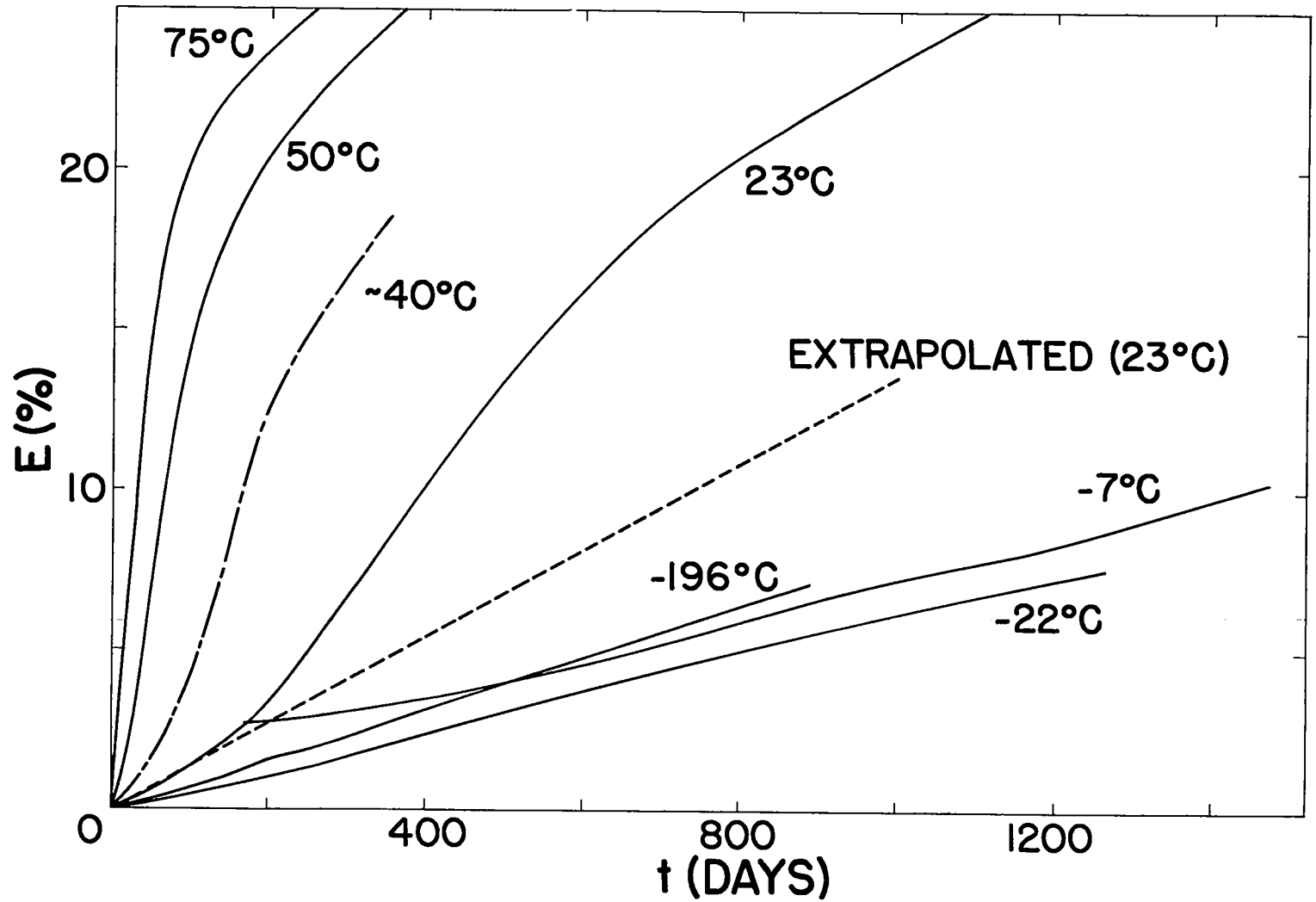

Fig. 5 Expansion isotherms of samples of LiH containing 40 mole % LiT and stored at low temperatures. The -7°C sample was stored at 23°C for 150 days before the temperature was reduced, and the 40°C storage temperature of the semi-dashed curve is only approximate.

isotherms obtained at storage temperatures of -7°C and below as contrasted to the high sensitivity to storage temperature observed at 23°C and above. The initial 23°C expansion was linear, and this slope has been extrapolated as a straight dashed line for comparison to the low temperature curves. The -196°C (liquid N_2) expansion curve was from measurements on the flotation densities of small crystalline samples rather than from bar samples. The broken curve labelled approximately 40°C was obtained from pressed pieces stored at ambient temperature within a drybox with poor temperature control.

3.2 Hardness

Hardness results obtained on some samples stored at 23°C as a function of increasing age are shown in Figure 6. The ordinate is given in absolute units on the left and in values relative to the unstrained single-crystal hardness on the right. The unstrained single-crystal hardness is indicated by the dashed line and is drawn as the approximate origin of the curves. The points and solid curve refer to average values for each sample, whereas the upper and lower bars and dashed curves refer to the maximum and minimum values, respectively. Low indenter loadings were required to prevent fracture of the fragile material at greater ages; this resulted in little penetration of the material and in reduced sensitivity. The minimum values were generally the least reliable for any given sample because of the somewhat porous nature of the pressed bar samples.

The curves show that the hardness increases to six times the original value in less than 250 days, but the rate of increase decreases with age. These results show that the salt, in expanding under the effects of β irradiation, has developed a high degree of stress. Extreme embrittlement of the aged samples made it impossible to continue the measurements without destruction of the samples after 250 days. The incidence of disintegration of

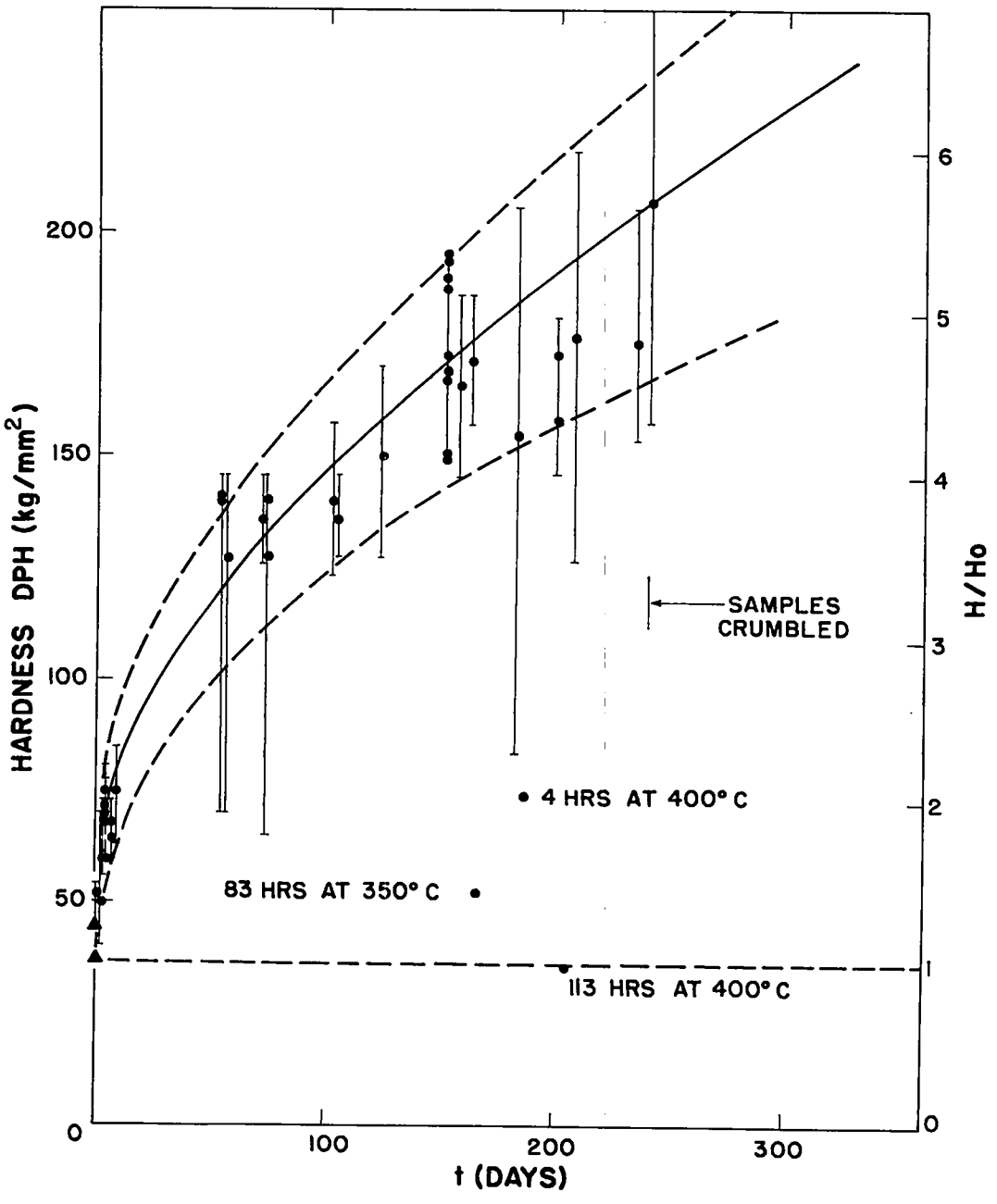

Fig. 6 Hardness increase observed in LiH samples containing 40 mole % LiT and stored at 23°C. The spread of some of the data is indicated by bars associated with the points and by the dashed curves. The variation of hardness with age and the results of various annealing experiments are compared to the single-crystal LiH hardness shown by the dashed line near the bottom of the figure.

room temperature samples also became appreciable at about this age. The extra hardness and the brittleness of old samples can be reduced by annealing the samples for some time at or near the hot-pressing temperature of 400°C. Plastic flow is sufficiently rapid at these temperatures to remove the internal stresses and the radiation-induced hardness, as indicated by the three points given in Figure 6 to illustrate annealing effects. In the last case, the unstrained hardness value was obtained after 5 days at 400°C, but it was simultaneously observed that the sample expanded 20% in volume to relieve the stress accumulated during storage of more than 200 days at room temperature. (The annealing process was observed to be accompanied by a loss of only 6% of the He^3 which had been accumulated in the sample by T decay and only 2% of the equivalent amount of Li metal which was also produced. This experiment, along with others, serves to indicate the tenacity with which the decay products are contained by the salt, even at relatively high temperatures.)

3.3 Outgassing

The outgassing isotherms obtained from LiT-containing bar samples stored at temperatures from -22° to 400°C are shown in Figure 7. The extreme range of the gas evolution rates observed as a function of storage temperature -- from 0.16 cc He^3/cc of salt stored at -7°C in 800 days to 65 cc of He^3/cc of salt stored for 800 days at 50°C -- makes it difficult to compare the results on the same graph, but the data are neither so complete nor so accurate as the expansion data and therefore are not presented here in so detailed a fashion. The deviations of outgassing curves for certain individual samples from the average curves, shown in the figure, are frequently quite extreme, which makes any detailed conclusions drawn from the features of the averaged curves of dubious value. With respect to the effect of the

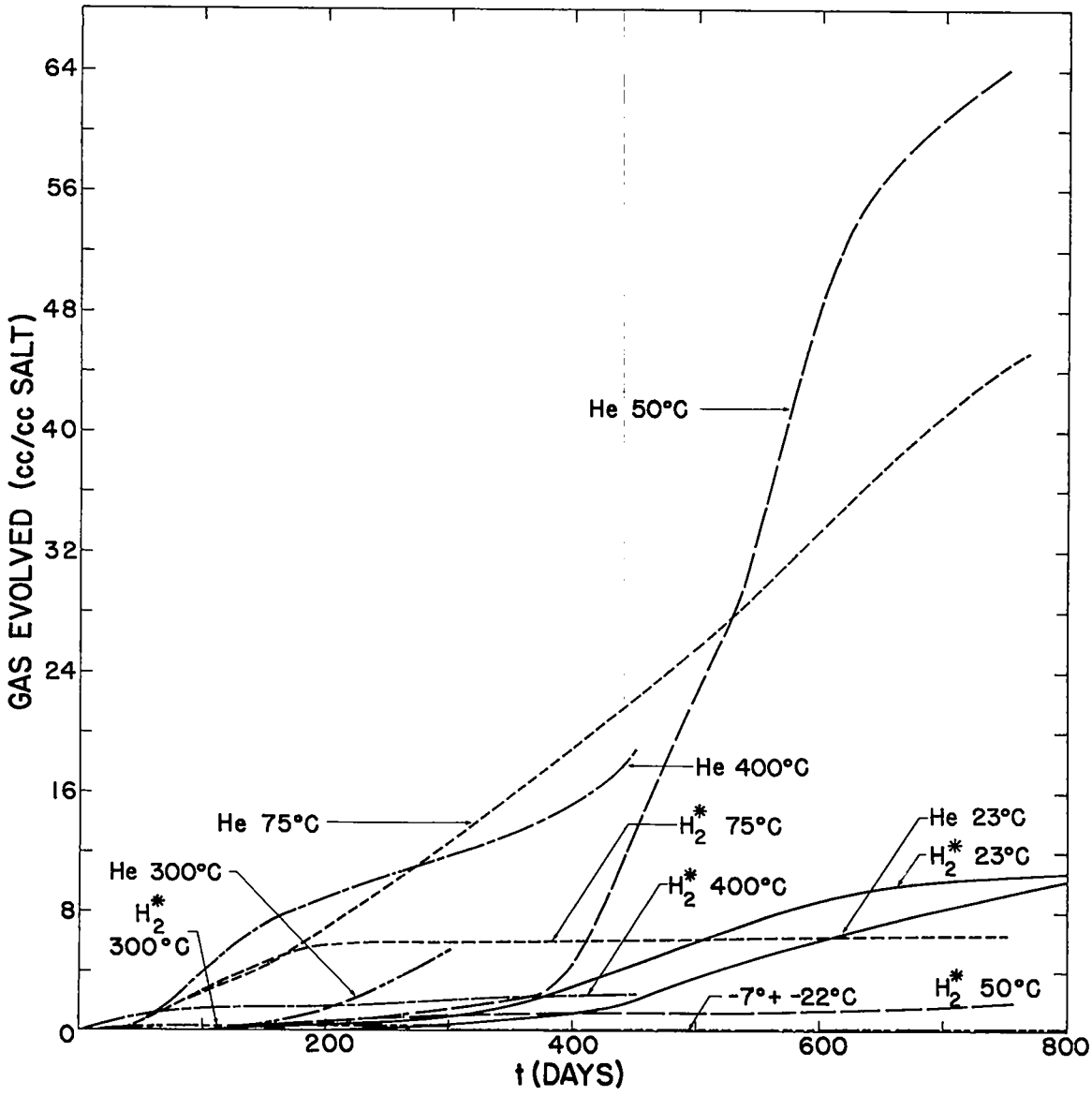

Fig. 7 Average outgassing of LiH samples containing 40 mole % LiT stored at the indicated temperatures. It is scarcely possible to indicate the small outgassing of samples stored at -7° and -22°C on the scale employed.

LiT concentration of the salts on the outgassing rate, it is found that the data for a given storage temperature (room temperature) can be normalized by plotting $x_T V$ vs $x_T t$. This fits the He evolution and, to a lesser extent, the H_2 evolution for all but very long storage times, similar to the E vs $x_T t$ plots used to normalize the expansion data. The data obtained at 300° and 400°C are probably subjected to the additional error of significant diffusion of He^3 through the glass containers.

The first gas obtained from any sample consists primarily of hydrogen isotopes, some from the reaction of moisture or hydroxide at the surface of the bar with the salt to form Li_2O, and the rest from radiation damage to the surface and bulk of the sample. Later the gas evolution rate increases greatly, and He^3 becomes the principal component. Again, the initial period is long for low storage temperatures and much shorter at high temperatures. The data cannot be explained by any simple model for gas diffusion through a solid. Too many factors change with age including "effective" gas pressure and surface area for a given sample. Some of the gas appears to be released in a sporadic manner, and this is probably related to the microfracturing of the embrittled material produced by radiation damage. Fracturing of the grains of the salt increases the effective surface area of a given sample, and this has the effect of reducing the average length of diffusion paths from the bulk of the crystals to the surfaces.

The disintegration of the bar samples often occurs with considerable vigor, frequently throwing fragments to all parts of the container, and may be compared to that of stressed glass Ruperts' drops.* As mentioned in Section 3.1, for bars stored at temperatures near 200°C, the breakup often

*This may be compared to the breakup of LiF crystals exposed to over 10^{18} n/cm^2 and subjected to over 10% expansion which was observed by Spaepen[41] and Senio and Tucker.[42]

occurs between grain fragments of the highly stressed compresses, and the amount of gas released is small. The rate of gas evolution often increases after disintegration -- although usually not as dramatically as shown in Figure 8. In Figure 8 the expansion and outgassing data obtained from a single bar sample containing 70 mole % LiT are plotted together for comparison. There was a very strong increase in He^3 evolution rate after the bar disintegrated following storage for 654 days at 23°C, but only a slight increase in gassing rate was noticed in a sample taken 4 days after the breakup. This is convincing evidence that the He^3 left the grain fragments after the disintegration of the sample. In most cases the onset of strong He^3 evolution occurred after a much greater time interval had elapsed since disintegration of the sample. Figure 8 also shows that the first marked increase in the rate of gas evolution occurs after the expansion rate reaches its maximum. The H_2*/He^3 ratio* in the evolved gas also drops after the maximum expansion rate has been passed, thus indicating recombination of H_2* with Li in the samples. The last two observations are fairly general for samples stored at 23°C.

3.4 Separated Phases in the Samples

Nuclear-magnetic-resonance (NMR) spectroscopy has been used to demonstrate the presence of He, molecular H_2, and metallic Li in heavily damaged pressed samples containing LiT. The He appears as the He^3 NMR band comparable to that reported for the gas.[43] Molecular H_2 shows as a narrow band in the NMR spectrum of T nuclei of the sample which is superimposed on the broad NMR absorption by the H^- ions of the crystal lattice.[44]

H_2 refers to any combination of H, D, and T. Generally, in this report H_2 is used also to mean any isotopic composition of hydrogen gas unless specified otherwise.

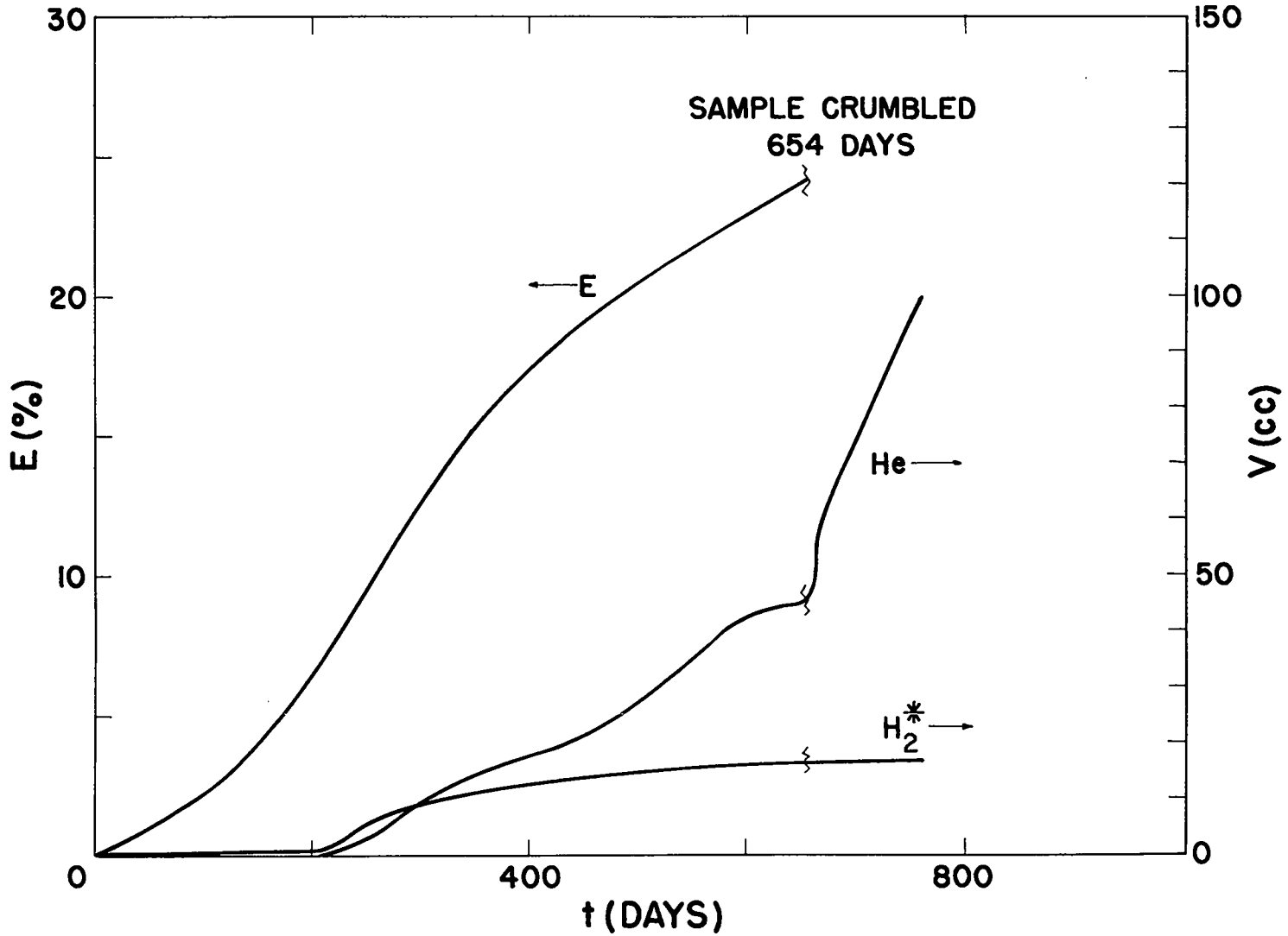

Fig. 8 Radiation-damage effects on a LiH sample containing 70 mole % LiT stored at 23°C. The upper curve shows the expansion of the sample and the time of disintegration for possible correlation with the outgassing results illustrated by the lower curves in the figure.

Metallic Li also appears as a narrow Li^7 NMR band superimposed upon the broad NMR absorption by the Li^+ ions of the sample and displaced by the characteristic Knight shift for the metal.[45]

Observations were made on two pressed samples of salt weighing from 1.6 to 2 g and containing 40% LiT, which were over 2000 days old and had been mainly stored at -7° and 23°C, respectively. The sample stored at -7°C appeared to be in good condition, whereas the sample stored at 23°C had undergone visible deterioration and rupture. The NMR observations are summarized in Table 2 for these samples in which about 11% of all H^- ions had been converted to He^3 by decay of T during storage.

Table 2. Nuclear-Magnetic-Resonance Observations of Species in Aged LiH Samples Containing LiT

Absorbing Nucleon	Absorbing Species	Observed Width of Characteristic Band	Comparative Intensity Found in Sample Stored at -7°C	Comparative Intensity Found in Sample Stored at 23°C
Li^7	Li^+ ion	10 gauss	strong	strong
	Li metal	0.5 gauss	weak	strong*
H^3	H^- ion	10 gauss	strong	strong
	H_2 gas	1-2 gauss	not observed	fairly strong
He^3	He atom	0.4 gauss	weak	weak**

*Area under Li metal NMR band was comparable to that of the Li^+-ion band in this sample.

**Helium-3 was less readily detected than the other nucleons, but the intensity of the He^3 signal in this sample was about one-fourth of that found in the sample stored at -7°C.

3.5 Precipitation of Li Metal

The electronic-spin paramagnetic-resonance (ESR) observation of Li metal in small crystals containing 40 to 50 mole % LiT does not give absolute values for the quantity of metal formed because the efficiency of the detection of this signal is low and is not known accurately. Estimates of the total amount of Li metal formed were made by intercomparing the intensity of the ESR absorption with expansion and outgassing results according to the mechanisms presented in Chapter 4. The advantage of the ESR measurements is that they permit us to observe the nucleation and precipitation of a particular phase, bcc Li metal, in the crystalline samples.

Evidence for the nucleation of the metallic Li phase in the LiH+LiT crystals is gained from observation of the width of the ESR absorption band. The newly formed metallic particles induce broadening which results in the observed maximum in the graph of half-width versus age illustrated in Figure 9. For a sample containing 40 mole % LiT and stored at 23°C, this maximum occurs at about 50 days. This maximum is associated with a rapid rise in the intensity of the ESR absorption, which rises at a maximum rate that is approximately proportional to the 3/2 power of t.

Subsequent narrowing of the ESR absorption band indicates that the average particle size increases as the total quantity of precipitated Li metal also increases. The size of the Li particles is small -- probably about 10 Å diameter on the average. Microscopic examination of some fracture faces in grains of old material reveals some large sheets or droplets of metallic Li and lenticular voids (which probably contained gas) up to 40 μ in diameter. These large particles evidently represent a small fraction of the total quantity of precipitated Li metal, and they do not influence the shape of the ESR absorption band.

Line broadening indicates that still smaller particles of Li metal are

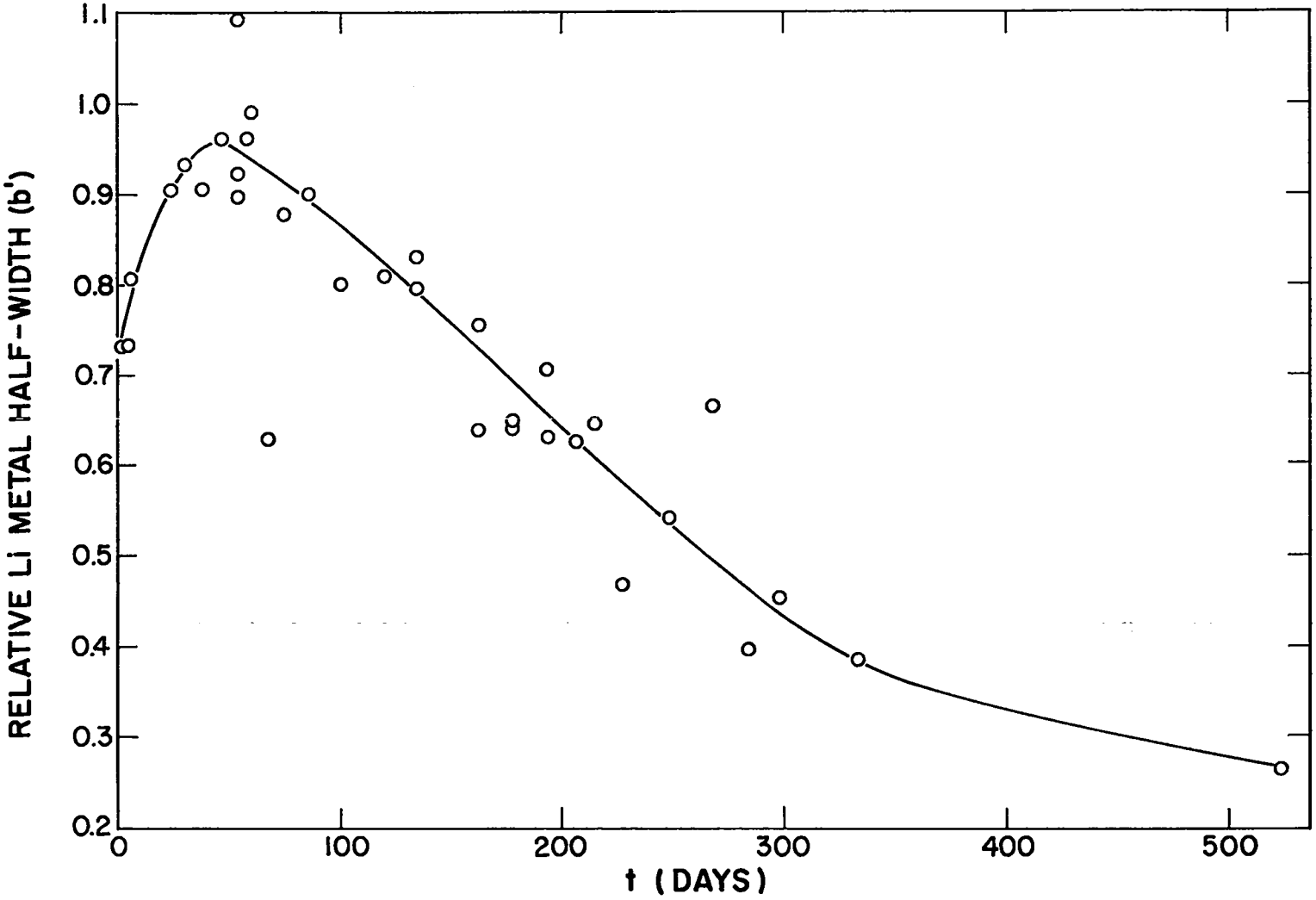

Fig. 9 Variation of the half-width of the ESR band during the formation of bcc Li metal in LiH sample containing 40 mole % LiT stored at 23°C. Values of b' are relative to the half-width of the DPPH standard employed which had an estimated half-width of 2.8 gauss.

formed in samples stored under liquid N_2 between measurements. Log-log plots of the growth of the ESR signal for metallic Li with age of two comparable samples* stored at different temperatures are given in Figure 10. The graph indicates that both nucleation and production of metallic Li are retarded by storage at -196°C. Additional experiments on samples stored and measured at -196°C indicate that bcc Li metal is not formed at this temperature.

A broader absorption band than that characteristic of the ESR absorption by bcc Li was observed in a sample kept at -196°C. This band bleaches out at room temperature with a half-life of about an hour and is replaced by the narrower band characteristic of bcc Li. This process is slowly reversed by long storage at -196°C. A rapid volume expansion also occurs at a comparable rate during flotation measurements made above room temperature on similar LiT-containing samples stored at -196°C. It is assumed that the broad ESR absorption is caused by a compressed fcc Li metal phase, which is observed at low temperature,[46] and that the rapid volume expansion corresponds to the room temperature transformation of the fcc Li metal to the bcc phase with the corresponding change in the ESR spectrum.

Similar Li metal transformations have been observed at higher temperatures in neutron-irradiated LiF. Using X-ray diffraction techniques, Lambert and Guinier[47] observed the fcc form of Li at room temperature in samples after neutron irradiation, and they were able to observe the transformation to the bcc form of Li after annealing the crystal at 200°C. Kim, Kaplan, and Bray[48] observed two Lorentzian-shaped ESR bands in LiF after intense neutron irradiation at 30°C; the narrow band, characteristic of bcc Li metal, was stable at the highest annealing temperature, but the broader band

*The comparatively high initial Li metal ESR intensities indicated in Figure 10 are caused by incomplete synthesis of the samples.

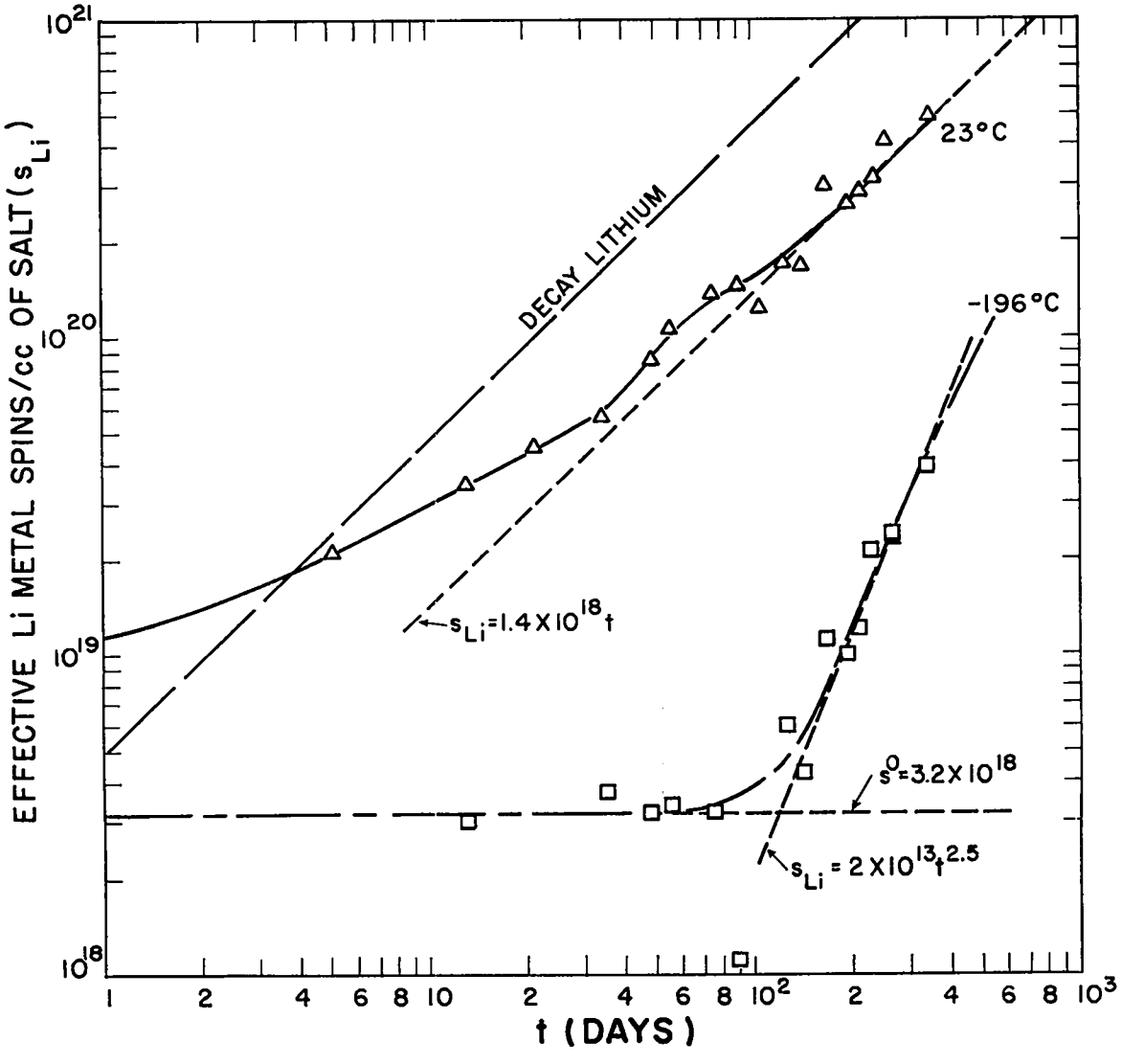

Fig. 10 Observation of the growth of the ESR absorption during the formation of bcc Li metal in samples of LiH containing 50 mole % LiT and stored at 23° and -196°C, respectively. Average slopes are indicated on the figure, and the initial concentration of uncombined Li metal was high in these samples.

had characteristics similar to those of the low temperature ESR band observed in LiH. The higher fcc to bcc Li metal transformation temperature observed in LiF is probably related to lower cation-vacancy mobility in LiF compared to LiH as illustrated by the electrical conductivity data.

3.6 Color Centers

Color-center formation in LiH and LiD was studied by the conventional methods of observing paramagnetic-resonance (ESR) and optical absorption bands formed by subjecting single crystals to energetic radiations. The principal effects are the formation of the F* and V* absorption bands, which are presumed to be the consequence of absorption by centers comparable to F and V centers in the alkali halides and lesser concentrations of other centers which effectively broaden the F and V_1 bands. Both bands are bleached by irradiating the crystal with F light, thus indicating mutual annihilation of the F and V_1 centers.

Optical absorption spectra of color centers produced in LiH crystals containing 5.56% LiT during storage at -193°C are illustrated in Figure 11. A small amount of Li colloid indicated by the initial spectrum was removed by subsequent exposure to β particles at -193°C. The F (or F*), V*, and β bands at 2.4, 3.5, and 4.7 ev, respectively, are the absorption bands attributed to the primary color centers produced in LiH crystals irradiated at low temperatures. The β band lies close to the first fundamental band in LiH, and it is difficult to observe unless thin samples are run against equally thin reference crystals. This was true for the sample whose spectra are reproduced in Figure 11. The β band is assumed to be caused by the change in the absorption characteristics of the ions surrounding the F center, in analogy with the explanation given for alkali halides. The formation of an M band after brief warming to room temperature is illustrated by the fourth spectrum

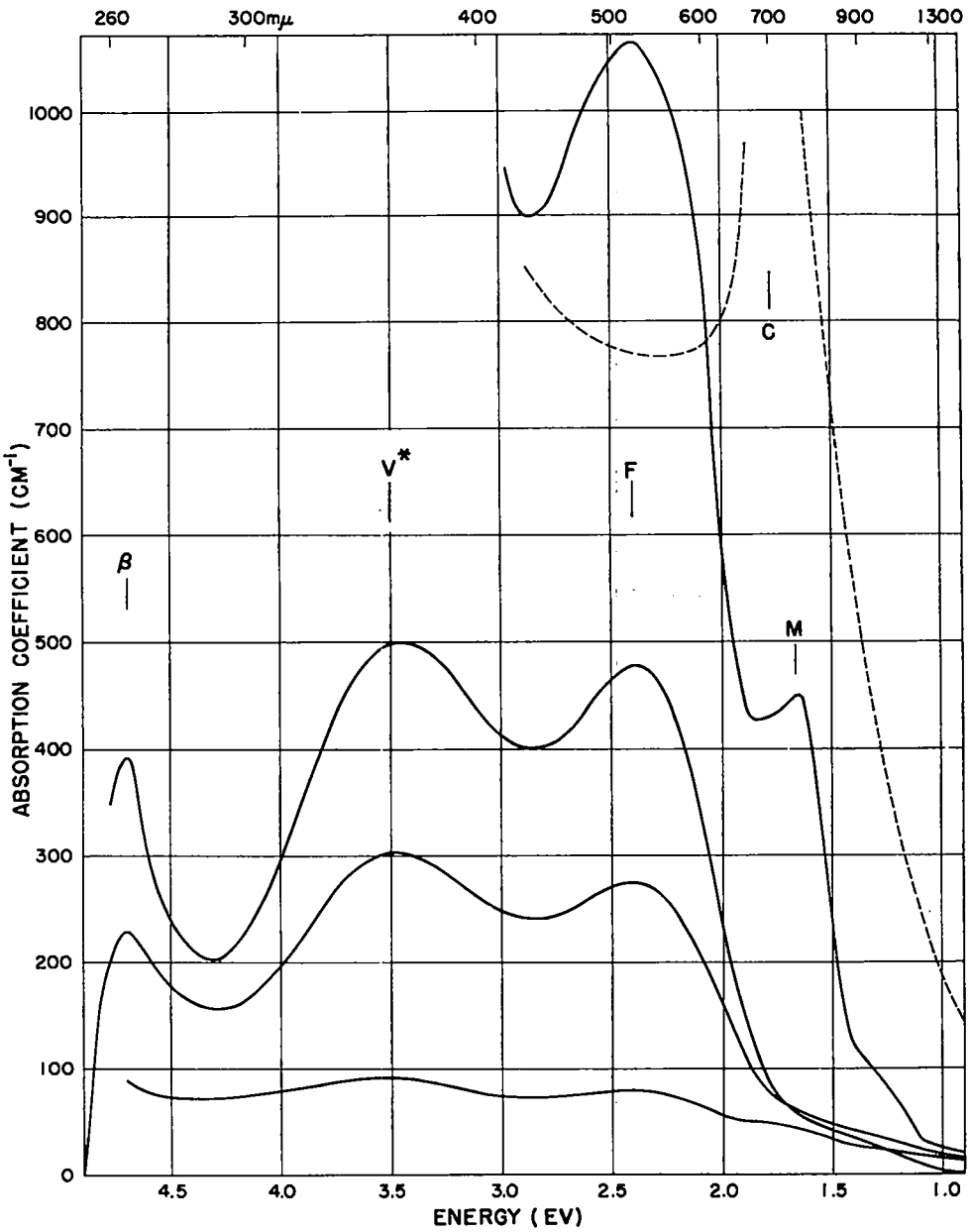

Fig. 11 Optical absorption by color centers produced at -193°C in a crystal of LiH containing 5.56% LiT. The growth of the principal F, V*, and β bands is indicated by the solid curves representing spectra taken after β exposure for 2.5 hr, 16.2 days, 28.1 days, and 62.4 days, respectively. Brief warming resulted in the formation of the M band illustrated by the last solid curve. Longer warming resulted in the formation of the Li colloid band illustrated by the dashed curve taken after exposure for 120 days.

in the figure. Subsequent spectra indicated that these M centers were destroyed during storage at -193°C, as had been observed previously; but a 20 hr warming to room temperature at a later time produced the intense Li colloid band illustrated by the dashed curve, which proved to be stable during continued storage at -193°C. Another sample which had been exposed to 6×10^{19} β/cc also showed the irreversible transformation of F centers to fcc Li colloid by corresponding changes in the ESR.

Several other centers which are evidently stabilized by impurity ions have been observed in less pure crystals, particularly after irradiation at room temperature. The S_1 band at 2.05 ev was observed in many samples after bleaching and thermal annealing for prolonged periods, and a similar band was also observed in some impure crystals at 2.3 ev and was called the S_2 band. Two bands seem to depend on the presence of Mg^{++} ion in doped crystals. The Mg band at 3.1 ev is probably caused by colloidal Mg. Another at 2.2 ev is called the Z band and has many properties which are similar to those of F bands, including the ability to trap another electron upon optical excitation at -196°C to undergo a Z to Z' transition. The formation of colloidal Li is normally accelerated by the presence of impurities in LiH, except that the Mg band is formed if large concentrations of MgH_2 are present.

In Figure 12, the absorption spectrum produced by low temperature X irradiation of LiD is compared to those produced by much shorter irradiation times on KCl and LiF. The width of the F* band in LiD is similar to that of the V* band, whereas the F bands in the halides are much narrower than the V bands. The energy of the crystalline zero-point vibrations also increases in the sequence KCl-LiF-LiD, which is the same as the sequence of the low temperature F-band half-widths. The V bands are all broad and have their maxima near 3.5 ev, but the V* band in LiD is relatively more

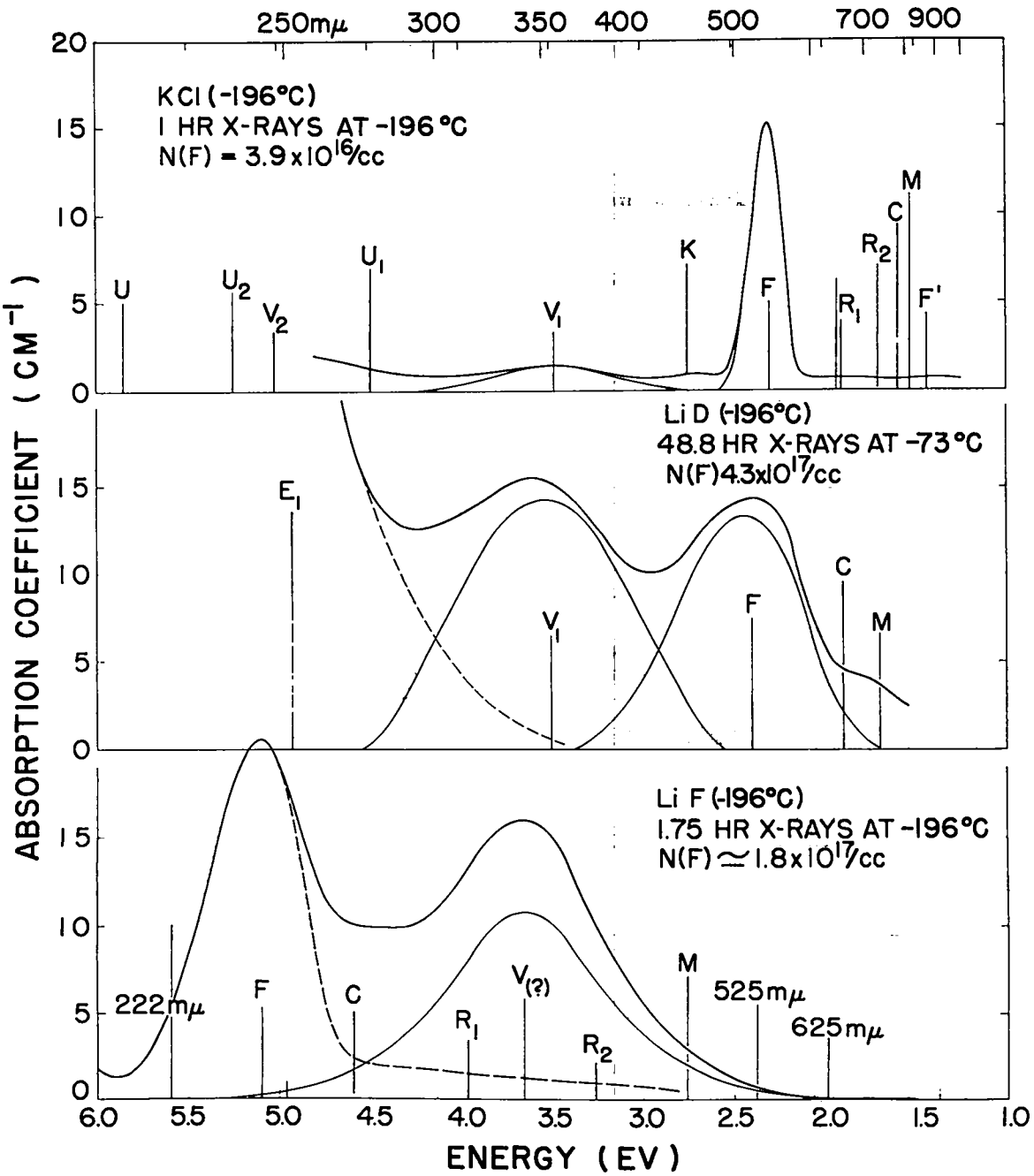

Fig. 12 Optical absorption of color centers produced in KCl, LiH, and LiF by low temperature X irradiation as indicated in the figure. The approximate shapes of the major F and V bands are illustrated in each case along with the positions of the other bands identified in the literature.

stable than the others. The first exciton absorption band at 4.9 ev in the Li hydrides is nearly at the position where one would expect to find the F band, on the simple assumption that the size of the anion vacancy determines the energy of the F-band absorption. This approximation is the basis of an empirical expression formulated by Ivey[49] to relate the alkali halide lattice parameter to the wavelengths of the F-band maxima observed at room temperature, which it does quite well. Levy[50] proposed another empirical expression for the energy of the F-band maxima in the alkali halides which takes the high frequency dielectric constant of the crystal into account. Levy's expression fits the alkali halides fairly well and gives about 2.4 ev for the expected energy of the F band in LiH.*

The F-center ESR has been examined in LiH irradiated at -193°C, and it has been found to have properties which are consistent with the accepted model of an F center as an electron trapped at an anion vacancy: (1) The ESR absorption band has a Gaussian band shape indicative of broadening by interactions between the F-center electrons and the nuclei of the neighboring ions. (2) The mean square width of the band was studied in crystals of different isotopic composition (Li^7H^1, Li^7D^2, Li^6H^1, Li^6D^2) and found to vary with the nuclear characteristics of the isotopes in a consistent manner. (3) The relaxation time of the F center is long, and the ESR signal is saturated by increasing the rf power level. These observations are consistent with those reported for F-center ESR's in alkali halide crystals.[52] LiH of normal isotopic composition exhibits an F-center ESR which has a mean square width of about 61 gauss and is centered at g = 2.004 ± 0.002 as illustrated in Figure 13. The Li colloid ESR is also shown in Figure 13 for

*The properties of color centers in LiH are described in a paper by Pretzel and Rushing,[51] and a description of color-center formation in crystals containing LiT is to be published in another paper.

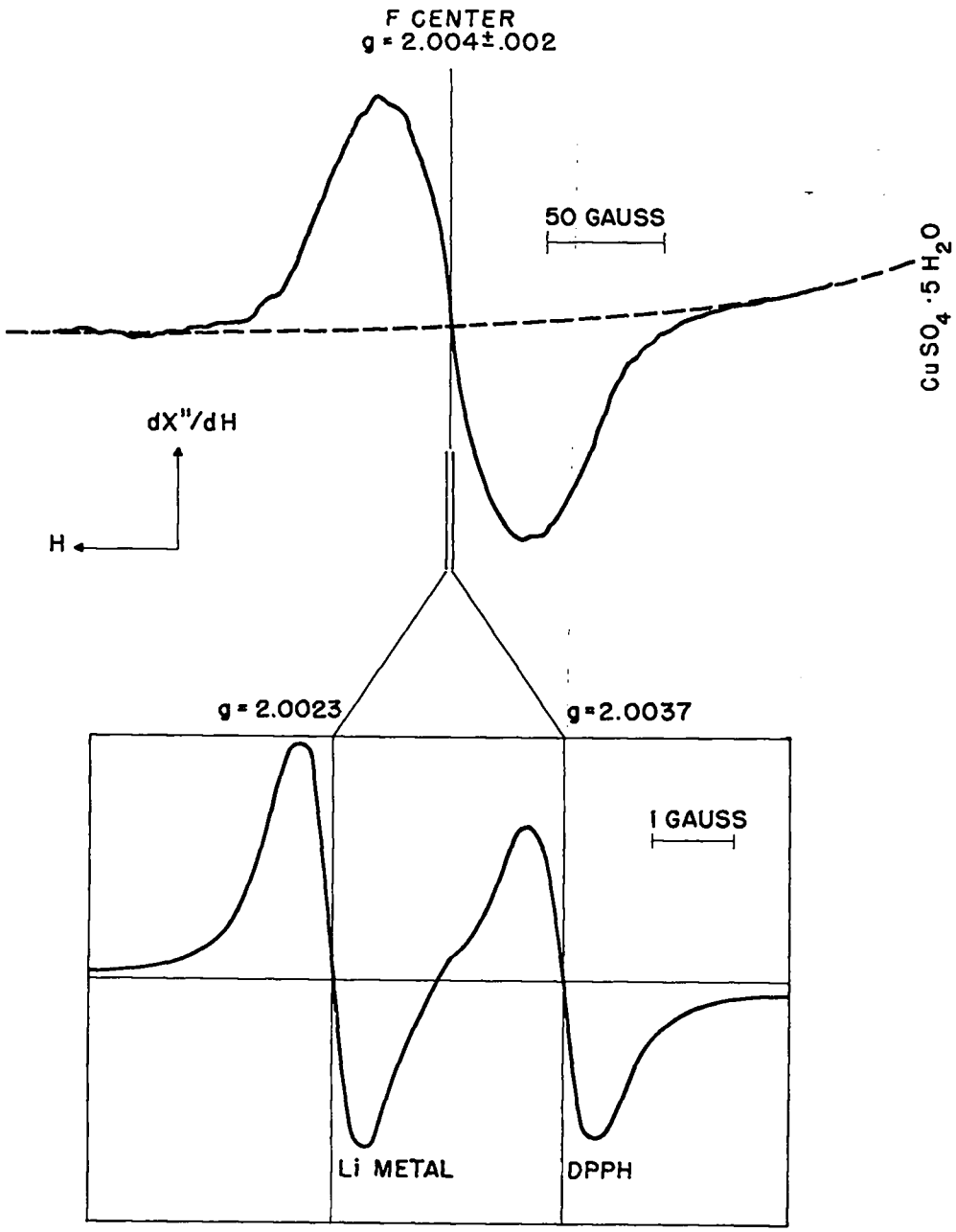

Fig. 13 F-center ESR absorption produced in a LiH crystal after exposure to approximately 10^{14} n/cc at -195°C and measured against a $CuSO_4 \cdot 5H_2O$ reference crystal. The insert shows the ESR absorptions obtained for bcc Li metal and the DPPH standard on an expanded H scale by using LiH crystals containing LiT and stored at 23°C.

comparison. The experimental g value for LiF[53] is also larger than the free-electron value, and similar asymmetric nuclear interactions are probably responsible for the shift in both crystals.*

The F band was identified by its association with the F-center ESR as demonstrated by several bleaching experiments since attempts to produce F centers by quenching H-deficient LiH from a high temperature only led to the production of Li colloid. The connection between the 2.4 ev optical absorption and the F-center ESR was established by making parallel measurements on: (1) "pure" LiH samples which were differentially bleached to form the M band, and (2) Mg-doped LiH crystals which contained a diamagnetic electron-trapping impurity and still showed a strong 3.5 ev band after the F centers were destroyed. The identity of the Li colloid (C) band at 1.9 ev was also established by the association between this band and the Li colloid ESR which was also identified in a crystal irradiated with Co^{60} γ rays at room temperature.

Since we have observed no ESR that could be attributed to the V centers in any of our crystals after irradiation at -193°C and since the H_2 molecule has a high binding energy, it is concluded that the 3.5 ev optical absorption band is caused by centers involving trapped H_2 molecules analogous to the V_1-center model proposed by Känzig and Woodruff.[55] According to this model the V_1 center in LiH would consist of a H_2 molecule at a H^--ion site, but such a center should not bleach readily in LiH because of the apparent instability of single holes (like traps involving X_2^--molecule ions found in the alkali halides which might serve as intermediates in a low temperature bleaching process) and the instability of the extra H^- ion produced by recombination of the V_1 center with electrons released from the F centers. The

*The F-center ESR results are reported in greater detail in a paper by Lewis and Pretzel.[54]

expected stability of colored LiH toward complete bleaching with F (or V_1) light at -193°C does exist, and the temperature of the sample must generally be raised to about 30°C to complete the optical bleaching process. It is probable that mobile lattice defects assist in the bleaching process at the higher temperature. In the LiD crystal X-rayed at -73°C (Figure 12), it was found that only a small fraction (9%) of the V_1 and F bands could be rapidly bleached with F light at -193°C, but the remainder bleached thermally at 37°C. A LiH V center consisting of a H_2 molecule in a pair of adjacent H^--ion sites (a self-trapped double hole in analogy to the self-trapped hole in the alkali halides) could readily combine with two electrons to re-form two H^- ions in normal lattice positions at low temperature. Such a center would be unstable because charge repulsion between the V_1 center and the adjacent anion vacancy would promote dissociation of the complex center at higher irradiation temperatures. This expectation is consistent with the observation that a larger fraction of the color induced by low temperature irradiation can be bleached optically at -193°C. The self-trapped double hole may be expected to absorb light in the region of the V_1 band in analogy with Delbecq, Smaller, and Yuster's[56] findings for the Cl_2^- self-trapped hole in KCl.

Observations on the LiT-containing crystals show that centers probably involving the decay product He^3 atoms also absorb under the complex V band. Up to the limits of the optical measurements, the absorption maximum of the V* band remained above that of the F band and its growth paralleled that of the F band illustrated in Figure 14. If the V* band were the result of absorption only by species containing H_2, the V*-band growth curve should rise to a maximum and drop like the curve in the lower left-hand corner of Figure 14 because of recombination of H_2 with electrons released by decay.

The result of concurrent measurements of optical absorption, ESR, and flotation temperature on samples cleaved from the LiH crystal containing

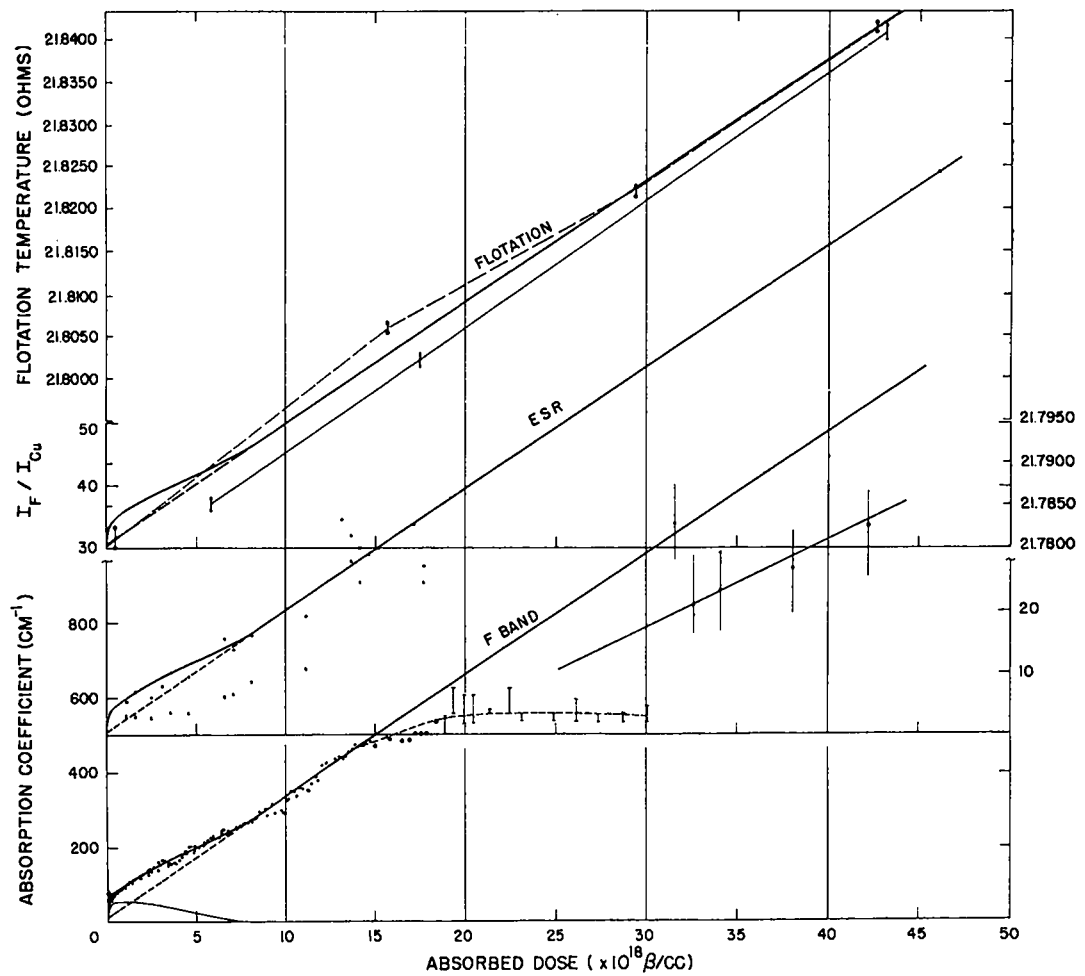

Fig. 14 Optical, ESR, and flotation temperature measurements on samples cleaved from a single LiH crystal containing 5.56% LiT and stored at -196°C. The heavy solid curve in the lower third of the figure indicates the growth of the F band. Scales for plotting I_F/I_{Cu} (the ESR intensity ratio) and flotation temperature (measured with a Pt-resistance thermometer) were chosen for comparison to the F-band growth curve.

5.56% LiT and stored at -196°C are given in Figure 14. Data from samples of the LiH crystal containing 1.35% LiT were also used to draw the initial portion of the F-center growth curve. F-center aggregation occurred at -196°C after 1×10^{18} β/cc in the less concentrated samples; this was indicated by the saturation and subsequent reduction of the F-center ESR with simultaneous growth of the aggregate ESR.* The linear portion of the F-band growth curve from approximately 8×10^{18} to 3×10^{19} β/cc was used to estimate the F-band oscillator strength to be $f = 0.19 \pm 0.03$. When this quantity and the measured refractive index and F-band half-width are inserted into the formula given by Smakula, the F-center concentration can be related to the maximum absorption in the F band by the expression $N_F = 3.0 \times 10^{16}$ α. A lower value for the oscillator strength was obtained by intercomparing the F band and the ESR spin density after 7×10^{18} β/cc, but, because of the low precision of this intercomparison, this result can be treated as a rough confirmation of the low oscillator strength derived from the slope. The points falling below the heavy F-band growth curve were disregarded because of the error introduced by a light leak around the sample. This was corrected before the last few points were taken, but probable errors related to the large spectrophotometer slit-widths which were required for these last measurements of optical absorption still indicate that the solid curve is probably the best representation of the true optical absorption values.

The results of the concurrent ESR and flotation density measurements in the two upper portions of Figure 14 are plotted to arbitrary scales chosen

---

*F-center aggregation at comparatively low concentrations has also been observed in other samples. This is evidently a structure-sensitive property of most of our single-crystal samples. Aggregation and Li-colloid formation appears to proceed even more readily in less-pure polycrystalline samples.

to demonstrate that the F-band growth curve can be drawn through these data within the relatively large errors of the determinations. The large ratios of F center to standard intensity observed in the ESR measurement are one reason for the scatter of the points in the central portion of the figure. The crosses indicate measurements taken at a higher microwave power level with consequent reduction of the I_F/I_{Cu} ratios because of saturation of the F-center ESR. The linear rise of the flotation temperature continued to much larger β doses than shown in Figure 14. ESR measurements on portions of the Li(H, T) crystal kept at -196°C for a longer period showed that the F-center concentration grew to approximately 9×10^{19}/cc.

Low temperature X-ray diffractometer measurements on powdered samples from the LiH crystal containing 5.56% LiT showed a 0.0020 ± 0.0007 Å average increase in lattice parameter after exposure to 6.7×10^{19} β/cc during storage at -196° and -27°C. The corresponding lattice expansion is $0.14_7 \pm 0.06\%$. Flotation density measurements on samples from the same single crystal gave a bulk expansion of $0.10_1 \pm 0.01\%$ for the same exposure. These results agree within the limits of error of the determinations, and they are consistent with the interpretation that interstitial He^3 atoms are formed by T decay in LiH at temperatures up to -27°C (Appendix A). According to the more accurate flotation measurements, the expansion associated with an interstitial He atom is about 12 $Å^3$.

Negligible lattice expansion was found by A. L. Giorgi in LiH crystals exposed to much larger doses at room temperature. This result is interpreted as indicating that interstitials are annihilated by mobile vacancies at higher temperatures, and this effect is taken into account in the interpretation of most of the expansion measurements which were made at room temperature or above. It is also possible that interstitials are destroyed in samples whose defect structure permits the aggregation of F centers at low temperatures.

3.7 Ionic Migration

The electrical conductivity of LiH and LiD single crystals was measured from room temperature to 650°C for both "pure" crystals and several crystals doped by the addition of Mg^{++}. A portion of the results is plotted on the graph in Figure 15 along with the results for oxide-containing LiH published by K. Moers.[57] The results obtained for the Li halides by Y. Haven[37] are also plotted on the same figure for comparison. It is evident from the figure that the conductivity of LiH is intermediate between those of LiF and LiCl. In this respect, LiH falls into a logical sequence with the Li halides -- especially when anion size, mass, polarizability, and lattice parameter are taken into consideration. Since the addition of $O^{=}$ impurity extends the region of intrinsic conductivity to lower temperatures, whereas the addition of Mg^{++} raises the total conductivity and extends the extrinsic conduction leg of the curve, the primary current carriers in LiH are Li^{+} ions moving by a cation-vacancy mechanism.

The activation energy for migration of a cation vacancy can be obtained from the extrinsic low temperature portion of the conductivity curves, particularly from those obtained with Mg^{++}-doped samples. If the activation energy is represented by the symbol U, and the energy required to form a Schottky defect pair by the symbol W, the following equation represents the electrical conductivity of LiH and LiD in the temperature range from 200° to 688°C:

$$\sigma = Ae^{-U/kT} + Be^{-(\frac{1}{2}W+U)/kT} \qquad (ohm^{-1}/cm)$$

For the energy terms the conductivity data give: U = 0.53 ± 0.05 ev, $(\frac{1}{2}W + U)$ = 1.72 ± 0.06 ev, and therefore W = 2.4 ± 0.2 ev. The pre-exponential factors are more complicated in interpretation, and the values

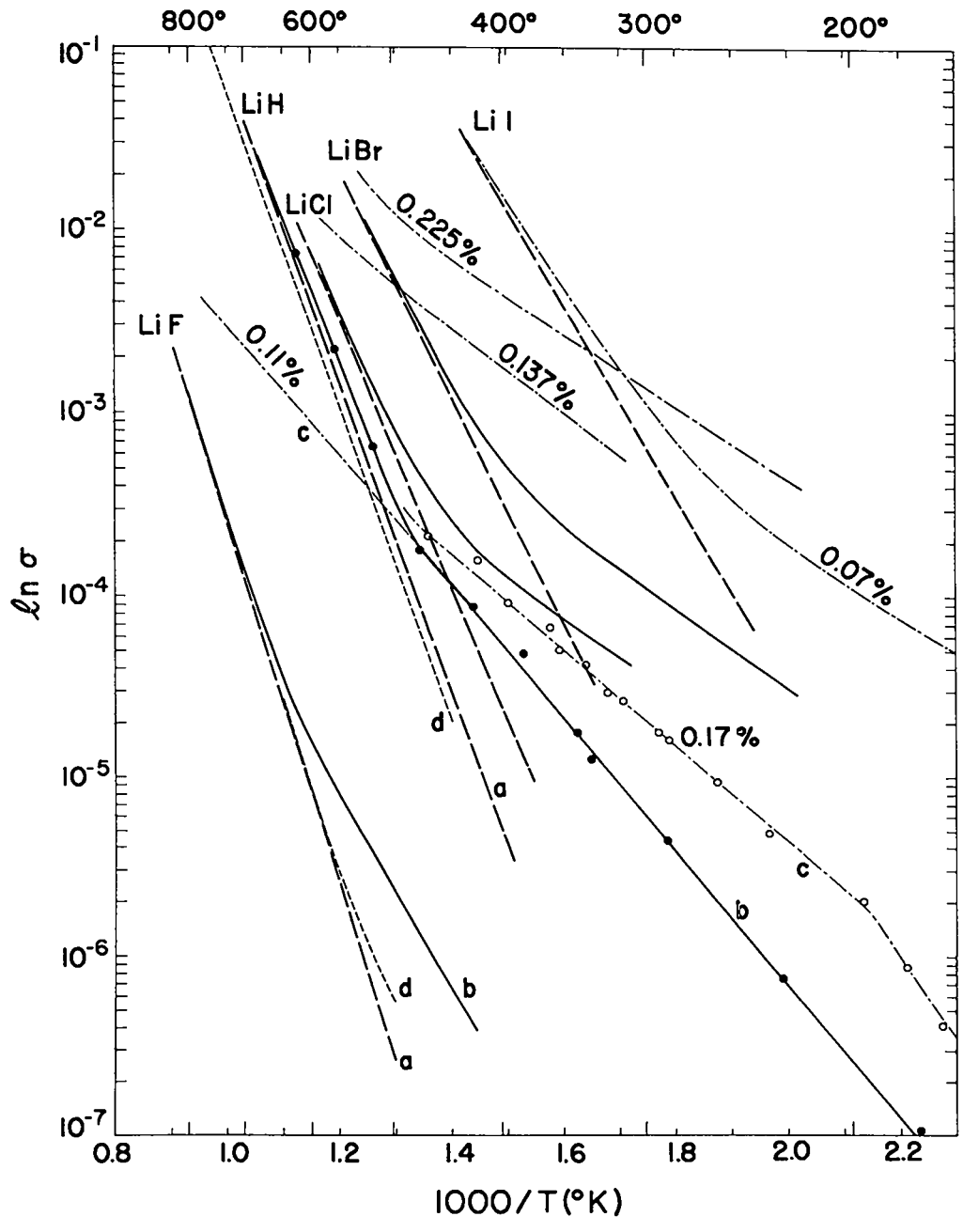

Fig. 15 Electrical conductivity of "pure" and Mg-doped LiH as a function of temperature compared to the Li halide measurements by Haven.[37] (a) Intrinsic conductivity of an ideal crystal, (b) conductivity of a "pure" crystal, (c) conductivity of a Mg-doped crystal with indicated impurity content, (d) conductivity of a crystal containing oxide from the measurements of Moers.[57]

for them are subject to relatively large errors.* For the intrinsic part of the curve, $B = 4 \times 10^7$ ohm^{-1}/cm for LiH and $B = 1 \times 10^7$ ohm^{-1}/cm for LiD. Since this term is dependent on the vibrational frequency of the lattice around the vacancy, it is expected that B for LiH should be larger than B for LiD and that both should have values which are larger than those obtained for the pre-exponential factor for the Li halides, as observed. The pre-exponential factor A should also be dependent on the concentration of impurities contributing vacancies to the conduction processes in the extrinsic leg of the conductivity curve. Values of A from 0.2 to 1 ohm^{-1}/cm are obtained; these are comparable to values often found for the alkali halides in this region. It is further noted that a region of steeper slope occurs in the conductivity curve for Mg-doped crystals in the region from 30° to 200°C. This is attributed to either the reversible precipitation of MgH_2 or to the association of divalent Mg^{++} ions with cation vacancies in the lattice to form divalent ion-vacancy complexes with an energy of formation E_c. For this region the slope is represented by $(E_c + U) = 0.75 \pm 0.05$ ev, from which $E_c = 0.2_2 \pm 0.1$ ev.

These results are valuable for consideration of diffusion or any other process involving transport of charge through the crystal lattice. In common with the alkali halides, we expect that the cation is the predominant diffusing species (diffusing by a cation-vacancy diffusion mechanism) and that the diffusion equations will include the same exponential factors as those obtained above. These measurements do not eliminate the possibility that uncharged defect pairs may have relatively high mobility and thus be responsible for the bulk of the diffusion in the crystals at low temperatures; but recent experiments on Cl^- diffusion in NaCl crystals[59] indicate that the activation

*The pre-exponential factors would be written more accurately as $A = A'/T$ and $B = B'/T$,[58] but the simpler description is adequate here.

energy for the migration of vacancy pairs is somewhat larger than for the migration of free anion vacancies.

An alternative mechanism has been proposed to account for the observation of enhanced anion diffusion in KCl and NaCl crystals which have been stressed by crushing.[60] Diffusion presumably occurs through dislocation networks and subgrain boundaries which offer a diffusion path requiring less activation energy than the bulk of the crystal. The structure-sensitive nature of anion diffusion compared to cation diffusion also examined in single crystals and pressed pellets[61] can be explained because the cation diffusion rate through the bulk crystal is usually much greater, and multivalent cation impurities further enhance the rate of cation diffusion; therefore, the total cation diffusion through defect networks must be comparatively larger to be detected. A reduction in the activation energy for cation migration at comparatively low temperatures has been found in electrical conductivity studies on solution-grown single crystals of alkali halides, which did not possess the usual knee in the conductivity curves until they were heated to approximately 500°C. This change has been related to observed changes in the dislocation network after heating,[62] and it may also indicate that cation vacancies have a higher mobility in the defect network.

A modification of the technique of Morrison and his coworkers[60] has been employed to study T diffusion from a crystal. A 1 cm cube cleaved from a LiH single crystal containing 1.35% LiT was used as the sample, and the T-evolution rate was determined by an ionization chamber in the thermally pumped H_2 gas cycle. Consistent results have been obtained only for the 150° to 300°C temperature range from a single experiment. The activation energy obtained for H^- diffusion in LiH in this low temperature range is 0.76 ev. This value is in agreement with activation energies for electrical conduction below the knee for some "pure" LiH crystals. It may

be that both results are related to ionic transport through dislocation networks by a mechanism similar to that proposed for Cl^- diffusion in crushed NaCl.

CHAPTER 4

INTERPRETATION

4.1 Comparison to Alkali Halides

From the results of the experiments discussed in the previous sections, it is concluded that LiH can be treated as a member of the alkali halides with respect to radiation damage and color-center formation. A model for some of the relatively simple point defects is illustrated in Figure 16. Most of the color centers represented in two dimensions in the figure are the defects proposed by Seitz[63] as the centers responsible for the various absorption bands observed in the alkali halides. Larger scale defects involving dislocations or large colloidal aggregates are too complicated to be shown in the figure.

Since Seitz's reviews, many experiments have been performed using advanced techniques to verify or modify the color-center model. The model for the F center, which was first proposed by de Boer,[64] has been given strong support by recent investigations using magnetic resonance[65] and polarized light.[66, 67] Further work with polarized light has not shown conclusively whether the M band is caused by absorption by the M center[68] or the $R_2(F_2)$ center of Figure 16. Similar uncertainty exists concerning the R bands. The assignment of the Z_1 and Z_2 bands to the centers illustrated in the figure is probably incorrect from considerations of symmetry.[69]

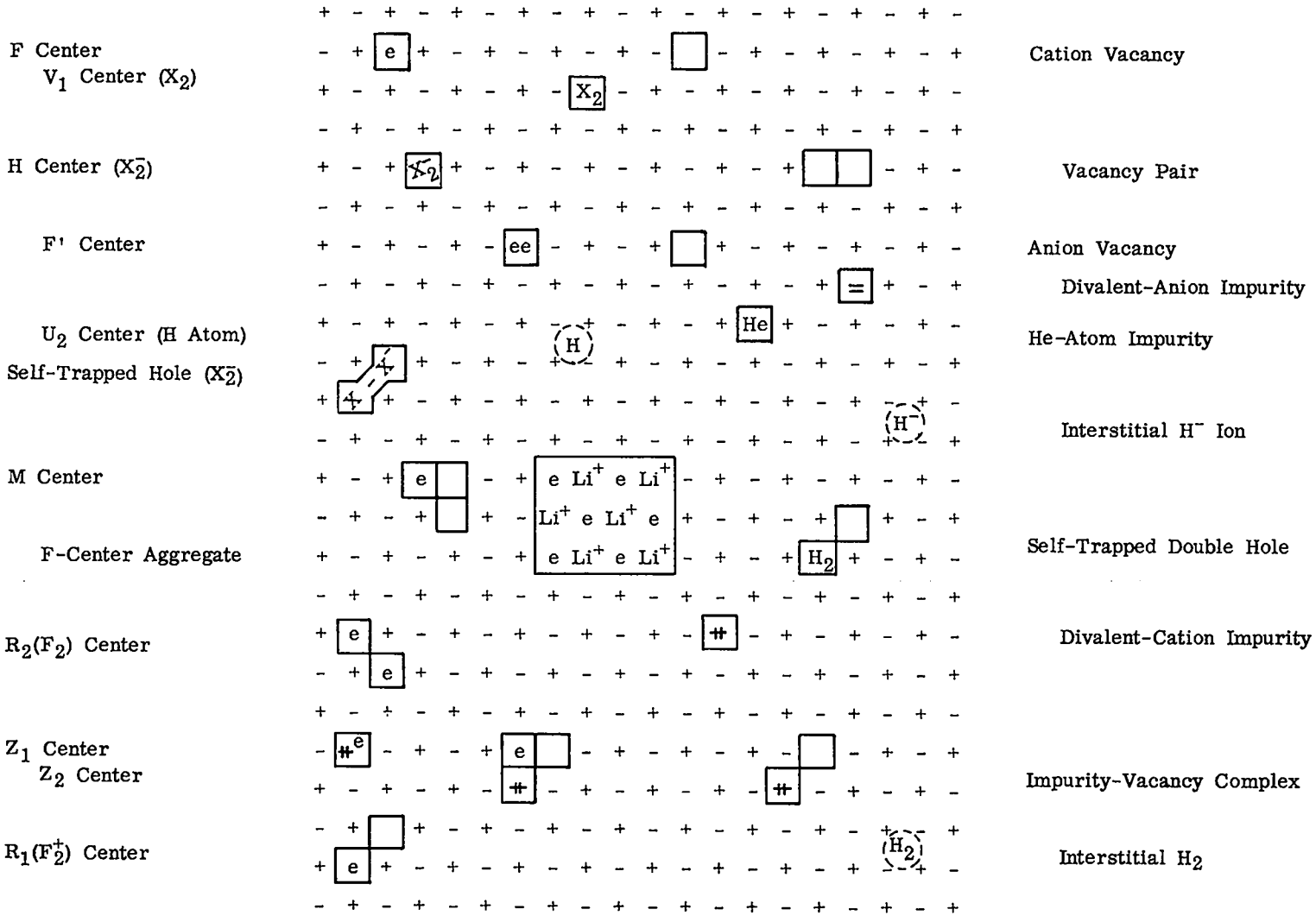

Fig. 16 Model for color centers and other lattice defects in the alkali halides and LiH.

Nevertheless, the divalent alkaline-earth impurity ions must be associated with the Z centers in some way. The results of a similar investigation of the V centers have shown that the hole-trap (electron deficient) centers are comparable in complexity to the electron-excess centers, but they are distinguished by a strong tendency to form molecular species. The V_1 center has not been observed by magnetic resonance, and Känzig and Woodruff[55] gave evidence to support their proposal that the V_1 center consists of a halogen molecule trapped at a halide-ion site. The X_2^- molecule ion has been observed as a self-trapped hole,[70] and as a self-trapped hole associated with a cation vacancy which corresponds to the model that Seitz originally proposed for the V_1 center.[71] The X_2^- molecule ion has also been detected in a single X^- lattice site, where it may be described as a trapped interstitial X atom or as a hole trapped by a crowdion, and in this configuration it is responsible for optical absorption in the H band.[72] V-type centers also include defects with paired electrons, such as X_2 or interstitial X^- which may give rise to optical absorption only, as well as more complicated species which have been analyzed by their magnetic-resonance spectrum.[73]

A comparable model for the important color centers in LiH has been described in Section 3.6. The F center is the same as in the alkali halides although the interactions of the F-center electron with the surrounding ions will have to be investigated more fully to interpret the large decrease in the F-band energy from the expected (Ivey) value.* The behavior of the M band seems to be consistent with observations in the alkali halides, except that both the M band and the Li-colloid band are shifted to lower energy in LiH compared to LiF, with the result that the familiar sequence of

*See, for example, the article on electron-excess color centers in alkali halides by Gourary and Adrian.[74]

electron-excess color centers given for KCl is maintained in LiH. Diamagnetic V centers which include the H_2 molecule are the prominent hole centers in LiH. These include the H_2 molecule trapped at a H^--ion site, which is analogous to Känzig and Woodruff's V_1 center, and the self-trapped double hole or H_2 molecule in a pair of adjacent H^--ion vacancies. No evidence for single hole centers, stable at -193°C in LiH, has yet been found.

Mechanical effects are intimately related to the formation of color centers. All of the color centers require the displacement of at least their neighboring ions to some extent, and their presence will therefore induce some strain into the crystal lattice. Interstitial atoms or ions repel neighboring ions most strongly and will thus force an increase in the volume of the unit cell of the crystal lattice that contains them. The self-trapped hole (X_2^- ion occupying two adjacent anion sites) is like the divalent impurity ion in that they both polarize the surrounding lattice in such a way as to effect a small volume change, which is positive for the case of the hole. The volume of the vacancy traps represented by the F, V_1, or M centers may also be somewhat larger or smaller than the volume of the lattice ions that they replace, because of some distortion of the surrounding lattice. If these centers are produced in a crystal, the bulk volume of the crystal will increase without a correspondingly large increase in the unit cell volume as determined by X-ray diffraction. If any pair of simple electron and hole traps (such as F and V_1 or H centers) are considered as the principal products of the irradiation of an alkali halide crystal, it can be seen that lattice strains and a net increase in the volume of the crystal must follow.

Any consideration of a mechanism for the formation of color centers in the alkali halides must include consideration of the properties of the crystal lattice with respect to the formation and diffusion of vacancies and other auxiliary defects, as well as the initial interactions of the ions of the crystal

with the energetic radiation employed. The primary interactions of the various radiations with solids have been described in the Introduction.[2-4] Fast neutrons may produce their effects by first displacing atoms or ions of the lattice, but X or γ rays start by ionizing the material. Ultraviolet light, in the region of the first exciton band of an alkali halide crystal, does not generally seem to have enough energy to ionize the halide simultaneously and create the necessary trapping defects, although under some circumstances it is capable of exciting the halide ions sufficiently to fill traps already present in the crystal. Ionization, primary or secondary, is the process responsible for most of the damage produced in the alkali halides studied under the irradiation conditions and intensities normally employed. Displacement collisions have also been observed, and they become important in crystals after prolonged exposure to neutrons or heavy charged particles.

Since F centers are formed as a result of the irradiation of the alkali halides, even at very low temperatures, the formation of the requisite number of negative ion vacancies at the rates observed is a very real problem indeed. From the results of measurements of electrical conductivity and self-diffusion in the salts, it is known that the mobilities of simple defects are far too low to account for the observed expansion of the crystals by the simple diffusion of vacancies into the samples from the free surfaces. To circumvent this difficulty, Seitz[2, 63] proposed that vacancies might be introduced into the crystal at the required high rate by the motion of dislocations through the crystal. It is assumed that these dislocations are propelled through the crystal by radiation-induced stresses and that they are capable of releasing vacancies from jogs in them as they move. Lin[75] has shown that the expansion of NaCl and KCl follows shortly after the beginning of the exposure to X rays, and the expansion parallels the increasing concentration of F centers. It has been further shown that the initial rate of coloration of a

sample can be enhanced by the introduction of free vacancies at low temperatures through the device of first using light absorbed in the F band to bleach out F centers formed in a preliminary X irradiation and then reirradiating the sample with X rays or with ultraviolet light.[76] As the irradiation of a crystal is continued at constant flux of X or γ rays, the free vacancies and clusters which may act as ready sources of free vacancies are used up. The propagation of dislocations through the strained lattice is also impeded until the "easy" or "rapid" type of coloration first observed is replaced by a "hard" or "slow" type.[77,78] The corresponding increases in the energy required to produce an F center are from 50 to 100 ev/center to about 1000 ev/center.[2] Physical hardening of the crystal seems to accompany the "slow" type of coloring, which may attain concentrations of F centers of the order of 10^{19}/cc or more, whereas the "rapid" coloration saturates at concentrations of about 10^{17} F centers/cc.[78] The maximum concentration can easily occur in the case of neutron-irradiated LiF.[79] Very high saturation concentration can also be reached with γ-irradiated NaCl or KCl by the device of first introducing strains into the crystals, either by quenching them from temperatures close to the melting point or by plastically deforming them prior to coloring.[78] Several measurements of bulk density or volume changes[75] have been made which support Seitz's assumption that one vacancy pair should be formed for each F center. It has also been shown that the lattice expansion of KCl X-rayed at room temperature is small compared to the observed volume increases.[80] Photoelastic measurements of the expansion of deuteron-bombarded LiF at room temperature also support the contention that a vacancy pair is created per F center produced.[81]

The expansion of LiF, X-irradiated at -179°C, has been attributed to the simultaneous formation of F centers and H centers[82] according to a mechanism for low temperature coloration proposed by Varley.[83] The

formation of H centers is roughly equivalent to the formation of the interstitial atoms postulated in Varley's mechanism. According to Varley, the color centers are formed as follows: (1) Impinging radiation doubly ionizes some of the anions to form unstable positive ions at anion sites. (2) The unstable positive ion is quickly repelled by the charges of the neighboring cations into an interstitial position in the lattice, where it regains one electron to become a neutral halogen atom. (3) The remaining anion vacancy traps the other electron to become an F center. Compared to the mechanism proposed by Seitz,[63] Varley's mechanism depends on the less probable event of double ionization as the first step, but it is free from dependence on some mechanism for the transportation of vacancies to the damage sites. For this reason Varley's mechanism could be the predominant one for low temperature coloration of the alkali halides, and Seitz's mechanism may be followed at room temperature and above. A modification of Varley's mechanism has been proposed by Klick[84] to circumvent the problem of the short lifetime of a doubly ionized halide ion. The mechanism involves the rapid production of an intermediate complex with a halogen molecule in a pair of anion vacancies, from which an anion vacancy dissociates because of charge repulsion, and both defects then trap electrons to produce a pair of F and H centers. We have obtained recent evidence which supports this mechanism for the low temperature coloration of NaCl and which also indicates that the Cl_2 molecule may trap two electrons to produce a Frenkel defect.

We have observed the lattice expansion of NaCl powder which was exposed to β radiation at -196° and -27°C in a mixture with 80 volume % LiH powder containing 5.56% LiT. The NaCl increased 0.0061 ± 0.0009 Å in lattice parameter for the average of three samples measured at -196°C. The corresponding expansion is 0.33 ± 0.05%. This result is too large to explain by the formation of F and H centers alone, according to Klick's mechanism,

because the energy requirement observed for F-center formation at low temperatures is 1000 to 2000 ev/F center, and the NaCl powder is calculated to have received an average dose of 4×10^{17} β/cc (or 0.6% of the LiH dose) for 0.01 cm particles homogeneously irradiated on the surface of the particles but inhomogeneously colored. The large expansion of the NaCl can be explained if it is assumed that interstitial Cl^- ions are produced at a net yield corresponding to the low energy requirement of about 50 ev/F center found in coloration experiments at room temperature and if the volume expansion per interstitial Cl^- ion is about 60 $\mathring{A}^3$ (Appendix A). Because of the relatively constant growth rates of F centers in alkali halides irradiated at low temperatures,[63,82] it is probable that the interstitial Cl^- ions are formed primarily by a competing process instead of through the recombination of F and H (or V) centers. These observations may be explained if the cross section for trapping both electrons by the Cl_2 molecule, just after the intermediate complex dissociates, is much larger than that for trapping one of the electrons at the anion vacancy, even though the rough calculations of Appendix A indicate that the anion vacancy is the deeper trap. The high total yield of F centers and interstitial Cl^- ions indicates that the initial step involving the loss of two electrons from one Cl^- ion, which was postulated by Varley and accepted by Klick, may be a serious limitation for the mechanism. It is likely that the mechanism given by Klick could operate without double ionization as the first step. A singly ionized Cl^- ion (a Cl atom) may have sufficient energy such that an intermediate Cl_2^- molecule ion (self-trapped hole) would be sufficiently excited to lose an electron to produce the Cl_2-vacancy intermediate complex proposed by Klick, and this complex and the surrounding lattice may still have enough energy to promote the dissociation of the anion vacancy from the complex before retrapping of the electrons occurs at the product defects.

The mechanism outlined above is consistent with observations of α-center production in alkali halide crystal irradiated at low temperatures.[63] A new interpretation of these observations is possible because the anion vacancies responsible for the α band are complementary defects to interstitial anions in the Frenkel defects postulated above. Rüchardt's[85] observations on the yield of α centers in KBr irradiated at temperatures down to -269°C and of their subsequent annealing behavior can be explained in this way. The increase in the yield of Frenkel defects at very low temperatures compared to the yield of F and H centers may occur because the defects tend to be produced close together under these conditions with a large increase in the probability that the F-center electron may recombine with the H center by an electron-tunneling process. It is interesting to note that Rüchardt's annealing curves for α centers in KBr resemble those obtained for Stage I annealing of Frenkel defects in Cu.[86]

4.2 Comparison to LiF

The comparison between radiation effects in LiH and the alkali halides can be carried somewhat further for LiF. This is true because radiation-damage studies on LiF have been extended to much higher effective doses than have been used on the other alkali halides by using pile neutrons to induce the energetic $Li^6(n, \alpha)H^3$ reaction. The cross section for the Li^6 fission reaction is large, and the 2.1 Mev α particles and 2.7 Mev tritons produced interact strongly with the ions of the crystal lattice to produce radiation damage by ionization and displacement collisions.[2]

Lithium fluoride is also particularly suitable for comparison to the Li hydrides because its crystallographic and physical properties are more similar to those of the hydrides than are those of the more "typical" alkali halides. (Most of the experimental work on color centers has been done on NaCl, KCl,

and KBr, and they were treated as "typical" by Seitz.[63]) Pauling[87] has considered the case of the Li halides and has discussed the effect of anion-anion repulsion on the properties of the salts. This effect is a function of the cation-anion radius ratio. In a more recent tabulation by Zachariasen, presented in Reference 88, the radius of the Li^+ ion was given as 0.68 Å and that of the F^- ion as 1.33 Å, from which the radius of the H^- ion in LiH is calculated to be 1.36 Å.

An account of the radiation effects on LiF, including the formation of color centers, displaced atoms, defect aggregates, and separate phases and including the effect of the presence of these defects on the volume, lattice parameter, and mechanical properties of the crystal, can be obtained from References 2, 41, 42, 79, 81, 82, and 89-93. A summary of much of the work on neutron-irradiated LiF is contained in a paper by Gilman and Johnston.[93] A brief summary of the results of the studies of radiation effects on LiF follows:

(1) At relatively low doses, F and V_1 centers may be formed in concentrations up to 10^{17} or 10^{18}/cc at room temperature; at low temperatures most of the data seem to indicate that F and H centers are formed. At higher doses at room temperature, interstitial defects predominate. Color-center concentrations quickly rise to 10^{18}/cc for LiF exposed to about 10^{13} n/cm^2; and the rate of formation of F centers, plus other magnetic centers, then decreases, until their concentration reaches about 10^{20}/cc with saturation after exposure to 10^{17} n/cm^2 according to the results of Bate and Heer.[79]

(2) Mechanical properties change significantly.[93] The bending yield stress for single crystals increases sharply for exposures of 10^{14} n/cm^2. The hardness increases more slowly up to 10^{16} n/cm^2, and then it rises rapidly to a limiting value of 240 kg/mm^2 at 10^{18} n/cm^2. This hardness

is about 2.5 times the initial hardness. Gilman and Johnston[93] have also shown that the dislocation structure of room temperature irradiated LiF is not significantly different from that of the unirradiated material. However, the internal stress fluctuations in the irradiated material probably result in a drag effect which reduces the velocity of dislocation motion for any given applied stress. This increased drag causes the hardening and embrittlement of the samples. Extreme embrittlement, a consequence of neutron exposures greater than 10^{18} n/cm^2, leads to rupture or formation of extremely friable samples. This effect is probably also related to the clustering of defects and the formation of separate phases. Also, microcleavages are observed in crystals exposed to 2×10^{18} n/cm^2 or more.

(3) Volume and lattice expansion of LiF, neutron irradiated at about 60°C, were shown to be equivalent by the work of Binder and Sturm.[91] They also demonstrated that the expansion is a linear function of dose from 10^{14} to 1.5×10^{15} n/cm^2. Their work indicates that interstitial defects of the Frenkel type account for at least 84% of the total volume expansion of LiF at 6×10^{16} n/cm^2. Seitz and Koehler[2] showed that all of their dilatational effects could reasonably be accounted for by a displacement mechanism of radiation damage. Willis and Smallman[92] found that the X-ray lattice parameter increases linearly with dose to about 10^{17} n/cm^2 at 55°C; it reaches a maximum value after about 3×10^{17} n/cm^2 and decreases thereafter as shown in Figure 17. The equivalence of lattice and volume expansion was demonstrated to a total expansion of 0.3%, but the parallel seems to continue farther if the density measurements of samples irradiated at 80°C by Spaepen[41] are compared to the lattice measurements by Willis and Smallman.[92]

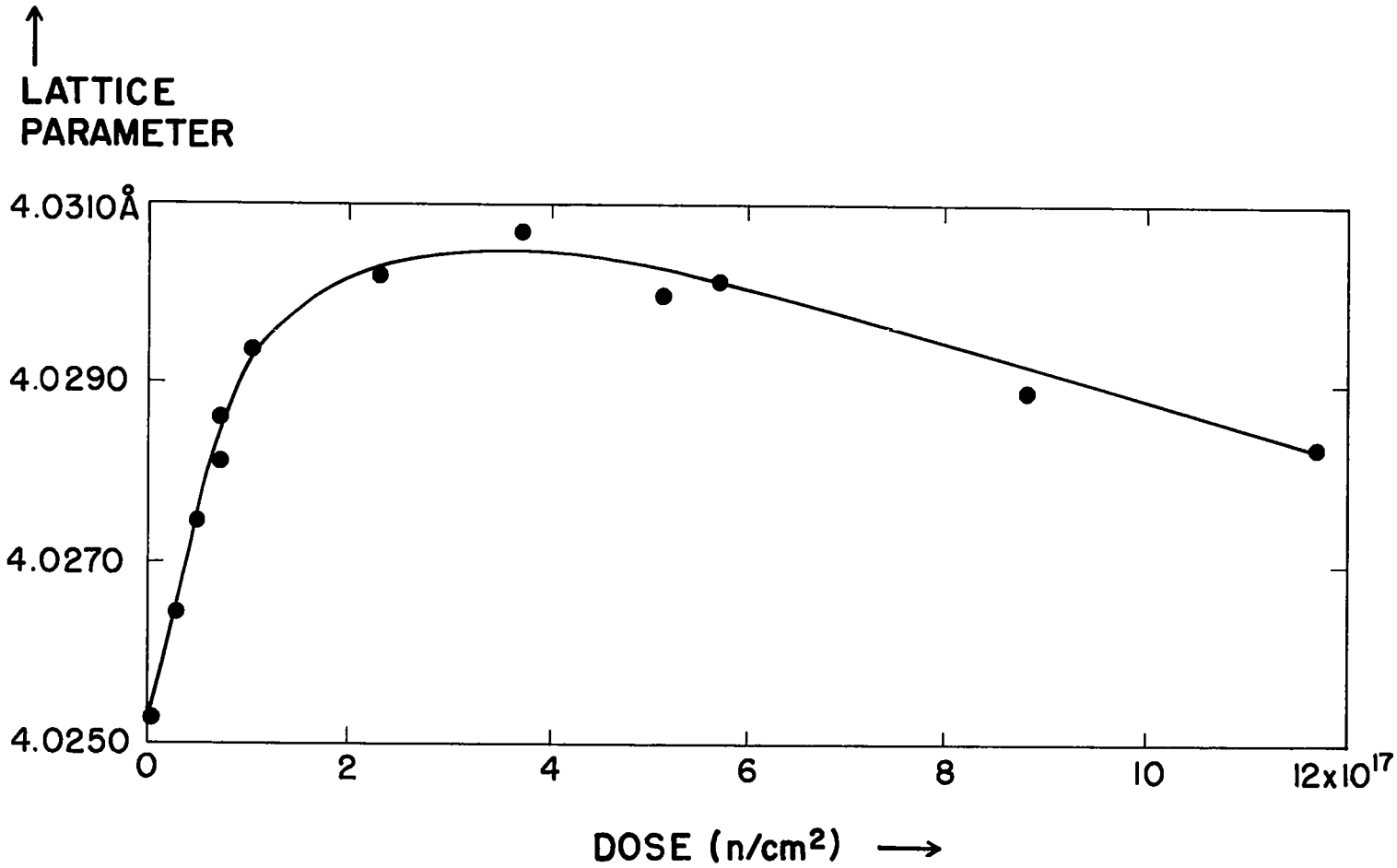

Fig. 17 Lattice expansion of neutron-irradiated LiF as a function of dose at 55°C. (After Willis and Smallman.[92])

Both results indicate that the efficiency* of the neutrons for producing expansion drops to a low value at doses from 10^{17} to 4×10^{17} n/cm^2, since both the volume and the lattice parameter remain relatively constant in this range. However, the volume expansion increases rapidly for doses between 4×10^{17} and 1.2×10^{18} n/cm^2, whereas the lattice parameter decreases steadily over the same dose range. For doses above 1.2×10^{18} n/cm^2 the expansion rate again decreases, and Spaepen's results indicate that the expansion is limited to a 22 to 24% increase in volume for doses of 2×10^{18} n/cm^2 or more. Most of the experiments were carried out inside reactor facilities at about 80°C. The only significantly different results that can be attributed to the irradiation temperature were obtained at 185°C by Senio and Tucker.[42] Their results show a remarkable decrease in both the volume and lattice expansions for comparable doses at the elevated temperature, which can probably be attributed to an annealing effect.**

---

*Bate and Heer[79] state that the efficiency of the neutrons for the production of magnetic centers starts at 15,000 per absorbed neutron at about 3×10^{13} n/cm^2, drops to 5000 at 6×10^{14} n/cm^2, then to 500 at 4×10^{16} n/cm^2, and becomes essentially zero at 10^{17} n/cm^2. These results are not entirely inconsistent with an average yield of 1000 to 2000 interstitials per neutron absorbed for 5×10^{16} n/cm^2 according to Seitz and Koehler.[2] The saturation of the production of magnetic centers at about 10^{17} n/cm^2 agrees with the expansion observations cited in the text.

**From Seitz and Koehler's[2] calculations we may assume that about 10^3 particles are displaced interstitially along the short path of each primary Li^6 fission particle. It is probable that the first effect of raising the irradiation temperature is to increase the rate of recombination of the Frenkel defect pairs produced in relatively high concentration around the tracks of the primary particles. Tritium β particles in the Li hydrides probably produce less than 10 lasting displacements over a much longer track by an ionization mechanism. Local defect concentrations are lower and recombination does not predominate to reduce the initial rate of defect formation for samples stored at elevated temperatures -- as Figures 3 and 4 show.

(4) The absence of the H band and the presence of the M band in room temperature irradiations of 10^{13} n/cm^2 indicates that there is some aggregation of defects to form M centers and interstitial F_2 molecules, even at low total doses. However, the formation of magnetic centers associated with Frenkel defect pairs proceeds rapidly until the rate of production is reduced at about 10^{17} n/cm^2. The F centers appear to be separated by more than six lattice units[79] and apparently do not interact much, even at the saturation value of about 10^{20}/cc; but continuing the irradiation after this increases only the degree of aggregation of the centers. Small angle X-ray scattering indicates that significant aggregation of the interstitials begins at about 5×10^{16} n/cm^2 and becomes predominant at 2×10^{17} n/cm^2. Distinct 10 to 20 Å cavities appear at 2×10^{18} n/cm^2. It is probable that the large volume expansion observed by Spaepen between 4×10^{17} and 1.2×10^{18} n/cm^2 is related to the inclusion of the necessary number of vacancies into the crystals to reduce the lattice strain and form the observed cavities. Aggregation forms metallic Li and free F_2 in the irradiated crystals. The F_2 has been observed by chemical means during dissolution of the crystals in water.[42] Lambert and Guinier[47,94] observed the metallic Li as thin platelets along the (100) cleavage planes by interpreting diffuse streaks in the X-ray patterns of heavily irradiated samples.

(5) Annealing of irradiation damage in neutron-irradiated LiF occurs in several stages and has been rather extensively studied. The color centers, lattice strain, and increase in hardness all are removed by annealing the samples for several hours at 400° or 500°C. For doses less than 2×10^{17} n/cm^2, almost all of the volume increase can be removed by annealing at 650°C.[41] Prolonged 450°C bleaching causes the more heavily irradiated crystals to become first clear and then cloudy as the cavity sizes begin to increase to microscopic dimensions.[42] Microscopic cavities can be observed

after annealing at temperatures above 600°C. These are observed to have a rectangular cross section,[42,92,93] and their dimensions continue to increase with increasing annealing temperature. Willis and Smallman[92] suggested that the bulk of the product He^4 and T from the neutron-induced Li^6 fission is contained in the square voids; but Gilman and Johnston[93] propose that little gas can be contained in the cavities because the sides of large cavities annealed for long times at 800°C do not bulge. They also give other evidence to show that gas pressures inside the cavities are small to support their contention that the cavities are basically an aggregation of the excess vacancies in the crystal. Senio[95] showed that some gas was contained in the cavities which he observed by the fact that their shape became spherical after a 15 hr anneal at a temperature just below the melting point.

4.3 Model for Li Hydrides Containing LiT

In the introduction we presented two very general equations to represent the decay and radiation-damage processes in the T-containing Li hydrides, and we mentioned the value of performing various experiments to help to understand the mechanisms by which these processes occur. In this section we shall try to derive a model for radiation effects in LiH, using the results summarized in Chapter 3 along with comparisons to radiation effects in the alkali halides and LiF.

The production of color centers in LiH is probably initiated by the same mechanism that was outlined for the alkali halides at the end of Section 4.1, but the products are different. ESR and X-ray measurements indicate that the H_2 molecule at an anion site in LiH is stable relative to the trapping of electrons to form H_2^- molecule ions or interstitial H^- ions. If an anion vacancy is available to accommodate the second H^- ion formed by retrapping both electrons released in the first stage of the mechanism, the

net effect of the process is to heat the crystal. Alternative mechanisms can be described for the production of two F centers and a H_2 molecule by which the molecule may be trapped in a single anion vacancy, an undissociated complex with a pair of anion vacancies, or an interstitial position. The first two possibilities were described in Section 3.6 as a V_1 center and a V_1-center anion-vacancy complex, but anion vacancies must be introduced from an external source to form F centers by either of these mechanisms. If either of these mechanisms is correct, it may be that the released electrons remain in F' centers or other shallow traps until anion vacancies are supplied by some mechanism, such as the one suggested by Seitz for the formation of F centers in the alkali halides. There is no evidence for the formation of interstitial H_2 molecules in LiH except by analogy with interstitial He atoms, which apparently have similar optical absorption characteristics. Rough calculations indicate that energy is required to produce an interstitial H_2 molecule and an F center by displacing the H_2 molecule from a lattice site, but this process is not nearly as unfavorable as the production of an interstitial H^- ion in LiH. The difference in the coloration mechanisms for LiH and the alkali halides at low temperatures may be reflected in the comparatively higher energy requirement for the formation of F centers in LiH. Although the mechanism for the production of F centers in LiH by radiation damage cannot be given unambiguously, the identification of the main centers produced by T decay in Li(H, T) samples with F centers and interstitial He atoms has been made, and the production of these centers has been correlated to the expansion of samples stored at low temperatures shown in Figure 14.

Aggregation plays an important role in most of our samples which were used for the expansion measurements, according to the results discussed in Sections 3.5 and 3.6. Mechanisms producing species as complex as these

aggregates are difficult to present, but a qualitative picture may be given by equating the F-center aggregates to the fcc form of Li metal colloid and then considering the phase transition which produces the bcc form of the Li colloid. The aggregation of defects containing He and H_2 in LiH is assumed to be similar to that observed in other materials, with concentration of aggregates at dislocations and impurities in the crystals. High local concentrations of lattice imperfections eventually lead to crystallite fracture and the escape of radiation-damage and decay products from the crystal lattice. The complicated effects of interactions between impurity aggregates and the crystalline dislocation network defy detailed description, although logical explanations can be made for some of the phenomena observed. Complications are further increased by defect recombination and thermal annealing of the damaged crystals. No attempt is made to present a detailed mechanism on an atomistic plane for the later stages in heavily damaged crystals, but some correlations are indicated on the phenomenological level.

Because the radiation source is an integral part of the T-containing Li hydrides, we have been able to accumulate much data on samples homogeneously irradiated under conditions of known (and arbitrarily adjustable) temperature and dose rate. It takes 6.45 days for the tritium β decay in LiH containing 40 mole % LiT to accumulate a dose of 2.6×10^9 roentgens, which is approximately equivalent to that produced by a slow neutron exposure of 10^{17} n/cm^2 in LiF samples of the dimensions used by several investigators.[41,42] During the same time 2.8×10^{19} He^3 atoms/cc are formed as impurities in the hydride, compared to concentrations of $2.2_3 \times 10^{16}$/cc of He and T by Li^6 fissions in LiF. These figures help to illustrate the comparative magnitude of the radiation doses experienced by some of our samples. For example, on this basis a 1400-day-old LiH sample containing 40 mole % LiT has experienced the equivalent of a neutron dose amounting to

2×10^{19} n/cm^2; also, more than 500 times the concentration of the impurity atoms formed in the LiF are present in the hydride sample. The expansion results indicate that this rough basis for comparison is approximately right.

We have made a comparison of the effectiveness of various types of radiation for producing color centers in LiH at low temperatures. F-center production in LiH crystals exposed to X rays, tritium β particles, and thermal neutrons is illustrated in Figure 18. These comprise most of the major classes of radiation: photons, electrons, and heavy charged particles from the neutron-induced fission of Li^6. The dose rates used increase in the order given, and all curves in the figure are plotted to the same absorbed energy scale. Since decay also produces F centers in LiH containing LiT, the effect of radiation damage by β particles was approximated by subtracting the yield of F centers by decay from the total yield (both indicated by dashed curves) to obtain the solid curve β(I). The initial part of the X-ray-yield curve seems as steep as curve β(I), but the yield in the second stage is lower. This could indicate a dependence on dose rate as well as on radiation type. The dashed curve shows that the saturation value for LiH X-rayed at 23°C (296°K) is also lower than the β(I) saturation level, but this may be a result of an increased recombination rate at the higher temperature in addition to the factors already given. The dose rates for neutron and β-particle irradiations nearly overlap at the limits used, yet the net yield for neutrons remains lower than for β particles over the entire range of exposures. This result probably indicates more recombination along the comparatively dense tracks of the heavy charged particles in the neutron-irradiated crystals. Since the F-center yield in LiF crystals is apparently somewhat higher than in LiH crystals exposed to neutrons, the comparison between neutron-irradiated LiF and LiH containing LiT is probably better than Figure 18 would indicate. The regular growth of the F-center concentration in LiH crystals containing

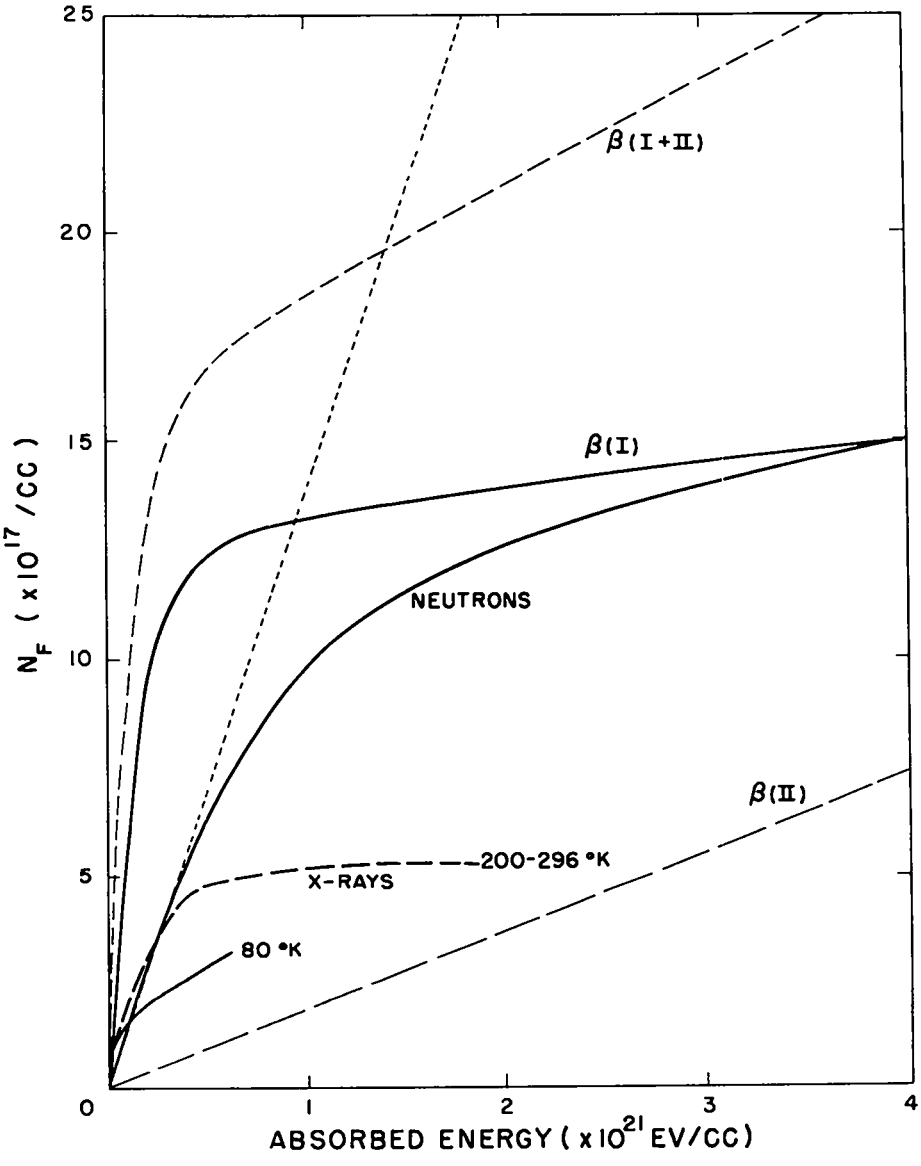

Fig. 18 F-center formation in LiH exposed to X rays, neutrons, and β particles at low temperatures. The solid curves illustrate the F-center growth at about -193°C (80°K) in samples absorbing 5.6×10^{18} ev/cc hr from X rays, (0.18 to 4.6) 10^{21} ev/cc hr from neutrons, and (0.29 to 1.18) 10^{20} ev/cc hr from tritium β particles. The dashed curve illustrates the saturation observed for X irradiation at room temperature. The upper dashed curve shows the total F-center growth in LiH containing LiT, and the dashed straight line, β(II), indicates F-center formation by β decay. The weak dotted line shows the F-center yield in a Mg-doped LiH crystal exposed to neutrons for comparison.

LiT is associated with steady expansion (Figure 14) which, because of the contribution of decay products, does not exhibit a saturation-induced step indicated for neutron-irradiation LiF.[41]

4.3.1 β Radiation Production of Point Defects

This discussion of radiation-damage processes follows the sequence of steps in the order of their relative importance in time starting at the lowest storage temperature. Some experimental evidence to support the proposed mechanism is included in the discussion of the various steps, and other results which support the consistency of the mechanism with the available data are presented in the last section.

Consistent with the plan, we begin by writing a mechanism for the radiation production of color centers which is drawn from the optical and ESR absorption studies on crystals irradiated at temperatures from -193° to -73°C.

$$2LiH_{(c)} \xrightleftharpoons{\beta(2[+][-])} 2[Li^{+}]_{(c)} + 2[e^{-}]_{(c)} + [H_2^{-}]_{(c)} + 2[+]_{(c)} \qquad (1)$$

This reaction permits easy bleaching of the F centers ($[e^{-}]_{(c)}$) by recombination with the self-trapped double hole $[H_2^{-}]_{(c)}$ at low temperatures, although the vacancy pairs $[+|-]_{(c)}$ (which may have been introduced from dislocation sources as postulated by Seitz) presumably remain after bleaching the color centers.

Alternatively, radiation may produce interstitial H_2 molecules in LiH instead of the complex postulated in Equation 1.

$$2LiH_{(c)} \xrightleftharpoons{\beta} 2[Li^{+}]_{(c)} + 2[e^{-}]_{(c)} + (H_2)_{(i)} \qquad (1')$$

The lattice parameter measurements do not distinguish between Equations 1 and 1' for low temperature radiation damage to LiH. If the interstitial molecule is more mobile than lattice vacancies at low temperatures, it may also explain the easy optical bleaching of a fraction of the centers produced at low temperatures which caused us to postulate the formation of the V_1-center-vacancy complex of Equation 1.

A third mechanism allows for the production of more stable V centers, first by dissociating the complex in the manner described in Section 4.1 to form V_1 centers in LiH, and second by allowing vacancy diffusion to produce a charge stabilized V_1-center-cation-vacancy complex $\left(\boxed{H_2|+}_{(c)}\right)$.

$$2LiH_{(c)} \xrightleftharpoons{\beta(\boxed{+|-})} 2\boxed{Li^+}_{(c)} + 2\boxed{e^-}_{(c)} + \underbrace{\boxed{H_2}_{(c)} + \boxed{+}_{(c)}}_{\downarrow\uparrow\ \boxed{H_2|+}_{(c)}} \qquad (1'')$$

The mechanism represented by Equation 1'' can also be considered to be the net result of the migration of vacancies under thermal activation upon the products of Equations 1 and 1'. The second step for Equation 1 is the release of a vacancy pair to the crystal lattice, and for Equation 1' it is the combination of the interstitial with mobile vacancies in the crystal to form the products of Equation 1''. Radiation damage by Equation 1'' would be consistent with an increase in F-center yield at higher temperatures because: (1) the total expansion is less than for Equation 1 and the lattice distortion is less than for Equation 1', and (2) the neutral complex produced has no coulomb attraction for electrons and should be comparatively stable toward bleaching.

The growth of F centers produced by radiation damage near -193°C is

shown in curve β(I) of Figure 18, and the recombination of the radiation damage products is illustrated by the curve in the lower left-hand corner of Figure 14. From Figure 14 it is evident that the expansion associated with radiation damage to LiH was not detected by the flotation density measurements, but that the larger effect due to LiT decay was observed. The reported failure to detect H_2 by NMR measurements on a sample containing 40% LiT which had been stored for a long time at -7°C (Section 3.4) is consistent with this interpretation drawn from Figure 14. For practical purposes, radiation damage may be neglected in interpreting expansion results for samples stored in the temperature range from -196° to -7°C. However, because of other processes which effectively stabilize radiation-damage products toward recombination, radiation damage cannot be ignored in the interpretation of expansion observations obtained at 23°C or at higher temperatures. At these temperatures the ionic mobilities in the LiH crystal lattice are so high that only the net reaction represented by Equation 1" needs to be considered.

4.3.2 β Decay Products

The production of F centers by the irreversible β decay of LiT is the predominant cause for the expansion illustrated in Figure 14. Measurements of lattice parameter and flotation temperature on samples from the LiH crystal containing 5.56% LiT have demonstrated that interstitial He^3 atoms are formed at -196° and -27°C, and that the corresponding crystal expansion is about 12 $\text{Å}^3/\beta$ decay. This result is in satisfactory agreement with a rough calculation of the expansion associated with the formation of an interstitial He atom which is presented in Appendix A.

$$LiT_{(c)} \longrightarrow \boxed{Li^+}_{(c)} + \boxed{e^-}_{(c)} + \left(He\right)_{(i)} \qquad (2)$$

Although the mechanism of Equation 2 is directly related to the F-center growth and volume expansion illustrated in Figure 14, most of our expansion measurements have been made near room temperature under such conditions that the aggregation of F centers and the combination of interstitial He atoms with mobile vacancies is expected.

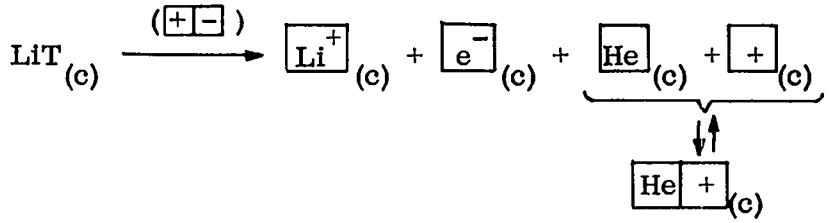

(2')

The net reaction expressed by Equation 2' is comparable to that represented by Equation 1'' with the important difference that twice the lattice expansion per F center according to Equation 1'' is indicated for those F centers produced by decay according to Equation 2'. This is the equivalent of saying that a He atom takes the place of a H_2 molecule in the V_1-type centers formed. Justification of the use of Equation 2' to interpret much of the expansion data is indicated by X-ray measurements which show no significant lattice expansion for samples containing 40% LiT after storage for 100 days at 23°C. A further justification of the use of Equation 2' is indicated by an expansion rate which corresponds to one vacancy pair per β decay in samples stored at -196°C and measured at about 40°C.

4.3.3 Aggregation of Point Defects

Measurements on LiH crystals containing 1.35% LiT have shown that the saturation concentration of free F centers may be low and that the ESR band typical of aggregates may begin to appear at F-center concentrations of about 10^{18}/cc even at -193°C. Since 3.7×10^{18} F centers/cc would be produced in LiH containing 40% LiT in 1 day by decay alone, it is evident

that aggregate production should be considered in the interpretation of most of our expansion results. Consistent with ESR results and with the X-ray detection of a fcc Li phase in neutron-irradiated LiF,[47,94] we propose that F-center aggregation first occurs without additional expansion.

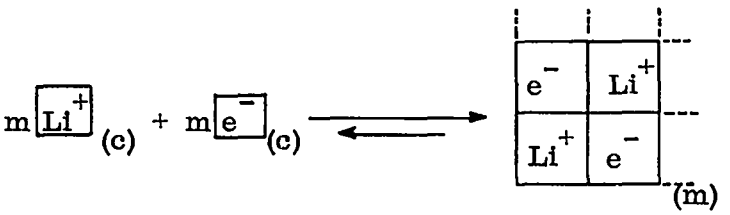

(3)

The size ranges from m = 2 (an F_2 center) to larger values, which become equivalent to compressed fcc Li metal.[46] The fcc metal phase is calculated to be under 17 to 30% compression, which may account for the variation in width of the Lorentzian-shaped ESR band observed in both LiH and LiF.* Consistent with X-ray observations of Li in LiF and with metallic decoration experiments on the alkali halides,[96] we expect Li aggregates in LiH to form on dislocation networks. Direct microscopic observation of Li decoration in LiH crystals containing LiT has not been made because of the dense coloration of these samples, but an example of impurity precipitation in LiH is given in Appendix B. The forces which tend to preserve the fcc lattice type and lattice parameter of the LiH host crystal in the sheetlike Li aggregates may be compared to those which produce abnormal phases in certain thin films formed on substrates of a different material.[97]

The energy of the damaged crystal is also reduced by aggregation of the defects containing He and H_2 by a similar mechanism

*Estimates based on the compressibility of bcc Li metal indicate that a force of about 200 kg/mm^2 would be needed to maintain a 17% compression. It is interesting to note that hardnesses of the order of 250 kg/mm^2 are induced in both LiH + 40% LiT and in neutron-irradiated LiF.[93]

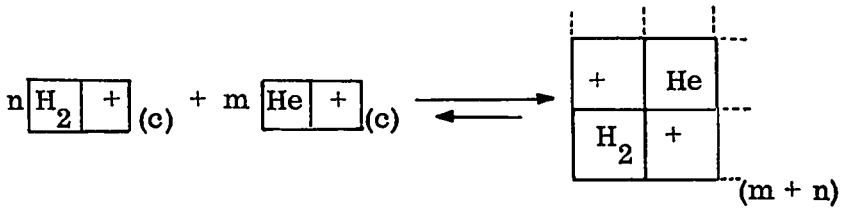

(4)

where in Equation 4 no net volume change is associated with the formation of small aggregates containing He and H_2 gas (also abbreviated as $He_{(g)}$ and $H_{(g)}$). Some reduction in volume may occur on aggregation if the cation vacancies are occupied by a fraction of the He or H_2 impurities, thus freeing some vacancy pairs to the crystal lattice. This assumption is needed to explain the relative values of the initial expansion rates at -196° and -22°C on the lattice vacancy model.

Calculated expansion rates for LiH containing 40% LiT can be obtained from the mechanisms illustrated by Equations 1" to 4 and compared to the observed initial expansion rates shown in Figure 19. By equating the volume of a vacancy pair ($\boxed{+}\boxed{-}$) to 17 $\mathring{A}^3$, the volume of an ion pair in a LiH crystal, and multiplying this by the T decay rate of 3.69×10^{18} disintegrations/cc day, the calculated volume expansion rate associated with Equation 2' is found to be 0.0062%/day. Comparable estimates could be made for Equation 1" if the radiation damage per decay were known; but the calculation can be turned around to estimate the radiation-damage yield from the experimental expansion rates since insufficient independent data on radiation-damage yields are available. The initial expansion rate observed (actually for the first 100 days) at -196°C was 0.006_7%/day (Figure 19), which is consistent with the calculated value and other measurements which indicate that Equation 1" is indeed reversible and that the radiation-damage contribution to the expansion of samples stored at low temperature is negligible.

The lower initial expansion rate of 0.004_4%/day found in samples stored at -22°C (Figure 19) is hard to explain on the vacancy model unless one

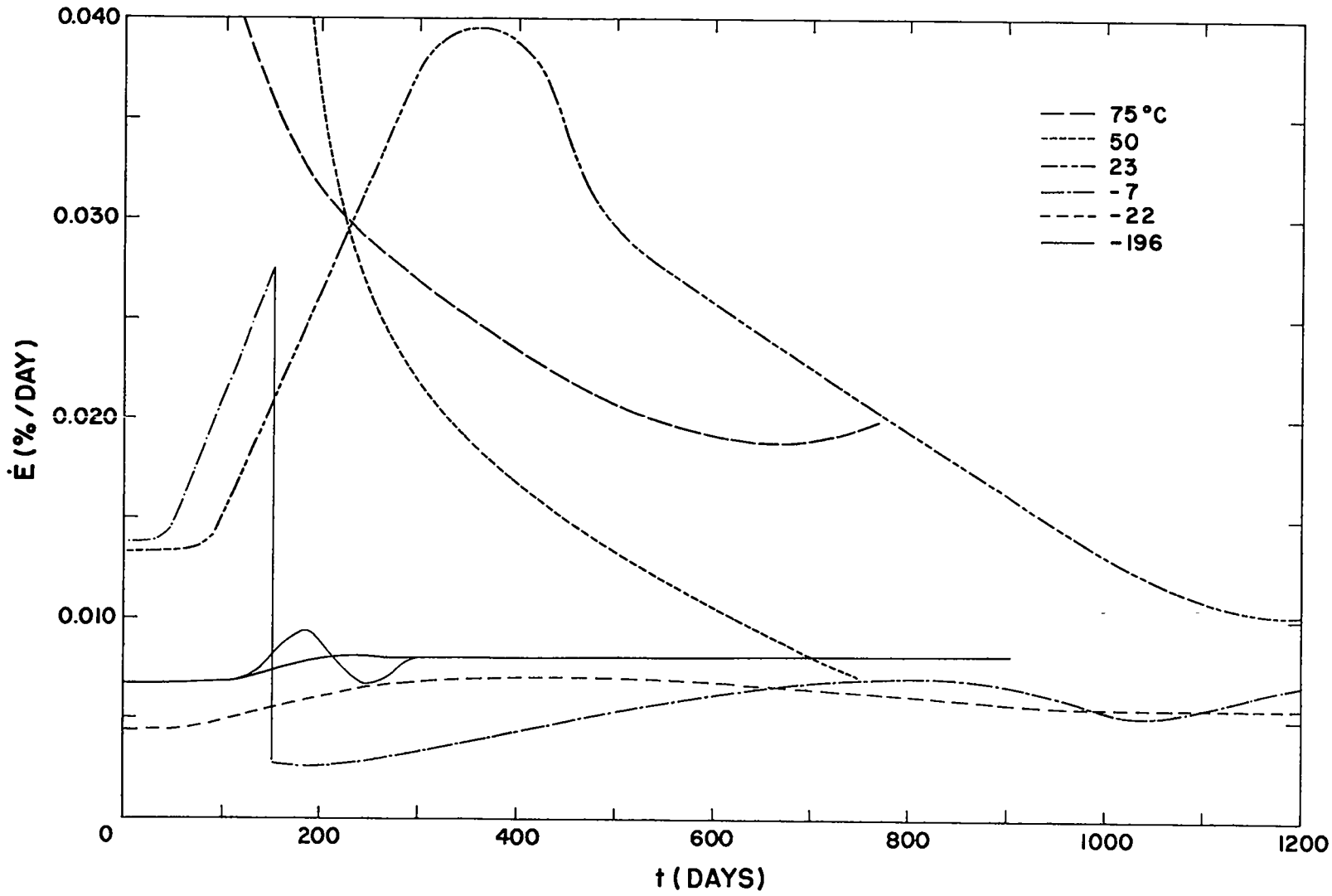

Fig. 19 Expansion rates calculated from the expansion isotherms of Fig. 5 for LiH samples containing 40 mole % LiT. The wave on the -196°C curve reflects an apparent "hump" on the expansion isotherm.

assumes the use of cation vacancies to store some fraction of the gaseous impurities in the aggregates as indicated previously. This result also agrees with the expansion observed in samples measured at low temperatures for which direct evidence for the formation of interstitial He atoms was obtained. Nevertheless, it is assumed that the interstitial He atoms were eliminated during storage for several hours at room temperature in these samples as well as in others. The low expansion rate of 0.002_8%/day found for the -7°C sample just after cooling to -7°C from previous storage at 23°C can be explained if it is assumed that H_2 formed at the higher temperature was destroyed by recombination and that the vacancies thus released to the crystal were used again for decay products.

If it is assumed that an expansion rate of 0.004_4%/day is required to accommodate the decay products by Equations 2' and 3 and some volume reduction in Equation 4 and that this rate will also fulfill the requirements of Equations 1", 3, and 4, for radiation damage at higher temperatures, a simple formula for radiation-damage yield can be written:

$$y = \frac{\left[\dot{E}(0) - 0.004_4\right]}{0.004_4}$$

in terms of $\dot{E}(0)$, the initial observed expansion rate.* Since y gives H_2 production according to Equation 1", the yield of F centers (in aggregate or fcc

*The actual precision of the determination of the initial expansion rate at -22°C was rather poor, $0.004_4 \pm 0.0015$%/day, but other evidence for selecting this value to insert in the formula includes: (1) It is 0.001_8%/day below the long-term average expansion rate at -22° and -7°C, which difference agrees with the expansion related to Li phase transformation in Section 4.3.4. (2) Since it is consistent with the -7°C expansion and since radiation damage contributes significantly to expansion measurements made at higher temperatures, this value probably is the best available estimate for the net expansion related to decay (Equations 2' through 4) for the analysis of the data obtained at higher temperatures.

Li) is 2y. By the application of the formula for radiation-damage yield to initial expansion rates of samples studied in the -22° to 50°C temperature range, the following values of y are obtained:

$$y(-22°C) = 0,\ y(-7°C) = 0,\ y(23°C) = 2,\ y(50°C) = 19$$

The increase in y with temperature is consistent with expectations from color-center studies. The formula for y has only been applied to those expansion data that show a steady expansion rate before the increase in rate, which (in the case of -196° and 23°C measurements) has been demonstrated to correspond to the production of bcc Li metal.

4.3.4 Precipitation of (bcc) Li Metal

When the F-center aggregates produced by Equation 3 become sufficiently large, they can become nuclei for the precipitation of the usual bcc-form of Li metal at temperatures above boiling N_2 (-196°C). Regardless of whether the mechanism involves the dissolution of F-center aggregates to re-form larger Li particles of the bcc form or only a simple martensitic transformation of fcc F-center aggregate to bcc Li metal is involved, the process requires expansion because the molar volume of bcc Li metal is about 28% greater than that of the LiH crystal in which it is formed. If, as before, we assume that this extra volume is introduced by the diffusion of vacancy pairs into the host crystal, the process of precipitation (or transformation) can be written:

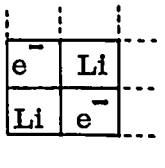

$$+\ 0.28m\ \boxed{+}\boxed{-}_{(c)} \rightleftharpoons mLi(s, bcc) \qquad (5)$$

Evidence for the forward reaction was obtained on comparable samples

stored at -196°C for over 100 days before warming them for ESR or expansion measurements which demonstrated that the bcc Li metal was formed with accompanying expansion of the samples in about 1 hr at room temperature. A reversal of Equation 5 occurred in a sample stored at -196°C for several months after bcc Li had been allowed to form at room temperature. It is not necessarily assumed that the martensitic transformation to fcc Li occurred with the large volume contraction indicated by the reverse of Equation 5, but an ESR band similar to that found before the transformation to bcc Li was produced.

Although bcc Li metal is not formed at -196°C in the samples, and although ESR and expansion data both indicate that little is formed in LiH samples containing 40% LiT for the first 100 days, nucleation and a rapid transformation to produce bcc Li then occurs in all samples measured at room temperature. An extension of the vacancy model to include steps 2' through 5 leads to a calculated increase in the expansion rate of 0.001_8%/day to give a total of 0.008_0%/day. This value agrees quite well with the observed value of 0.008_2%/day (Figure 19) obtained from later expansion measurements on samples stored at -196°C. Later expansion measurements on samples stored at -22° and -7°C are consistent with a 0.006_2%/day expansion rate, which is also 0.001_8%/day higher than the initial -22°C rate. This result is also in agreement with Equation 5 if the reasoning used previously is applied to explain the low initial -22°C expansion rate.

The ESR and expansion measurements on samples stored at 23°C are also consistent with the interpretation that the strong maximum in the 23°C expansion rate, illustrated in Figure 19, is also associated with the transformation of fcc Li (F-center aggregates) to bcc Li metal according to Equation 5. The association between the expansion data and the ESR observations of the formation of bcc Li metal are discussed in the final section, along

with detailed descriptions of the model adopted and some possible alternatives. In summary, it was found that a (vacancy) diffusion-controlled Li metal transformation following Equation 5 could account for both the qualitative features of the 23°C expansion-rate curve (Figure 19) and the quantitative 23°C expansion (Figure 5), assuming the radiation-damage yield previously found from the initial 23°C expansion rate (y = 2). The model explains the total expansion rather well through the maximum rate at 300 days and up to about 500 days. The total expansion observed after 500 days is too large to be accounted for by an expansion at the initial rate plus that required to form the bcc Li detected (Equation 5). The discrepancy can be explained by assuming either that H_2 and He gas aggregates require more volume per defect than indicated by Equation 4 in more heavily damaged crystals, or that y has increased slightly above the initial value (y = 2) during the period of rapid expansion and some recombination has occurred.* After 700 days storage at 23°C, the expansion rate drops below the 0.022%/day rate calculated for steady damage at the initial rate plus formation of bcc Li metal (Equation 5); other processes (recombination is assumed to be the first) are required to explain the continued drop in the 23°C expansion rate below this value.

The features of the 50°C expansion rate curve shown in Figure 20 are similar to those of the 23°C curve (although on a different scale) and a similar explanation is assumed. Compared to the 23°C interpretation it is

*That y increases during rapid expansion is indicated by the application of the modified yield formula to the maximum average expansion rate at 23°C which gives y = 2.5 after about 500 days. Although this increase in y is scarcely beyond the accuracy expected of the model, an increasing yield may be explained if accelerated Li precipitation according to Equation 5 is accompanied by a reduction in the average concentrations of the intermediates with a consequent increase in the fraction of H_2 molecules aggregating according to Equation 4.

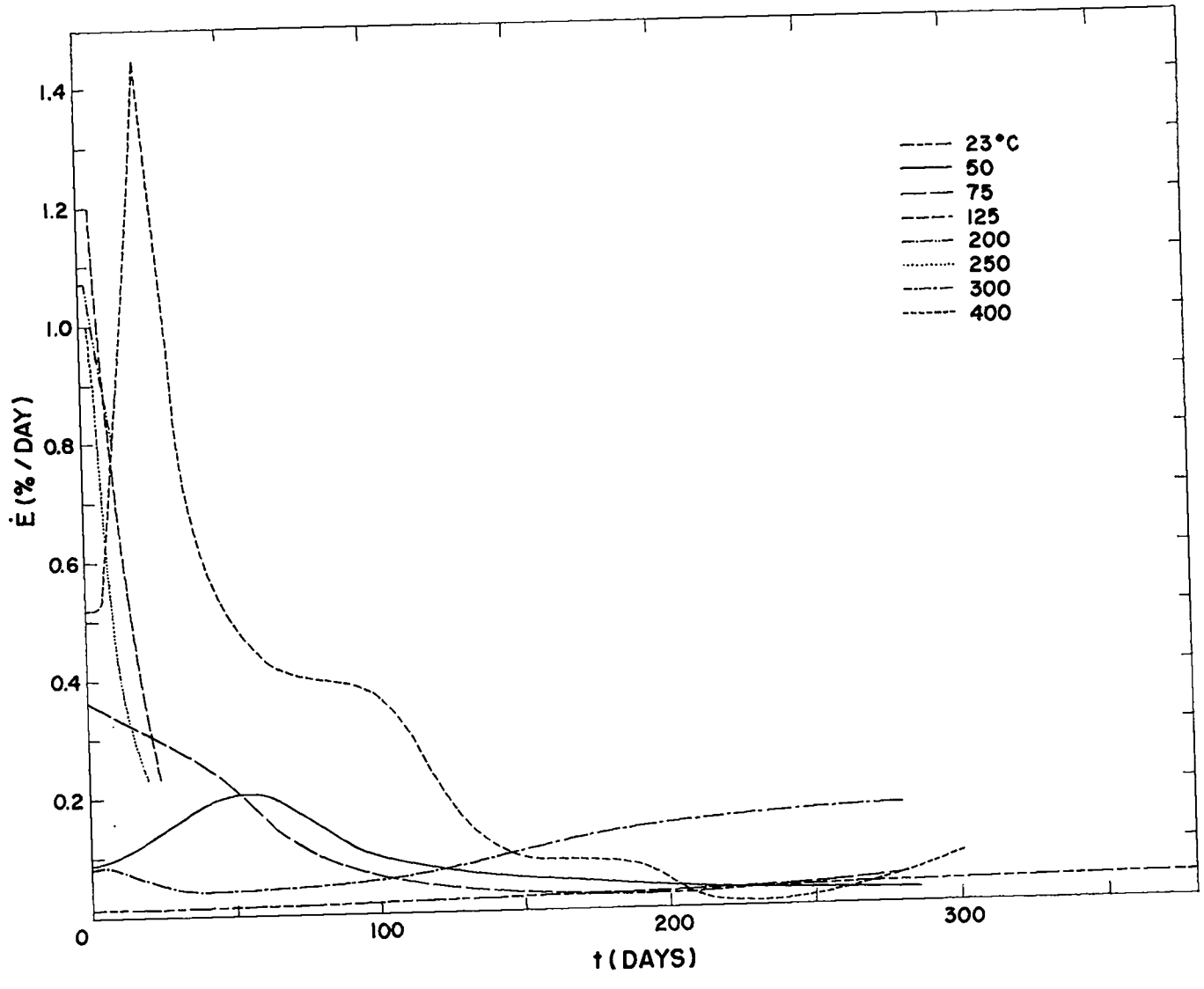

Fig. 20 Expansion rates for LiH samples containing 40 mole % LiT and taken from the high temperature expansion isotherms of Figs. 3 and 4.

found that recombination is important after storage at 50°C for 76 days.

The 75° and 125°C expansion rate data of Figure 20 show that the initial rates are the maximum rates observed, and the subsequent reduction is attributed to the recombination of radiation-damage products, which is considered in the following section. Since no significant buildup of the concentration of F-center aggregates (fcc Li) occurred before the maximum expansion rate is observed, an estimate of the radiation-damage yield was obtained by letting $y = (\dot{E} - 0.0062)/0.0080$. This expression is similar to that previously used, but it includes the expansion for bcc Li metal formation according to Equation 5. The values found from the initial expansion rates are: y(75°C) = 44 and y(125°C) = 150. The maximum (125°C) yield corresponds to an energy requirement per LiH dissociation which approaches that generally given for ion-pair production by energetic radiation (20 to 30 ev/ion pair).

4.3.5 Recombination and Cavitation

The temperature dependence of the initial and maximum expansion rates observed for LiH samples containing 40% LiT is illustrated in Figure 21. The rate obtained at 125°C, corresponding to $y \approx 150$, is a maximum of the curve of log $\dot{E}$ vs 1/T. The expansion of the samples is a consequence of: (1) a fixed decay rate and subsequent changes in the state of aggregation of the decay products, and (2) a variable net radiation-damage yield for each storage temperature with reasonably constant steady-state concentrations of products of intermediate stability which produce the more stable products by Equations 1" through 5. Since the high yield for the net reaction at 125°C of about 300 ion pairs per tritium β particle is comparable to the maximum production of ion pairs expected from the first step of the radiation-damage process, the net yield should not be increased by raising

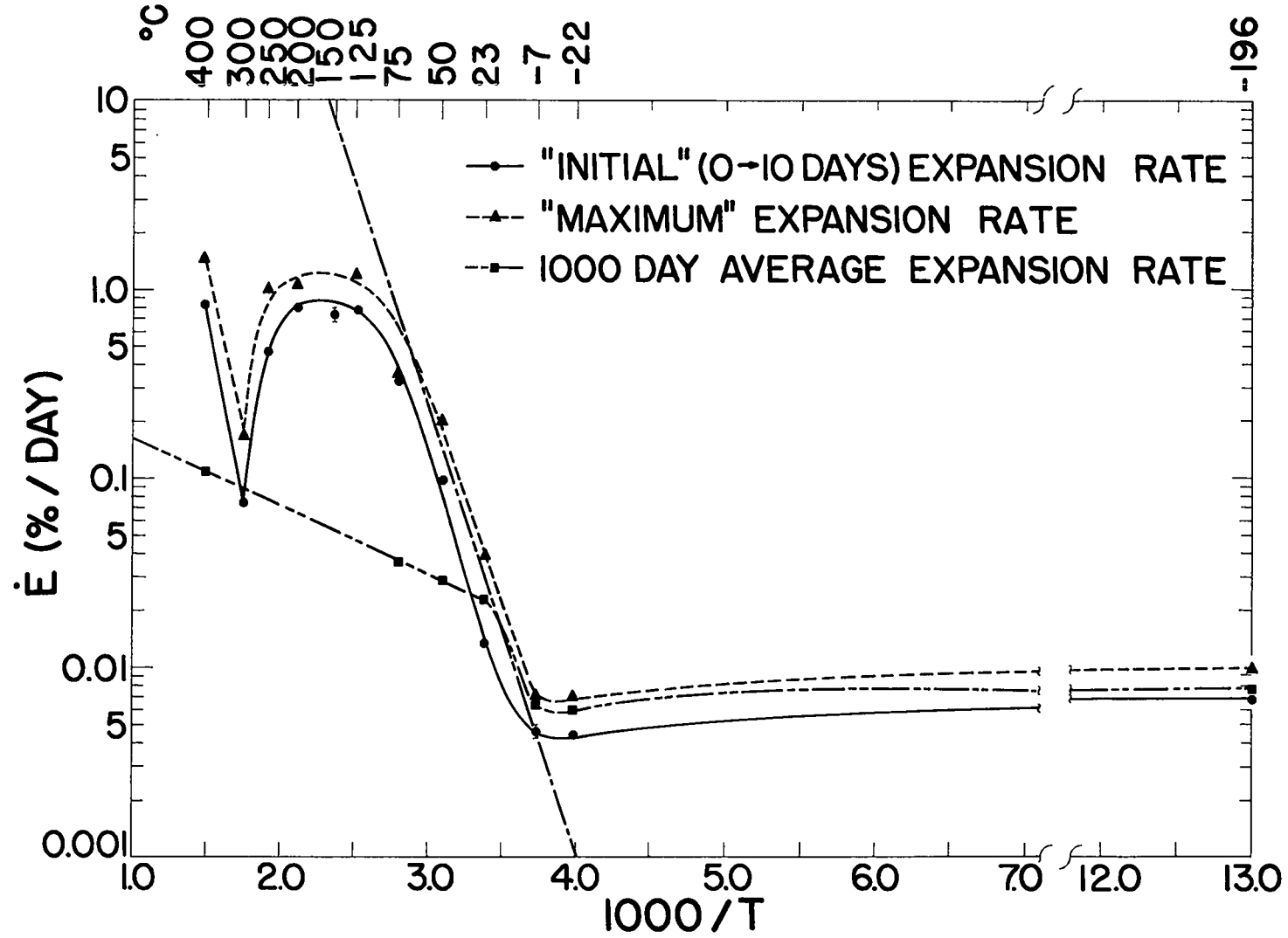

Fig. 21 Temperature dependence of initial, maximum, and 1000-day-average expansion rates of LiH samples containing 40 mole % LiT. The semi-dashed line corresponds to an average activation energy of 0.5_5 ev.

the temperature above 125°C. Raising the temperature further should increase the rate of all reactions except the radiation-limited forward reaction, Equation 1", with the result that the net reverse reaction ending with recombination of the products of Equation 1" is enhanced and the net radiation-damage yield is lowered.

Thermal bleaching studies in color-center experiments have shown that these unstable defects are removed more rapidly as the crystal lattice is restored to (thermodynamic) equilibrium at elevated temperatures. The steady-state concentrations of intermediates (including color centers) may even rise because of the increasing radiation-damage yield in the range from -7° to 125°C, but above this temperature they must fall for the reasons given above. This observation is confirmed by the bleaching of samples heat-treated at 400°C. The fact that expansion observations follow the temperature dependence postulated for net radiation-damage yield may be explained if it is assumed that a steady-state concentration of vacancies (and vacancy pairs) is established and that these are utilized in the forward reactions (Equations 1" through 5) and produced by the reverse reactions.

Recombination as described above is presumably responsible for the reduction in the initial expansion rates observed above 125°C. It is also important in determining the concentration of metastable intermediates (color centers and aggregates) and, through this, has an influence on the net radiation-damage yields at temperatures below 125°C. At the lowest temperatures studied, direct recombination affects the essentially complete reversal of Equation 1, 1', or 1" within 2 days. Another form of recombination is required to explain the decrease in expansion rate observed after longer storage time at 23°C or above; namely, the recombination of separated $H_2\left(H_{2_{(g)}}\right)$ and Li metal [Li(s,bcc)] phases within the samples. Since the reaction occurs (by a direct or an indirect process) between separated aggregate phases

within the LiH parent crystal, the result of the recombination will leave a volume equivalent to 1.57 vacancy pairs (designated 1.57 $\boxed{+}\boxed{-}_{(g)}$) at the site of the recombining aggregates. We have called this process cavitation, and it is probable that the gas-free rectangular-sided cavities observed by Gilman and Johnston[93] in neutron-irradiated and annealed LiF were formed by a similar process. Using the abbreviated notation for aggregates introduced above, an equation may be written to describe this recombination and cavitation process.

$$2Li(s,bcc) + H_{2(g)} \longrightarrow 2LiH_{(c)} + 1.57\ \boxed{+}\boxed{-}_{(g)} \qquad (6)$$

Since dissociation of LiH is negligible under the experimental conditions, the recombination reaction is not indicated as reversible. The vacancy volume within the cavities is not readily available to accommodate fresh radiation-damage or decay products, as would be true of vacancies left by the reverse of Equation 5 through 1"; but another equilibrium exists between the cavities, the dissolved lattice vacancies, and the free surface of the crystalline samples.

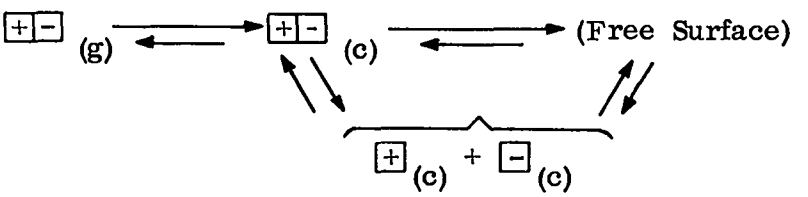

(7)

The disappearance of vacancies at a free surface of a crystal corresponds to a contraction of the sample and an effective reversal of the mechanism which introduced the vacancies during the radiation-damage process. The driving force for the removal of cavities from the crystal is presumably the excess surface energy required by their presence. Under these conditions it may be possible for a relatively small pressure of residual He gas

to maintain the cavity volume in a crystal.

The best mechanism to explain the reduction in expansion rate and net radiation-damage yield from a maximum value as observed in all samples stored at temperatures from 23° to 300°C is probably slightly different from that discussed above. According to our previous discussion, we might expect that diffusing F centers or Li atoms would recombine with H_2 in cavities (which may also contain He atoms) to leave cavities containing He at a reduced pressure without much net reduction in cavity volume.* On the other hand, H_2 molecules diffusing to a Li particle or F-center aggregate leave a vacant volume which can be directly used for the transformation of accumulating Li atoms to bcc Li metal. The increasing ratio of Li metal particles to gas cavities (because Li is the product of both radiation damage and decay) increases the probability that a H_2 molecule should meet a Li particle in its path and thus lead to a decrease in net radiation-damage yield and expansion rate.

The expansion rate data (Figure 20) indicate that recombination reduces the initial maximum rate after about 2 days at 200°C, 2-1/2 days at 250°C, 4 days at 125°C, and 5 days at 300°C. The shift of the initiation of rapid recombination to 200°C from the 125°C temperature for maximum yield indicates that both temperature and concentration of radiation-damage products influence the rate of recombination as expected. The 75°C sample indicates uncertain initiation of recombination between 2 and 50 days but, unfortunately, the early thermal history of this sample was irregular. In the discussion of the effect of the Li metal transformation on the expansion rate, it was shown that recombination must be considered to account for the reduction in expansion rate observed after 76 days of storage at 50°C and after 700 days of

*Evidence for this is the reduction of H_2/He ratio in gas obtained after annealing samples used in grinding experiments by T. Newton.[98]

storage at 23°C. Continued observation of the 23°C sample beyond 2000 days showed a rate comparable to the lowest initially observed at -22°C. The net yield of radiation-damage must be zero, with effective reuse of vacancies in this aged sample. The results for the 300°C sample given in Figure 20 indicate that the initial yield of y(300°C) = 20 drops to less than one-half this value, and it is probable that most of the H_2 produced recombines and is replaced by He in the cavities during the period of low expansion rate from 30 to 90 days.

The most striking example of expansion by cavitation is provided by the samples stored at 400°C. The thermally induced recombination of radiation-damage products which is nearly complete at 300°C must be essentially complete at 400°C as verified by the bleached appearance of the samples. In passing from 300° to 400°C the material is transformed from a brittle substance into one which undergoes plastic flow at usual strain rates. Then to explain the observation of a very high expansion rate, we postulate that vacancy transport into the crystal (presumably by a dislocation mechanism) is rapid compared to the defect bleaching process. The excess vacancies then aggregate to form cavities which are less accessible for reuse to accommodate other metastable radiation-damage products. The net effect of this aggregation is an increase in vacancy production, as the concentration of dissolved vacancies is reduced by the equivalent of a nucleation-precipitation process. The subsequent decrease in expansion rate observed after 20 days (and 20% expansion) is explained by postulating that the cavity surfaces are so large that the cavities compete with the free surfaces of the crystal as sources of vacancies. The proposed mechanism is like the reverse of Equation 7.

$$\text{(Free Surface)} \xrightleftharpoons{\beta} \boxed{+|-}_{(c)} \xrightleftharpoons{\beta} \boxed{+|-}_{(g)} \qquad (8)$$

From Equation 8 alone it might be expected that a steady state might be found after the cavity surfaces become so large that they yield vacancies to the crystal as fast as they collect them. The expansion of the crystals continues at a low rate after 200 days or so (80% expansion) because the build-up of decay products increases the He pressure in the cavities. The increased rate of expansion after 250 days may indicate hydrostatic equilibrium between He gas pressure and the confining cavities with subsequent increases in average cavity volume.

4.3.6 Escape of Impurities

Another mechanism which produces a reduction in the net yield of radiation-damage products contained by the crystals and in the expansion rate of the samples is the escape of impurities from the samples. The experimental evidence for such processes is given by the He and H_2 outgassing measurements and by the observation of the extrusion of some Li metal from grain boundaries at the surface of some of the samples.

The simplest form of "impurity" escape is represented by Equation 7, in which vacancies diffuse to free surfaces of the crystalline grains of the sample and thus escape. Since the stresses which induce expansion presumably tend to compress the grains of the sample together, the disappearance of a layer of vacancies at a free surface of a grain can occur by the displacement of the grains toward each other. In the case of gaseous impurities, H_2 and He, the pressure produced by their accumulation at cavities concentrated at grain boundaries may prevent a compressive displacement of the grains. To actually "escape" from the sample, the H_2 and He gasses must reach the sample surface by direct diffusion, by gaseous diffusion through fissures developed at the grain boundaries, or by gaseous diffusion through microfissures developed by the aggregation of cavities along the

subgrain boundaries of the crystalline grains.

$$H_{2(g)} + He_{(g)} \longrightarrow \begin{pmatrix}\text{Fissure or Diffusion}\\ \text{Intermediate}\end{pmatrix} \longrightarrow \begin{pmatrix}H_2, \text{ He in}\\ \text{Free Volume}\end{pmatrix} \qquad (9)$$

Because of its metallic nature, little of the Li produced actually "escapes" through the boundary represented by the original sample surfaces by direct diffusion through the surfaces or by extrusion from the grain boundaries. Most of the Li which diffuses to the grain boundaries or forms large particles observed at microcracks within the crystalline grains of the samples probably remains there as large particles or sheets, which may help to maintain the entity of some aged samples by effectively cementing the grains together.

$$\text{Li(s, bcc)} \longrightarrow \begin{pmatrix}\text{Grain Boundaries, Fissures,}\\ \text{or Diffusion Intermediates}\end{pmatrix} \longrightarrow \text{(Li in Free Volume)} \qquad (9')$$

The extent of loss of Li by Equation 9' is evidently less than the loss of He by Equation 9, and the latter estimate is more easily obtained from outgassing data.

From the He outgassing data it is found that less than 0.1% of the He produced by decay (Equation 2') is released before the maximum expansion rates are attained at 23°C (or 50°C), but after this the He-outgassing rate increases about 100-fold with 2 to 5% of the He released within 100 days after the maximum rate has been reached. These observations are coincident with the onset of cracking connected with the friable nature of the samples and with the increased scatter of measurement of Li metal ESR. Thus, the effects of impurity escape and recombination combine to reduce the 23°C growth rate below the value expected on a steady radiation-damage plus bcc Li metal-formation model discussed in Section 4.3.4.

The irregular increase in He-outgassing rate with increasing storage

time at 23° to 75°C indicates a continuing breakup of the crystal grains with gas released through the new fissures either directly or by diffusion through the enhanced crystal surface area of the samples. Following these continuing crystallite breakups, the He-evolution rates may increase another order of magnitude until as much as 10 or 15% or as little as 2% of the total He may be released in 800 days.

At the other extremes of temperature, more regular outgassing prevails. The low temperature samples (-7° and -22°C) have not fractured, and only 0.04% of the He contained in the sample stored at -7°C had escaped within 800 days. Although one expects that the He escape from samples stored at 300° and 400°C occurs by a more regular diffusion-controlled process than at the intermediate temperatures, the net path for crystalline diffusion is reduced by expanding the samples to a lower density. An increase in outgassing rate approximately paralleling expansion might be expected on this basis, and such increases in the 300° and 400°C outgassing rates are roughly observed.

The H_2 outgassing rates are affected by LiOH decomposition and by H_2 reaction with Li as the He-H_2 mixture passes over Li particles during the escape of gasses through fissures and grain boundaries. The changes in H_2/He ratio in the evolved gasses qualitatively reflect the changes in net radiation-damage yield with the age of different samples, but this ratio is not a reliable index of the magnitude of the yield itself. One reason for this is that most of the gas comes from fissures in which the H_2 has been subjected to recombination according to Equation 6.

It does not seem possible to draw quantitative conclusions regarding the effects of impurity escape, or specifically of He outgassing, on the net expansion of aged samples. The extent of the observed outgassing losses do seem large enough to account for the magnitude of some of the fluctuations in expansion rate observed for old samples.

4.3.7 Aged Samples

The concept that recombination cancels radiation damage in old samples and that a regular correlation exists between the state of stored decay products and the storage temperature was stimulated by the observation that a straight line could be drawn through 1000-day-average expansion rates as a function of temperature (Figure 21). An interpretation of this observation was sought on the basis that "aged" samples expand according to the net reaction:

$$LiT_{(c)} \xrightarrow{(x\square+\square-)} Li(s,bcc) + \underbrace{He(g,p)}_{\downarrow\ (He\ in\ Free\ Volume)} \qquad (10)$$

The volume required to store the decay products is represented by x vacancy pairs, and it could logically range from x = 0.28 ($\dot{E}$ = 0.002%/day) for He escaping at the decay rate, through x = 1.28 ($\dot{E}$ = 0.008%/day) according to Equations 2' to 5, and to x = 10 ($\dot{E}$ = 0.06%/day) from the estimated pressure of stored He gas in the 400°C sample after 1000 days.*

Although a condition of hydrostatic equilibrium may be obtained at 400°C, the brittle nature exhibited by the salt at 23°C makes it less likely that such considerations might control the expansion rate at this lower

*These assume conditions of approximately hydrostatic equilibrium for the stored gas in the samples stored at 400°C; the observed average rate of expansion for the 450- to 1000-day interval is $\dot{E}$ = 0.038%/day, which corresponds to an average loss of 50% of the He produced during this period, and this figure does not violently contradict expectations. The later rate of $\dot{E}$(1000) = 0.004%/day obtained at 400°C indicates a higher rate of outgassing if it is assumed that hydrostatic equilibrium is maintained.

temperature.* If the He gas were produced in hydrostatic equilibrium at the pressure calculated for the voids, the room temperature 1000-day expansion rate should be 0.027%/day compared to an observed rate of 0.014%/day. After 2000 days the rate drops to between 0.003 and 0.006%/day. The latter could be explained either as primarily the effect of decay (Equations 2' to 5) plus recombination (Equation 6) or as the effect of a large He outgassing rate on Equation 10. There is evidence for both explanations, but the NMR observation of a strong H_2 absorption in the 2000-day-old sample stored at 23°C proved that the criterion of complete recombination in "aged" samples is not fulfilled. Grinding experiments performed by T. Newton[98] on samples stored at 23°C for 128 days indicated that some of the He was contained in cavities as large as 2000 Å in average diameter. Other observations support the explanation that the cavities are neither spherical nor randomly distributed, but that they are probably small in one dimension and concentrated along dislocations or subgrain boundaries which serve as incipient cleavage planes.

4.3.8 Discussion

Ultimately, it is diffusion that plays the predominant role in controlling net radiation damage by: (1) supplying vacancy pairs to accommodate point defects produced by Equation 1", (2) controlling the rate of stabilization of point defects by aggregation, following Equations 3 and 4, (3) supplying vacancy pairs to allow the martensitic transformation of F-center aggregates into bcc Li metal according to Equation 5, and (4) finally allowing recombination

*The value of x given by Equation 10 may be calculated for a 1000-day-old sample stored at 23°C if it is assumed that the He gas contained in the 21.5% expanded volume is at a mean pressure of 425 atm. If a mean surface tension of 200 dynes/cm is assumed for LiH in spherical cavities, a mean cavity diameter of ~200 Å and a mean value of x = 4 is obtained.

and escape of defects to free surfaces. The importance of vacancy diffusion in controlling the expansion rates of samples stored at -7° to 125°C (presumably by the diffusion-controlled Reactions 1" through 5) is illustrated by Figure 21 in which a straight line through the "initial" or "maximum" expansion rates in the indicated temperature range has a slope of $0.5_5 \pm 0.1$ ev. This value is in agreement with the value 0.53 ev obtained for the activation energy for cation vacancy diffusion from electrical conductivity measurements. The agreement can be explained if vacancy pairs have essentially the same activation energy for diffusion as do cation vacancies in LiH, or if the mechanisms are controlled by a second step requiring the diffusion of the separated cation vacancy in case vacancy pairs are much more mobile than either single vacancy. It is not known whether vacancy pairs are generally less mobile than anion vacancies, as reported for NaCl,[59] or more mobile, as previously postulated.[63] In either case, the mechanism controlling the expansion of LiH crystals may involve dislocation motion or diffusion through dislocation networks, and it would then be rather complicated.

The application of a diffusion-controlled martensitic transformation according to Equation 5 together with ESR studies of bcc Li metal formation, using results of the type described in Section 3.5, led to suitable agreement with the 23°C expansion results for the first 500 days. To test the postulated correlation, log $\dot{E}$ was plotted against log S (the bcc Li ESR spin density). After the initial bcc Li metal nucleation period, a linear relation between the two variables was obtained. A linear plot of the concentration of bcc Li metal atoms, N_{Li}, versus the concentration of vacancy pairs introduced into the crystal, $N_{\boxed{+}\boxed{-}}$, was made by estimating a detection efficiency of 1.3% for the ESR measurements on a 23°C sample and using 17 $\mathring{A}^3$ per vacancy pair to calculate $N_{\boxed{+}\boxed{-}}$ from the 23°C expansion. A portion of the results is given in Figure 22, in which only half of the linear part of the

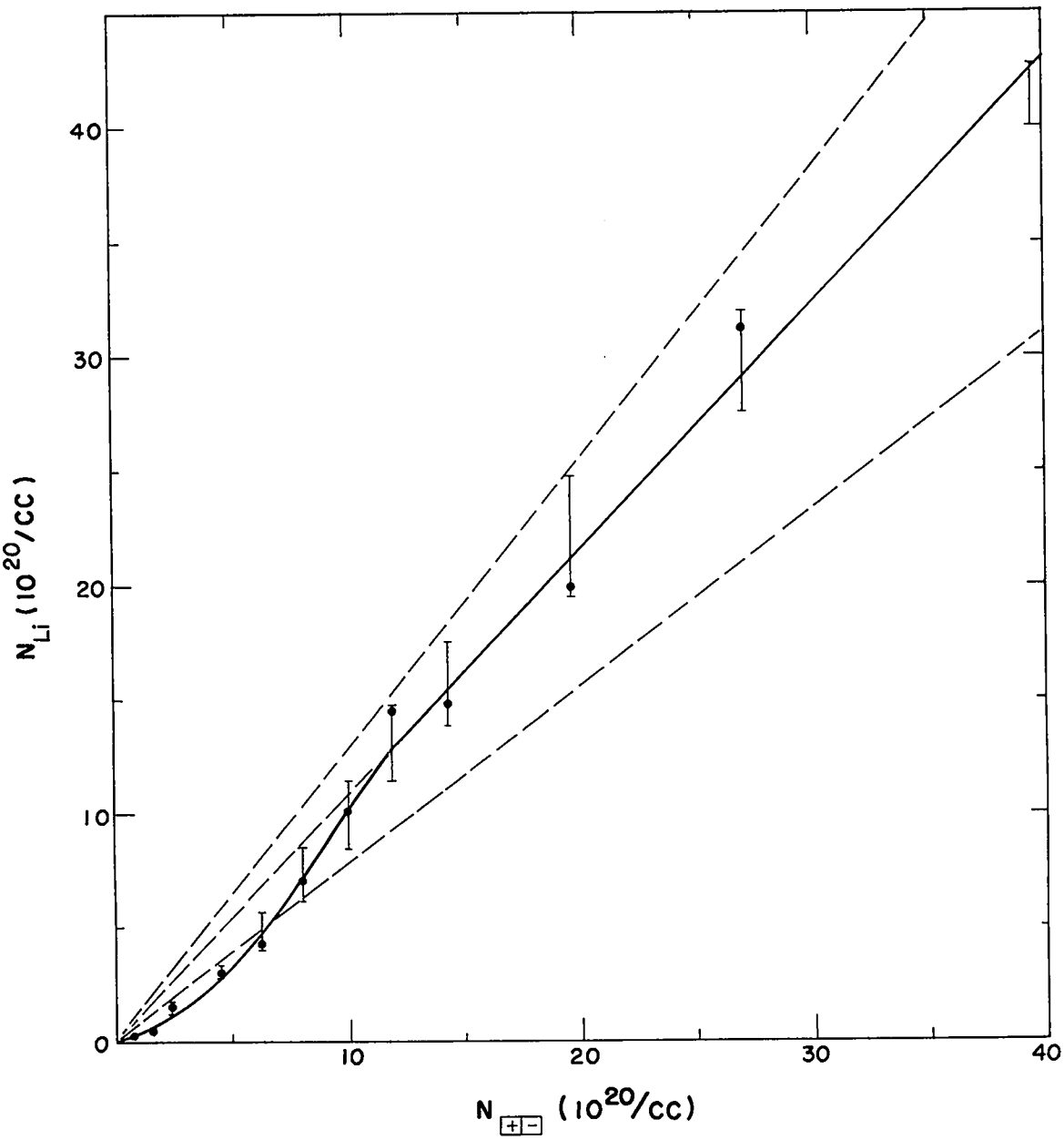

Fig. 22 Relation between the concentrations of bcc Li metal atoms and of vacancy pairs in LiH samples containing 40 mole % LiT stored at 23°C. $N_{Li} = 76S_{Li}$ was used to calculate the ordinate from the ESR bcc Li spin density, S_{Li}. $N_{[+|-]}$ was obtained from the expansion data. The bars through the points indicate the uncertainty of the ESR measurements.

curve is shown in order to illustrate better the deviation from linearity observed in the initial stages. Slopes were calculated assuming bcc Li metal formation by β decay alone (Equations 2' through 5) and radiation damage alone (Equations 1", 3, 4, and 5), and these are given for comparison with the observed slope of 1.08. This slope is only slightly less than that calculated for a radiation-damage yield of y = 2 which is estimated from the initial 23°C expansion rate (Section 4.3.3).

This yield was used to obtain an independent estimate of the rate of "total" F-center production (F centers plus aggregates), which enables one to compare the ESR data on the rate of formation of bcc Li metal in LiH containing LiT to the theory of the diffusion-limited growth of precipitate particles given by Ham.[99] Ham's equation can be written:

$$\ln \left(C_0/C\right) = \alpha t^n$$

where C_0 is the initial solute concentration in a supersaturated solid solution, C is the concentration of solute remaining in solution at any time t, α is a constant dependent upon the concentration of precipitate particles and concentrations and diffusion parameters controlling the rate of accumulation at the particles, and n is a parameter which depends upon the nature of the accumulation at the growing particles and is described by Ham in detail. The application of Ham's theory to the precipitation of Li in Ge is given by Reiss.[100] It was found that n = 3/2, indicating that spherical particles grow in Ge with low dislocation densities, whereas platelike particles are formed at high dislocation densities according to the finding that n = 1. To account for the steady production of "dissolved Li" in LiH containing LiT at 23°C by Equations 1", 2', 3, and 4, it was assumed that $C_0 = 5N_t\lambda t$ or 5 times the production of He^3 atoms by the T decay. The concentration of "dissolved Li" at any time, t, was obtained from C_0 by subtracting the amount

of bcc Li metal precipitated, N_{Li}, obtained from ESR results and the efficiency of detection. The resulting plot of $\log\left(C_0/C\right)$ vs t^n gave excellent agreement with n = 1 and with an equation of the form $\ln\left(C_0/C\right) = 4.6 \times 10^{-3} t$, with t given in days. This result is consistent with microscopic observations which have shown that Li particles in LiH tend to grow as sheets or discs in samples stored at 23°C. On the other hand, limited measurements of bcc Li metal growth in LiH samples stored at -196°C between observations agree better with n = 3/2 and with a regular spherical growth of particles after warming from this low temperature. Other characteristics indicate that the nature of the bcc Li particles formed in samples stored at low temperature may be different from Li produced in samples stored at 23°C. The ESR observations indicate greater line width and higher detection efficiency for particles produced in samples stored at -196°C. Evidently the bcc Li particles formed in samples stored at -196°C are of comparatively small size.

Thus it has been shown that the data for radiation-damaged LiH are consistent with a diffusion-controlled mechanism for expansion and bcc Li metal formation following the proposed mechanism. According to Equation 5, the diffusing entities which permit the transition of F-center aggregates into the less dense bcc Li metal are vacancies rather than Li atoms as in the case of Li in Ge.[100] Vacancy diffusion has also been shown to be valuable in explaining the temperature dependence of LiH expansion presented earlier in this section. The expansions calculated from the bcc Li concentrations found by ESR through the use of the model agree with the 23°C expansions observed during the first 500 days, as noted in Section 4.3.4. Therefore, the model for radiation damage to LiH containing LiT meets this test for internal consistency.

Since we have introduced the subject of radiation damage in LiH by

comparison to various studies made on neutron-irradiated LiF, we conclude by intercomparing radiation damage to these two materials in more detail. In Figure 23 the LiF expansion data obtained by Spaepen[41] for crystals irradiated at 80°C and by Senio and Tucker[42] for samples irradiated at 30° and 185°C are compared to the expansion of LiH samples containing 40 mole % LiT stored at -22°to 75°C. The initial rapid rise and plateau observed by Spaepen at 80°C has already been compared to the X-ray expansion measurements by Willis and Smallman in Section 4.2, and similar X-ray expansion measurements by Senio and Tucker on LiF irradiated at 30° and 185°C are illustrated in Figure 23 against an expanded ordinate scale. All of the results indicate that the expansion caused by interstitial defects in LiF reaches a maximum at 0.4 to 0.6% expansion or about 3×10^{20} defects/cc. This is somewhat greater than the maximum concentration of point defects observed in LiH. Figure 14 illustrates why LiH crystals expand in a comparatively regular fashion near the origin and do not exhibit a step in the expansion curve similar to LiF crystals which expand by a reversible radiation-damage process. After the step in the LiF expansion data, there is a general agreement between the 80°C LiF curve and the 75°C LiH curve, and between the 30°C LiF curve and the 23°C LiH curve, which supports the intercomparison of the samples by equating a dose of 10^{17} n/cm^2 to 6.45 days for a sample containing 40 mole % LiT. The very low expansion observed by Senio and Tucker at 185°C can be accounted for if rapid recombination of point defects generated by the Li^6 fission fragments is assumed (somewhat like the low LiH expansion at 300°C), so that the net yield of stabilized radiation-damage products is also low.

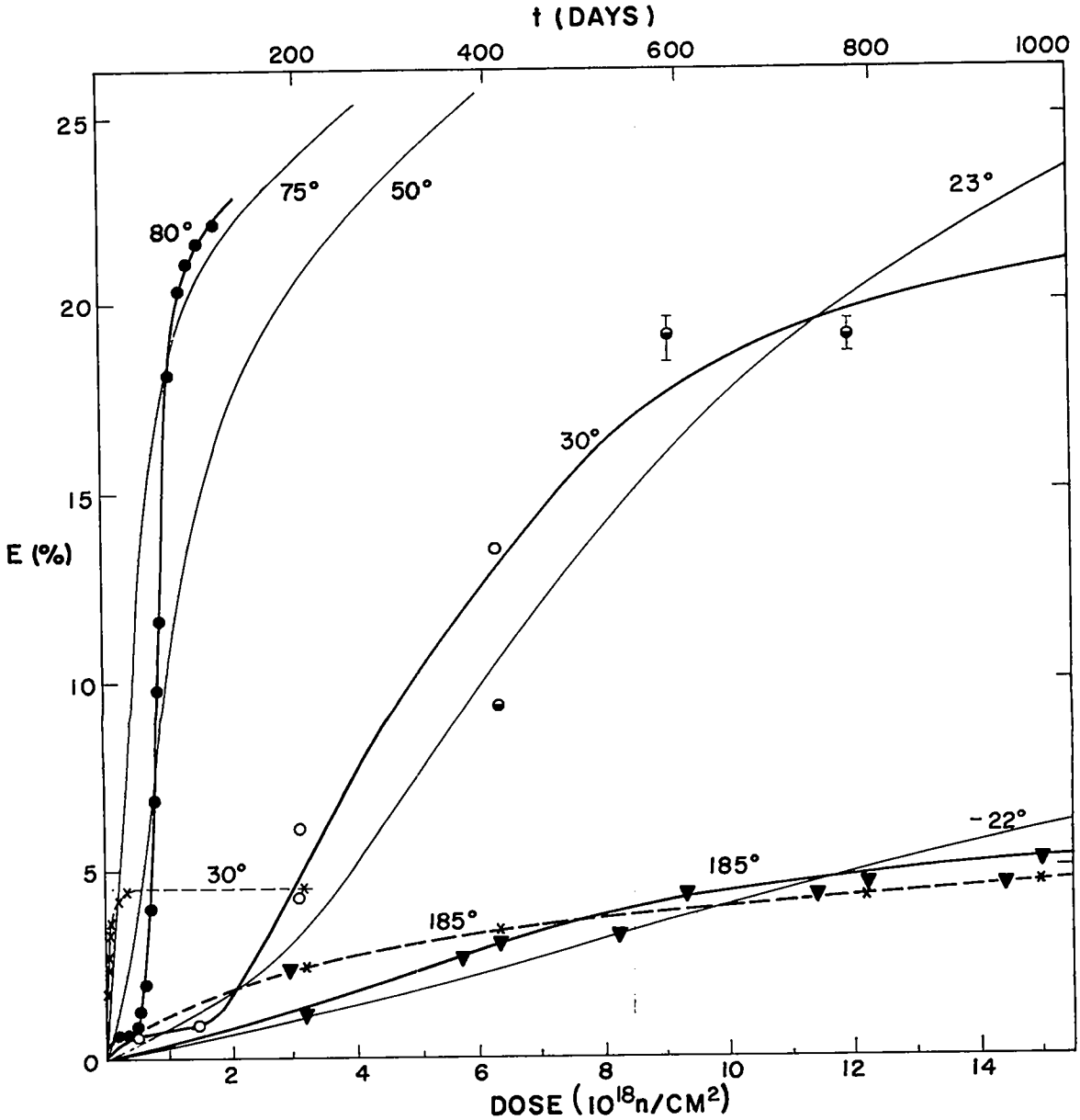

Fig. 23 The expansion of neutron-irradiated LiF compared to LiH samples containing 40 mole % LiT: (●) LiF volume expansion at 80°C (Spaepen[41]); (○) and (◒) LiF volume expansion at 30°C of single crystals and pressed pellets (Senio and Tucker[42]); (▼) LiF volume expansion at 185°C[42]; (X) LiF X-ray lattice expansion at 30° and 185°C plotted to 10X scale.[42] Weaker curves show LiH expansion results in the -22° to 75°C temperature range.

APPENDIX A

CALCULATED PROPERTIES OF LATTICE DEFECTS

A.1 Vacancies

The volume of a vacancy pair is estimated from the volume of an ion pair plus the distortion of the ions around the vacant lattice sites. This distortion reduces the volume in the case of metals, but it increases the vacancy volume in the case of ionic crystals because of the charge repulsion between the nearest-neighbor ions of the vacancies.[101] This increase in vacancy volume is of the order of 10% of the volume of the replaced ion. Activation volumes for ionic transport are even larger,[102] but the reverse displacement polarization of ions of opposite charge to the missing ion reduces the apparent vacancy volume at larger distances, and the net volume increase observed in radiation-damage studies is expected to be closer to the ion pair volume. Thus the expansion rate of $0.006_7 \pm 0.0004$%/day observed for LiH containing 40% LiT, calculated on the assumption of Equation 2', corresponds to a volume of $16._9 \pm 1.0$ Å^3/vacancy pair compared to 16.8 Å^3/ion pair calculated from the LiD parameters given in Table 1. This result is in satisfactory agreement with the model.

A.2 Interstitials

The crystal expansion caused by interstitial lattice defects is directly

related to the lattice strain as has been demonstrated to within 6% for neutron-irradiated LiF.[91] For a homogeneous random distribution of interstitials, calculations based on the elastic continuum model have demonstrated the equivalence of the average lattice expansion and the geometrical crystal expansion.[103] Both are dependent on the product of the interstitial concentration and on an average lattice expansion per interstitial. A detailed calculation of the expansion per interstitial defect would be extremely complex, and it would involve more detailed knowledge than we possess of such parameters as ionic sizes, repulsion potentials, and polarization. The lattice would expand to the parameter corresponding to the spacing of the displaced ions adjacent to the interstitial if perfect symmetry of hard-sphere ions were maintained; but this extreme is avoided by elastic displacements of the ions at some distance from the defect, and by compression of ions neighboring the interstitial in the direction of the strain axes, with displacements normal to the strain axes to occupy some of the extra volume created by displacements away from the defect. As expected, this relaxation is also greater in the case of metals such as Cu than in ionic crystals such as the alkali halides.[2] Eshelby estimated that nearly 90% of the strain energy is contained within $2r_o$ of the defect; the entire expansion occurs in the immediate neighborhood of the imperfection with the extra volume transmitted to the surface by elastic displacements of the type $\vec{u} = c\left(\vec{r}/r^3\right)$.[104]

The simplified calculation used here to estimate the average volume increase per interstitial defect equates this expansion with that of the shell of nearest neighbor ions (1/8 of NaCl unit cell) to the interstitial.

This model is illustrated in Figure A.1.

From the difference between one-half body diagonal and the anion radius for LiH, it is found that a sphere of 0.41 Å radius could fit into the tetrahedral vacancy at the center of the cube without distortion. The radius of a He atom is estimated as 0.93 to 1.01 Å, depending on the coordination number,[87,88] so that the neighboring H^- ions must be displaced 0.52 to 0.60 Å outwards to accommodate a He atom in the interstitial position. The associated volume increase is therefore 10 to 12 $Å^3$ per interstitial He atom in LiH. This result is in surprisingly good agreement with the observed value 12.4 ± 0.6 $Å^3/\beta$ decay (see Section 3.6) considering the very crude nature of the calculation. This result corresponds to an expansion that is three times the volume of the interstitial atom compared to expected values of one to five times the volume of the interstitial atom.[2] Corresponding results of calculations for an interstitial (spherical) H_2 molecule with 1.30 to 1.36 Å radius give 21 to 23 $Å^3$ per interstitial H_2 in LiH, which

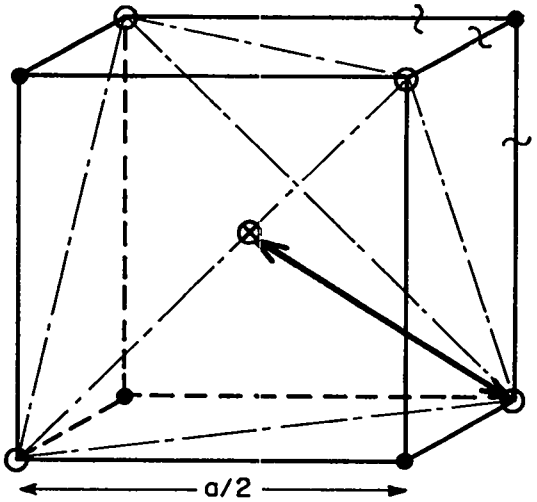

Fig. A.1 An interstitial atom ⊗ in a simple cube of a NaCl-type crystal lattice causing outward displacements ⟷ of the tetrahedron of four neighboring anions ○ in the directions of the body diagonals. The four neighboring cations ● are assumed to also expand to maintain the symmetry of the cube in going from $\frac{1}{2}a_o$ to $\frac{1}{2}a_d$ on the side. The jagged lines indicate the approximate positions of anion-cation contact in LiH.

is quite large compared to 1.2 $\mathring{A}^3$ per interstitial H atom calculated from the small, 0.52 $\mathring{A}$, size of the H atom.

A.3 Interstitial Ions

The calculation of the displacement caused by an interstitial ion is a little more complicated than for a neutral atom because the presence of the interstitial charge results in polarization of the surrounding lattice ions. For simplicity it has been assumed that the net effect of polarization displacements cancels out at distances affecting the measurements, although they may be significant in the immediate neighborhood of the defect. The model illustrated by Figure A.1 was used to calculate the volume expansion per interstitial anion in LiH, LiF, and NaCl, and the results are presented in Table A.1. The anion radii used were mostly taken from Zachariasen's table given by Kittel[88] for coordination numbers 6 and 8.

Table A.1 Calculated Expansion Per Interstitial Anion Defect

Quantity	LiH	LiF	NaCl
$\frac{1}{2}a_o$ ($\mathring{A}$)	2.042	2.014	2.820
r_- ($\mathring{A}$)	1.36 - 1.44	1.33 - 1.41	1.81 - 1.89
Void Radius ($\mathring{A}$)	0.41	0.41	0.63
Displacement ($\mathring{A}$)	0.95 - 1.03	0.92 - 1.00	1.18 - 1.26
$V = \left(\frac{1}{2}a_d\right)^3 \left(\mathring{A}^3\right)$	31.0 - 33.7	30.7 - 31.7	74.6 - 80.6
$V_0 = \left(\frac{1}{2}a_o\right)^3 \left(\mathring{A}^3\right)$	8.5	8.2	22.4
$E = V - V_0 \left(\mathring{A}^3\right)$	22.5 - 25.2	22.3 - 23.5	52 - 58

The expansion per interstitial Cl^- ion in NaCl seems small compared to the lattice expansion of β-irradiated NaCl powder, but it is of the right order of magnitude, and the result can be made consistent with the experiment if the

net yield of Frenkel defects in NaCl is assumed to be high. The expansions per interstitial anion in Table A.1 are all slightly larger than the ion-pair volume in the corresponding salt, and they are about two times the volume of the interstitial ion used in the calculation.

A.4 Stability of Interstitial Anions

In this section the relative stability of interstitial anions, which may be formed by the recombination of radiation-damage products at low temperatures, is estimated by approximate energy calculations for LiH, LiF, and NaCl. Calculations for the recombination of X_2 molecules (V_1 centers) with a pair of F centers are carried out for all three salts, and calculations for the recombination of an H center with an F center are made for the alkali halides. The net reactions are:

$$\boxed{X_2}_{(c)} + 2\boxed{e^-}_{(c)} \longrightarrow \boxed{X^-}_{(c)} + \left(X^-\right)_{(i)} + 2\boxed{-}_{(c)} \quad \ldots \qquad (A.1)$$

$$\boxed{X_2^-}_{(c)} + \boxed{e^-}_{(c)} \longrightarrow \boxed{X^-}_{(c)} + \left(X^-\right)_{(i)} + \boxed{-}_{(c)} \quad \ldots \qquad (A.2)$$

For the purposes of calculation, the net reactions are divided into two major steps with the first step in each case requiring the photo-ionization of the F center. It has been assumed that the energy required to transfer the electron into the conduction band is 0.5 ev greater than the energy of the F-band maximum for each salt.[51,63,89] Step A:

$$\boxed{e^-}_{(c)} \longrightarrow \boxed{-}_{(c)} + e^-_{(c)} \qquad E_A = E_F + 0.5 \text{ ev.}$$

The second step is far more difficult because it involves the energies of processes that are known only for the gas phase, and the distortion energy involved in forming the interstitial anion. For Reaction A.1 the second step

was estimated as follows in Step B:

$$\boxed{X_2}_{(c)} + 2e^-_{(c)} \longrightarrow X_{2(g)} + 2e^-_{(g)} + \boxed{-}_{(c)} \qquad E \sim 0$$

$$X_{2(g)} \longrightarrow 2X_{(g)} \qquad E = E(\text{diss})^{(105)}$$

$$2X_{(g)} + 2e^-_{(g)} \longrightarrow 2X^-_{(g)} \qquad E = 2E(\text{e.a.})^{(106)}$$

$$X^-_{(g)} + \boxed{-}_{(c)} \longrightarrow \boxed{X^-}_{(c)} \qquad E \approx \tfrac{1}{2}\phi - P$$

$$X^-_{(g)} \longrightarrow (X^-)_{(i)} \qquad E \approx E(\text{displ}) + P'$$

$$\boxed{X_2}_{(c)} + 2e^-_{(c)} \longrightarrow \boxed{X^-}_{(c)} + (X^-)_{(i)} \qquad E_B' \approx E(\text{diss}) + 2E(\text{e.a.}) + \tfrac{1}{2}\phi + E(\text{displ})$$

The energy for the first step was estimated by assuming negligible distortion around the molecule in the anion site and neglecting the difference between the conduction band and the vacuum level. The dissociation energy and electron affinities required for the second and third steps are available for the gas phase from the references.[105,106] The energy of placing an anion in the vacant site in the fourth step is estimated as one-half the lattice energy of the crystal per ion pair $\frac{1}{2}\phi$ minus the polarization energy of the anion vacancy P. The displacement energy is very crudely estimated as equal to the change in electrostatic energy of the neighbors to the interstitial in expanding to the configuration illustrated in Figure A.1 with the total repulsive energy assumed constant. If each interaction between the eight ions of Figure A.1 is counted once, the estimated displacement energy becomes $E(\text{displ}) \approx (0.870)(4e^2/a_o)(a_d - a_o)/a_d \approx 0.870(4\phi_e/\alpha)(a_d - a_o)/a_d$, where the numerical factor is obtained from the symmetry of the ions, the symbols

ϕ_e and α refer to electrostatic energy per ion pair in the crystal and the Madelung term, respectively, and the values a_o and a_d are taken from Table A-1. Other electrostatic interactions between the interstitial ion and the lattice ions cancel except for the polarization term P' which, for simplicity, was assumed to be approximately equal to the polarization energy of the vacant lattice point P. The results of these calculations are summarized in Table A.2.

Table A.2 Energy Relations for the Recombination of Color Centers (ev)

Reaction A.1		LiH	LiF	NaCl
Step A:	$E_A = 2(E_F + 0.5)$	5.8	10.8	6.2
Step B:	$E_B = E(\text{diss}) + 2E(\text{e.a.}) + \frac{1}{2}\phi + E(\text{displ})$			
	$E(\text{diss})$	4.52	1.64	2.52
	$2E(\text{e.a.})$	-1.46	-7.12	-7.44
	$\frac{1}{2}\phi$	-4.7_2	-5.3_0	-4.0_1
	$E(\text{displ})$	~8.1	~9.1	~6.0
	$E_B \approx$	+6.4	-1.7	-2.9
Reaction A.1:	$E_1 = E_A + E_B \approx$	+12.2	+9.1	+3.3

Reaction A.2		LiF	NaCl
Step A:	$E_A = E_F + 0.5$	5.4	3.1
Step B:	$E_B = E''(\text{diss}) + E(\text{e.a.}) + E(\text{displ}) + P' - E'(\text{displ})$		
	$= E(\text{diss}) + 2E(\text{e.a.}) + \frac{1}{2}\phi + E(\text{displ})$		
	$E''(\text{diss}) = E(\text{diss}) + E(\text{e.a.})$	-2.0	-1.2
	$P^{(101)}$	~-1.2	-1.2
	$E'(\text{displ}) \approx P - \frac{1}{2}\phi$	+4.1	+2.8
	$E_B \approx$	-1.7	-2.9
Reaction A.2:	$E_2 = E_A + E_B \approx$	+3.7	+0.2

The second step of Reaction A.2 is still harder to estimate because it involves more unknown quantities. They can be broken down as follows:

Reaction A.2, Step B:

$$\boxed{X_2^-}_{(c)} + e^-_{(c)} \longrightarrow X_{2(g)}^- + e^-_{(g)} + \boxed{-}_{(c)} \qquad E \approx -\tfrac{1}{2}\phi - E'(\text{displ}) + P$$

$$X_{2(g)}^- \longrightarrow X_{(g)}^- + X_{(g)} \qquad E = E''(\text{diss})$$

$$X_{(g)} + e^-_{(g)} \longrightarrow X_{(g)}^- \qquad E = E(\text{e.a.})$$

$$X_{(g)}^- + \boxed{-}_{(c)} \longrightarrow \boxed{X^-}_{(c)} \qquad E \approx \tfrac{1}{2}\phi - P$$

$$X_{(g)}^- \longrightarrow \textcircled{X^-}_{(i)} \qquad E \approx E(\text{displ}) + P'$$

$$X_{2\,(c)}^- + e^-_{(c)} \longrightarrow \boxed{X^-}_{(c)} + \textcircled{X^-}_{(i)} \qquad E_B \approx E''(\text{diss}) + E(\text{e.a.}) + E(\text{displ}) - E'(\text{displ}) + P'$$

The properties of the X_2^- ion in the anion site are assumed to be similar to those of an X^- ion except for the extra distortion indicated by the interactions with two next-neighbor X^- ions deduced from the ESR spectra of the H center.[55] The probable value of E'(displ) has been assumed to be $\frac{1}{2}$E(displ) calculated before for the interstitial anion. Since gaseous X_2^- ions have not been observed, it is assumed that the most probable value for E'' is less than or equal to zero, and it is certainly less than $\frac{1}{2}$E(diss), the binding energy for a H atom in a H_2 molecule. As before, the value for the polarization energy associated with an interstitial anion P' is assumed to be equal to the polarization energy of an anion vacancy P which has been calculated by Mott and Littleton for NaCl.[101]

An alternative path may be used to estimate the energy change in Step B of Reaction A.2.

$$\boxed{X_2^-}_{(c)} + e^-_{(c)} \longrightarrow X_{2(g)} + 2e^-_{(g)} + \boxed{-}_{(c)} \qquad E \approx -\tfrac{1}{2}\phi - E'(\text{displ}) + P \approx 0$$

$$X_{2(g)} \longrightarrow 2X_{(g)} \qquad E = E(\text{diss})$$

$$2X_{(g)} + 2e^-_{(g)} \longrightarrow 2X^-_{(g)} \qquad E = 2E(\text{e.a.})$$

$$X^-_{(g)} + \boxed{-}_{(c)} \longrightarrow \boxed{X^-}_{(c)} \qquad E \approx \tfrac{1}{2}\phi - P$$

$$X^-_{(g)} \longrightarrow \left(X^-\right)_{(i)} \qquad E \approx E(\text{displ}) + P'$$

$$\boxed{X_2^-}_{(c)} + e^-_{(c)} \longrightarrow \boxed{X^-}_{(c)} + \left(X^-\right)_{(i)} \qquad E_B \approx E(\text{diss}) + 2E(\text{e.a.}) + \tfrac{1}{2}\phi + E(\text{displ})$$

The net result is the same as for Step B of Reaction A.1. The evaluation of the energy for the modified first step comes from the observation that H centers decompose spontaneously at -173°C in LiF (and presumably similarly in NaCl) with the release of electrons into the conduction band.[107] Therefore the energy for the process $\boxed{X_2^-}_{(c)} \longrightarrow \boxed{X_2}_{(c)} + e^-_{(c)}$ is from 0 to 0.1 ev. This is the same as the energy for the first step if the energy change represented by the first step of Reaction A.1, Step B, is still taken as zero. From an intercomparison of the two paths presented for Step B of Reaction A.2, two properties of the X_2^- ion may be estimated: (1) The displacement energy of the H center is approximately $E'(\text{displ}) \approx P - \tfrac{1}{2}\phi$. (2) The dissociation energy of a gaseous X_2^- molecule ion is approximately $E''(\text{diss}) \approx E(\text{diss}) + E(\text{e.a.})$.

The results of the calculations for Step A and Step B of Reaction A.1 for LiH, LiF, and NaCl are contained in the first part of Table A.2. The results of similar calculations for the major steps of Reaction A.2 are also listed for LiF and NaCl, along with the approximate calculations of E'(displ) and E''(diss) outlined in the preceding paragraph.

It is possible to draw some conclusions from the results given in Table A.2, as long as the approximate nature of the calculations used is not forgotten and comparisons of the conclusions with other experimental observations are made. From the values for Step B of Reaction A.1 it appears evident that interstitial H^- ions in LiH are unstable compared to the corresponding anions formed in LiF and NaCl. This is consistent with the lattice expansion results on mixed powders discussed in Sections 3.6 and 4.1 which indicate that interstitial Cl^- ions were formed in the NaCl, but that only interstitial He atoms occurred in the LiH powder containing LiT. The energetics favor the formation of a mobile hole (H atom) as a possible intermediate when the first electron is trapped at a $\boxed{H_2}_{(c)}$ center in LiH, and if this eventually combines with an anion vacancy, or a defect that can supply a vacancy, and another electron, the recombination process can be completed without forming an interstitial.

From the examples under consideration, it appears that interstitial anions could be most readily formed by the recombination of F and H centers in NaCl. Some mechanism like that proposed here is required to account for the lattice expansion observed in NaCl exposed to β particles from LiT, because the energy required for direct displacements of Na^+ ions is about 25 ev compared to 1.7 ev maximum energy acquired by collision with an 18 kev electron.[2, 3] This was not true in the case of neutron-irradiated LiF[91] for which the displacement mechanism could account for the concentration of interstitials observed.[2]

APPENDIX B

PRECIPITATE DISTRIBUTION

No microscopic observations of Li colloid precipitated in relatively clear crystals of LiH have been made, but the decoration of various planes inside clear LiH crystal with precipitated Cu has been observed. This result is presented as some small justification for the assumption that the precipitation of Li colloid in LiH is comparable at some stages to the decoration of alkali halides with alkali or noble metals.[96] The Cu precipitate came from metal which was included with the Li metal before the synthesis of the crystal; it evidently dissolved as a hydride in the molten LiH and precipitated in bands as the single crystal grew. These bands of Cu precipitate appeared periodically throughout the length of the crystal with a common primary orientation relative to the axis of the crystal.

The Cu distribution in a thin plate cleaved from the LiH crystal is illustrated in the photograph of Figure B.1. The approximate identifications of the planes bearing the Cu precipitate "feathers" are given on the photograph, as well as the directions of the intersections of these planes with the upper cleavage surface of the LiH crystal. The orientation of the various cleavage faces of the LiH crystal are also indicated. The figure shows a predominance of bands oriented parallel to the $(\bar{1}1\bar{1})$ plane, although a complementary band in the $(11\bar{1})$ plane is shown in the center of the figure.

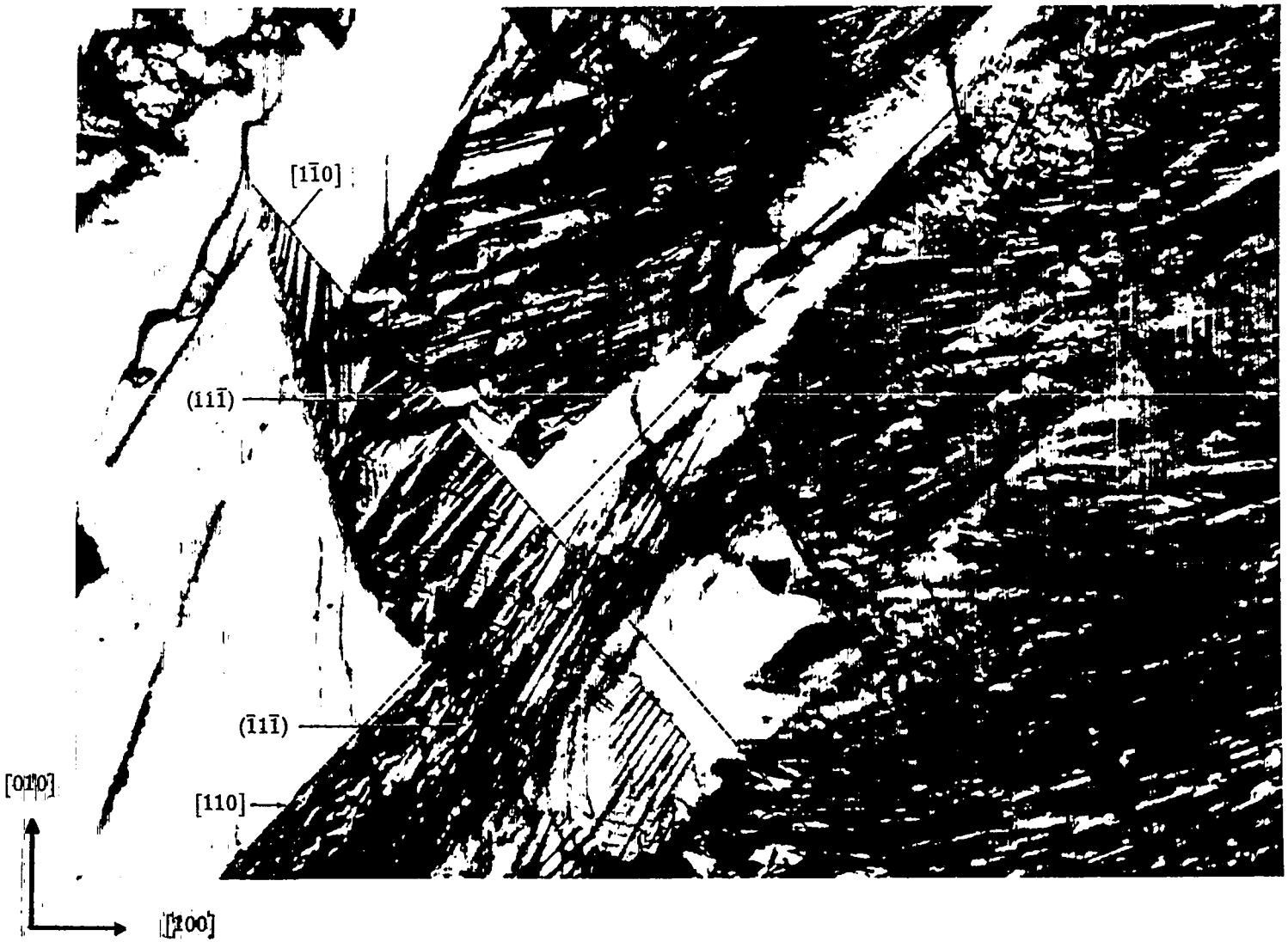

Fig. B.1 Precipitated Cu in LiH. Photographed by J. M. Wellnitz, H-4. (Approximately 60X)

REFERENCES

(1) W. M. Jones, Phys. Rev. 100, 124 (1955); and G. H. Jenks, F. H. Sweeton, and J. A. Ghormley, Phys. Rev. 80, 990 (1950)

(2) F. Seitz and J. S. Koehler, Solid State Phys. 2, 308 (1956)

(3) G. J. Dienes and G. H. Vineyard, Radiation Effects in Solids, Interscience, New York (1957)

(4) J. J. Harwood et al., (ed.), The Effects of Radiation on Materials, Reinhold, New York (1958)

(5) E. A. Hylleraas, Z. Physik 63, 771 (1930)

(6) D. H. Ewing and F. Seitz, Phys. Rev. 50, 760 (1936)

(7) S. O. Lundqvist, Arkiv Fysik 8, 177 (1954)

(8) P. O. Löwdin, Advances in Phys. 5, No. 17 (1956)

(9) A. Morita and K. Takahashi, Progr. Theoret. Phys. 19, 257 (1958)

(10) E. C. Baughan, Trans. Faraday Soc. 55, 736 (1959)

(11) J. Kasarnowsky, Z. Physik 61, 236 (1930)

(12) G. Herzberg, Spectra of Diatomic Molecules (2nd Ed.), pp. 375-7, Van Nostrand, New York (1950)

(13) L. Pauling, The Nature of the Chemical Bond, pp. 64-73, Cornell University Press, Ithaca (1940)

(14) M. S. Ahmed, Phil. Mag. 42, 997 (1950)

(15) J. M. Bijvoet and K. Lonsdale, Phil. Mag. 44, 204 (1953)

(16) I. Waller and S. O. Lundqvist, Arkiv Fysik 7, 121 (1952)

(17) F. E. Pretzel, G. N. Rupert, C. L. Mader, E. K. Storms, G. V. Gritton, and C. C. Rushing, J. Phys. Chem. Solids 16, 10 (1960)

(18) International Table of Atomic Weights (1956)

(19) E. Staritsky and D. J. Walker, J. Anal. Chem. 28, 1055 (1956)

(20) H. E. Swanson and E. Tatge, J. C. Fel. Reports, NBS (1949); and H. E. Swanson and R. K. Fuyat, Nat. Bur. Standards Circ. 539, II, 41 (1953)

(21) Handbook of Chemistry and Physics (39th Ed.), Chemical Rubber Publishing Co., Cleveland (1957)

(22) T. R. P. Gibb, Jr., and C. E. Messer, Tufts University Report NYO-3957 (May 2, 1954); and Tufts University Report NYO-8022 (Aug. 31, 1957)

(23) International Critical Tables, McGraw-Hill, New York (1926-33)

(24) I. R. Tannenbaum and F. H. Ellinger, Los Alamos Scientific Laboratory Report LAMS-1650 (March 4, 1954)

(25) A. Zalkin, Lawrence Radiation Laboratory, Livermore, Report UCRL-4239 (Nov. 16, 1953)

(26) H. Laquer, Los Alamos Scientific Laboratory Report LA-1505 (AECD-3706) (Dec. 9, 1952)

(27) S. S. Ballard, L. S. Combes, and K. A. McCarthy, J. Opt. Soc. Am. 41, 772 (1951)

(28) F. Birch (ed.), Handbook of Physical Constants, Geological Society of America, New York (1942)

(29) A. P. Ubbelohde, Trans. Faraday Soc. 32, 526 (1936)

(30) C. K. Stambaugh and P. M. Harris, Phys. Rev. 86, 651 (1952)

(31) D. L. Martin, Phil. Mag. 46, 751 (1953)

(32) C. E. Messer, E. B. Damon, P. C. Maybury, J. Mellor, and R. A. Seales, J. Phys. Chem. 62, 220 (1958)

(33) American Institute of Physics Handbook, McGraw-Hill, New York (1957)

(34) S. R. Gunn and L. G. Green, J. Am. Chem. Soc. 80, 4782 (1958)

(35) D. F. C. Morris, Acta Cryst. 9 (Part 2), 197 (1956)

(36) J. Sherman, Chem. Rev. 11, 93 (1932)

(37) Y. Haven, Rec. trav. chim. 69, 1471 (1950)

(38) C. P. Bean, Thesis, University of Illinois, Urbana (1952)

(39) K. Höjendahl, Kgl. Danske Viderskab. Selskab. Mat. Fys. Medd. 16, No. 2 (1938); and N. F. Mott and R. W. Gurney, Electronic Processes in Ionic Crystals, p. 12, Oxford, London (1940)

(40) Z. Gyulai, Z. Physik 46, 80 (1928)

(41) J. Spaepen, Phys. Rev. Letters 1, 281 (1958)

(42) P. Senio and C. W. Tucker, Jr., Knolls Atomic Power Laboratory Report KAPL-1727 (June 25, 1957)

(43) H. L. Anderson, Phys. Rev. 76, 1460 (1949)

(44) M. P. Klein and W. Ramsey, Lawrence Radiation Laboratory Progress Report, Livermore, UCRL-4500, p. 17 (May 5, 1955) (classified)

(45) M. Gueron and Ch. Ryter, Phys. Rev. Letters 3, 338 (1959); and P. J. Ring, J. G. O'Keefe, and P. J. Bray, Phys. Rev. Letters 1, 453 (1958)

(46) D. Hull and H. M. Rosenberg, Phil. Mag. Series 8, 4, 303 (1959); and C. S. Barrett, Phys. Rev. 72, 245 (1947)

(47) M. Lambert and A. Guinier, Compt. rend. 246, 1678 (1958)

(48) Y. W. Kim, R. Kaplan, and P. J. Bray, Phys. Rev. 117, 740 (1960)

(49) H. F. Ivey, Phys. Rev. 72, 341 (1947)

(50) M. Levy, Nature 177, 241 (1956)

(51) F. E. Pretzel and C. C. Rushing, J. Phys. Chem. Solids 17, 232 (1961)

(52) A. F. Kip, C. Kittel, R. A. Levy, and A. M. Portis, Phys. Rev. 91, 1066 (1953)

(53) N. W. Lord, Phys. Rev. 105, 756 (1957)

(54) W. B. Lewis and F. E. Pretzel, J. Phys. Chem. Solids 19, 139 (1961)

(55) W. Känzig and T. O. Woodruff, J. Phys. Chem. Solids 9, 70 (1959)

(56) C. J. Delbecq, B. Smaller, and P. H. Yuster, Phys. Rev. 111, 1235 (1958)

(57) K. Moers, Z. anorg. u. allgem. Chem. 113, 179 (1920)

(58) E. A. Giess, Thesis, Alfred University, Alfred, N. Y. (1958)

(59) N. Laurance, Phys. Rev. 120, 57 (1960)

(60) G. W. Barr, I. M. Hoodless, J. A. Morrison, and R. Rudham, Trans. Faraday Soc. 56, 697 (1960)

(61) J. F. Laurent and J. Benard, Compt. rend. 241, 1204 (1955); and F. Noyer and J. F. Laurent, Compt. rend. 242, 3068 (1956)

(62) T. J. Gray, 1959 International Symposium on Color Centers, Corvallis, Oregon

(63) F. Seitz, Rev. Modern Phys. 26, 7 (1954)

(64) J. H. de Boer, Rec. trav. chim. 56, 301 (1937)

(65) G. Feher, Phys. Rev. 105, 1122 (1957)

(66) C. Z. van Doorn, Philips Res. Rep. 12, 309 (1957)

(67) J. Lambe and W. D. Compton, Phys. Rev. 106, 684 (1957)

(68) H. Pick, Z. Physik 159, 69 (1960)

(69) E. J. West and W. D. Compton, Phys. Rev. 108, 576 (1957)

(70) T. O. Woodruff and W. Känzig, J. Phys. Chem. Solids 5, 268 (1958)

(71) W. Känzig, Phys. Rev. Letters 4, 117 (1960)

(72) W. Känzig and T. O. Woodruff, Phys. Rev. 109, 220 (1958)

(73) M. H. Cohen, W. Känzig, and T. O. Woodruff, Phys. Rev. 108, 1096 (1957)

(74) B. S. Gourary and F. J. Adrian, Solid State Phys. 10, 128 (1960)

(75) Lan-Ying Lin, Phys. Rev. 102, 968 (1956)

(76) H. W. Etzel, Phys. Rev. 100, 1643 (1955)

(77) I. L. Mador, R. F. Wallis, M. C. Williams, and R. C. Herman, Phys. Rev. 96, 617 (1954)

(78) R. B. Gordon and A. S. Nowick, Phys. Rev. 101, 977 (1956); and A. S. Nowick, Phys. Rev. 111, 16 (1958)

(79) R. T. Bate and C. V. Heer, J. Phys. Chem. Solids 7, 14 (1958)

(80) C. R. Berry, Phys. Rev. 98, 934 (1955)

(81) W. Primak, C. J. Delbecq, and P. H. Yuster, Phys. Rev. 98, 1708 (1955)

(82) D. A. Wiegand and R. Smoluchowski, Phys. Rev. 110, 991 (1958)

(83) J. H. O. Varley, Nature 174, 886 (1954)

(84) C. C. Klick, Phys. Rev. 120, 760 (1960)

(85) R. Rüchardt, Phys. Rev. 103, 873 (1956); and Z. Physik 140, 574 (1955)

(86) J. W. Corbett and R. M. Walker, Phys. Rev. 115, 67 (1959)

(87) L. Pauling, The Nature of the Chemical Bond, pp. 352-63, Cornell University Press, Ithaca (1940)

(88) C. Kittel, Introduction to Solid State Physics, p. 40, John Wiley, New York (1953)

(89) P. Pringsheim and P. H. Yuster, J. Chem. Phys. 18, 293 (1950); and C. J. Delbecq and P. H. Yuster, J. Chem. Phys. 21, 794 (1953)

(90) F. F. Morehead and F. Daniels, J. Chem. Phys. 27, 1318 (1957)

(91) D. Binder and W. J. Sturm, Phys. Rev. 96, 1519 (1954); and Phys. Rev. 107, 106 (1957)

(92) B. T. M. Willis and R. E. Smallman, UKAEA, Report AERE M/R 2266 (May 1957); and Phil. Mag. 2, 1018 (1957)

(93) J. J. Gilman and W. G. Johnston, J. Appl. Phys. 29, 877 (1958)

(94) M. Lambert and A. Guinier, Compt. rend. 245, 526 (1957)

(95) P. Senio, Science 126, 208 (1957)

(96) S. Amelinckx, Phil. Mag., Series 8, 1, 269 (1956)

(97) L. G. Schulz, J. Chem. Phys. 18, 996 (1950); and Acta Cryst. 4, 483 (1951)

(98) T. Newton, Los Alamos Scientific Laboratory Internal Document

(99) F. S. Ham, J. Appl. Phys. 30, 1518 (1959)

(100) H. Reiss, J. Appl. Phys. 30, 1141 (1959)

(101) N. F. Mott and M. J. Littleton, Trans. Faraday Soc. 34, 485 (1938)

(102) W. Biermann, Z. Physik Chem. nf25, 253 (1960)

(103) J. D. Eshelby, Solid State Phys. 3, 79 (1956)

(104) J. D. Eshelby, J. Appl. Phys. 25, 255 (1954)

(105) F. D. Rossini et al., Nat. Bur. Standards Circ. No. 500 (1952)

(106) D. Cubicciotti, J. Chem. Phys. 31, 1646 (1959)

(107) W. Känzig, J. Phys. Chem. Solids 17, 88 (1960)